WADC TECHNICAL REPORT 57-353
PART II

SOUND PROPAGATION NEAR THE EARTH'S SURFACE AS INFLUENCED BY WEATHER CONDITIONS

M. D. Burkhard
H. B. Karplus
H. J. Sabine

Armour Research Foundation

DECEMBER 1960

Contract Nos. AF 33(616)-2470 and AF 33(616)-5091
Project No. 7210
Task No. 71709

BIOMEDICAL LABORATORY
AEROSPACE MEDICAL DIVISION
WRIGHT AIR DEVELOPMENT DIVISION
AIR RESEARCH AND DEVELOPMENT COMMAND
UNITED STATES AIR FORCE
WRIGHT-PATTERSON AIR FORCE BASE, OHIO

1,000 – May 1961 – 27-1,014

FOREWORD

This report was prepared by the Armour Research Foundation of Illinois Institute of Technology under Contract Nos. AF 33(616)-2470 and AF 33(616)-5091 for the Aerospace Medical Division, Wright Air Development Division,* Wright-Patterson Air Force Base, Ohio. The work was in support of Project No. 7210, "Generation, Propagation, Action, and Control of Acoustic Energy," Task No. 71709, "Experimental Studies of Acoustic Energy Generation and Propagation." Technical supervision of the research program was the responsibility of Dr. Henning E. von Gierke and John N. Cole of the Bioacoustics Branch, Biomedical Laboratory, Aerospace Medical Division.

The work was carried out by H. B. Karplus and H. J. Sabine, under the supervision of Dr. R. W. Benson and M. D. Burkhard. The airplane was piloted by N. Collings and the field recording site was operated by L. D. Williams. Data were recorded on charts and reduced to tabular form by L. D. Williams, C. Caccavari, K. E. Feith, D. Lubman, L. Sprainis, and L. Silverman. H. B. Karplus, M. D. Burkhard, and H. J. Sabine carried out the mathematical analysis with the aid of J. G. Haynes and T. Engelhardt of the Mathematical Services Section.

* Wright Air Development Division was formerly Wright Air Development Center (WADC).

ABSTRACT

The effects of weather on the propagation of sound from an elevated source to the ground have been studied. Variations in attenuation were reported in Part I for weather in all seasons in the Chicago area. Part I was limited to source elevations of 14-1/2°, 30°, and 90° above the horizon. In this study measurements have been extended to include weather conditions in Arizona and propagation angles down to 2° elevation above the horizon.

Attenuations have been correlated with absolute humidity, temperature, temperature gradient, wind velocity, and wind direction. For source elevations of 5° and higher and source altitudes above a few hundred feet, only temperature and absolute humidity have a significant effect on attenuation. For source elevations of less than 5°, large attenuations occur in the presence of strong wind and temperature gradients. These are due to upwind refraction of sound and the resulting creation of shadow zones on the ground.

PUBLICATION REVIEW

E. L. de WILTON, Capt., MC, USN
Acting Chief, Biomedical Laboratory
Aerospace Medical Division

TABLE OF CONTENTS

LIST OF ILLUSTRATIONS

LIST OF ILLUSTRATIONS (Continued)

LIST OF ILLUSTRATIONS (Continued)

EXPERIMENTAL PROCEDURE

The flight program for angles of 14-1/2° and greater was identical to the previous year's program. This consisted of six circular passes at various altitudes and various radii and 16 straight passes of the airplane over the recording microphone at four different altitudes. A graphical representation of these flight patterns is shown in Fig. 4.

Since it was impossible to maintain a low enough altitude to fly circular passes for low angles, the airplane was flown in straight line dives directly at the microphone. Flight patterns are illustrated in Fig. 5. Elevation and azimuth angles were maintained constant in these passes. The angles of elevation selected were 15°, 10°, 5°, and 2°. The length of the flight path was 9600 feet. It was approached in two directions. This required a landing strip where the pilot could land if necessary, but under normal operating procedure the airplane would touch the ground and immediately climb back to altitude. These flights, therefore, yield only two measurements of the azimuthal variation of sound pressure level. At the Illinois site the directions were due east and due west and at the Arizona site directions were 15° south of east and 15° north of west. In order to establish the repeatability of the data obtained, two such complete flight patterns were flown for each independent series of flights. The number of approaches was, therefore, 16, two for each angle of elevation and two for each direction of approach.

In order to maintain the accuracy of the flight path for the lower angles of elevation the pilot was guided by one of a series of steady lights mounted on a pole and a single flashing light mounted on the ground at a distance of 100 feet from the pole. These lights are illustrated in the photograph, Fig. 6, and diagrammatically in Fig. 7, which show the orientation of the aircraft with respect to the lights. A single light on the pole was energized for each of the different dive passes and the pilot was able to keep in line with the steady light and the flashing light on the ground in order to maintain both elevation and azimuth. The technique was simple and accurate. In addition, the observer on the ground checked the plane with a sighting transit and radioed instructions for corrections to the pilot.

The 38 airplane passes which constituted one flight (one day's operation) are summarized in Table I (Appendix A).

MEASUREMENT APPARATUS

Measurement of weather variables was done with the same apparatus and procedures as in the previous study. Details are given in Part I. Sound levels for the circle and overhead passes were measured and analyzed in exactly the same manner as before. Tape recordings were made at the test site of the sound levels received by a microphone mounted 5 feet above the ground. The tape signals were passed through octave band filters and an integrating circuit which averaged the sound pressure level over a 1-second time interval. The output of this circuit was fed to a chart recorder from which the final sound pressure level data was read. This apparatus and procedure is fully described in Part I.

For the dive passes, the 1-second time integration was not available, because of the rapid changes in sound level as the airplane approached the microphone. After octave band analysis, the tape signals were therefore recorded directly on a high speed level recorder. By suitable scaling of the time axis of the recorder chart, sound pressure levels were read as a function of source distance. A typical recording is shown in Fig. 8. The apparatus and procedure is described fully in Appendix B.

SECTION III

DATA REDUCTION

During the period covered by this report there were 110 flights (55 at La Fox, 55 at Phoenix) during each of which there were six circular passes, 16 overhead passes, and 16 dive passes. The circular and overhead passes yielded a total of approximately 40,000 readings and the dive passes 130,000 readings. Some of these readings had inadequate signal-to-noise ratio for reasonable accuracy. However, a large majority of data is valid. The sound level readings and the associated meteorological data were transferred to IBM cards, and all further computations and statistical analyses of the data were carried out by means of an IBM 650 electronic computer.

ATTENUATION

The method of obtaining attenuations from the data may be indicated in the following way. We define attenuation, A, as the difference between the sound levels, L_{d1} and L_{d2}, at the microphone for transmission of the sound in the same direction over distances, d_1 and d_2, respectively. Thus,

$$A = L_{d1} - L_{d2}, \text{ db} \qquad (1)$$

Next, that portion of the level difference due to spherical spreading is removed from A, leaving only the atmospheric attenuation, A_a, which represents the losses for transmission of plane waves:

$$A_a = L_{d1} - L_{d2} - 20 \log (d_2/d_1) \qquad (2)$$

For convenience an atmospheric attenuation coefficient, α_a, the attenuation in db per 1000 feet is introduced.

$$\alpha_a = A_a / (d_2 - d_1) \text{ for } d_1 \text{ and } d_2 \text{ given in 1000 feet.} \qquad (3)$$

Although the use of an attenuation coefficient implies a constant attenuation or loss proportional to distance, such an assumption may not be valid. For example, variation of sound velocity with altitude, a common occurrence, gives rise to shadow regions by refraction of the sound waves. The attenuation of sound transmitted through a shadow region may be non-linear with distance, thus giving an attenuation coefficient dependent both on the distance interval and on its position with respect to the source. Attenuation, A_a, defined as above in Eq. (2) results from all losses other than spherical spreading encountered in the propagation of the sound, including molecular absorption, scattering, and refraction effects.

For each day's operation, attenuations, A, were obtained along each line of propagation. Thus, for propagation at a 30° elevation angle, the attenuation was observed as the difference between the average level in the circular passes coded 1, 3, and 5 in Table I. (See Fig. 4, also.) This gives attenuation over three different distances along the line of propagation. Attenuations along the 14.5° line of propagation were obtained in this manner, also. For propagation along the vertical, or 90° elevation angle, the attenuation was taken as the difference of average maximum levels for the various altitudes, the four separate overhead passes at any one altitude being averaged together. Rapid fluctuations were ignored by integrating the sound energy over a 1-second period, as noted above.

For the dive passes, sound levels were read off for distances of 300, 425, 600, 850, 1200, 1700, 2400, 3400, 4800, 6800, and 9600 feet (maintaining a ratio of $\sqrt{2}$). Attenuations were computed by subtracting the level at each distance from the level at 300 feet. Attenuations were computed and averaged separately for dive passes (and sound propagation) with and against the wind component.

CORRELATION

Circle and Overhead Passes

The principal aim of the investigation is to determine whether attenuation of sound from an airborne source depends significantly on meteorological conditions in the vicinity. Dependence may be established by statistically evaluating the correlation between attenuation and the various weather quantities measured.

If it assumed that the attenuation is the sum of linear functions of the weather parameters (or of functions of the parameters), the attenuation quantities defined by Eqs. (1), (2), and (3) may be expressed by the regression equations:

$$A = \bar{A} + m_1 (P_1 - \bar{P}_1) + m_2 (P_2 - \bar{P}_2) + \ldots\ldots\ldots\ldots\ldots \quad (4)$$

$$A_a = \bar{A}_a + m_1 (P_1 - \bar{P}_1) + m_2 (P_2 - \bar{P}_2) + \ldots\ldots\ldots\ldots\ldots \quad (5)$$

or

$$a = \bar{a} + M_1 (P_1 - \bar{P}_1) + M_2 (P_2 - \bar{P}_2) + \ldots\ldots\ldots\ldots\ldots \quad (6)$$

P_1, and P_2, etc., are either directly observed weather parameters or functions of the observed parameters which may be expected to approach a linear relationship to the attenuation more closely.

$\bar{A}$, $\bar{P}_1$, $\bar{P}_2$, etc., are the mean values of the attenuation and the weather parameters, or their functions, respectively, based on the observed data. The multiple regression coefficients, m_1, m_2, etc., are computed to give the statistically predicted change in attenuation per unit change in the corresponding weather parameter or function. The coefficients, M, are $m/(d_2-d_1)$, or db per thousand feet per unit change in weather parameter.

For the circle passes multiple regression coefficients were computed for the following weather parameters:

T Temperature at flight altitudes, °F

g Temperature gradient between ground and flight altitude, °F/1000 ft

W Wind velocity averaged between ground and flight altitude, ft/sec.

G Wind gradient between ground and flight altitude, ft/sec/1000 ft.

H Humidity function = $(T + 45)/h^2$

T = ground temperature, °F

h = absolute humidity at ground, gm/m^3

Maximum, minimum, and mean values of these parameters and their standard deviations for Illinois and Arizona are given in Table II (Appendix A).

These correlations differ from those of the previous period only in the use of the humidity function, H, instead of absolute humidity. This function is based on the theoretical expression relating molecular absorption to absolute humidity, temperature, and frequency. For a given distance interval, the molecular attenuation in db is of the form*:

$$A_H \propto \frac{f\,F(T)}{(h/h_m)^2 + (h_m/h)^2} \quad (7)$$

where

f = frequency

h_m = absolute humidity for which maximum absorption occurs

$h_m^2 \propto f$

* Reference 1, pp 13-14.

The humidity, h, was so high in relation to h_m in nearly every case that a simplified form of this equation,

$$A_H \propto f\, F(T)\, h_m^2 / h^2 \tag{8}$$

or

$$A_H = k f^2 F(T) / h^2 = k f^2 H$$

where k is an experimental constant, could be substituted in which no assumption had to be made on any of the parameters and yet permitted the same function to be used for all frequencies. The function of temperature that was used was approximated by a linear function without introducing a significant error. The form of the function is given by:

$$F(T) = T + 45 \quad °F \tag{9}$$

The values for temperatures between zero and 100°F have been plotted from data supplied by Nyborg and Mintzer* in Fig. 9. It will be seen that an assumption of a linear function does not introduce an appreciable error. The actual humidity function, H, used is then given by:

$$H = \frac{T + 45}{h^2} \tag{10}$$

Regression coefficients were computed individually for all of the distance intervals for which attenuations were determined.

Dive Passes

The same type of regression analysis was applied to the dive pass data, except that the east components of the wind velocity and wind gradient were substituted for the scalar values. These computations showed a very strong dependence of attenuation on wind velocity and direction, on temperature gradient, and on angle of source elevation, indicating the expected influence of shadow effects. In order to study these effects in more detail, a revised computer program for all of the dive pass data was set up, comprising the following steps:

1. All cases in which the signal level was less than 7 db above the ambient noise level were eliminated from the computations. This would only partially correct for the effects of noise interference, since the remaining data would tend to be weighted toward higher average signal levels and the

* Reference 1, p 152.

average attenuations would be correspondingly smaller than their true values.

2. Residual attenuations were computed for all distance intervals in the dive passes referred to 300 ft from the source. These are defined as:

$$A_o = A - A_H - 20 \log (d_2/d_1)$$

$$= A_a - A_H$$

The molecular absorption, A_H, was computed from the regression coefficients relating attenuation to the humidity function, H, as determined experimentally from the circle pass data. The value of H was in turn computed for each day's flight from the observed values of temperature and absolute humidity. The residual attenuation, A_o, is therefore due to all other effects, including scattering, refraction, and shadow phenomena.

3. Simple regression coefficients, b, were computed for four weather parameter functions:

$W \cos \phi$ = component of wind velocity, averaged between ground and 600 ft. altitude, parallel to line of dive pass

$(W \cos \phi)^{2/3}$

$(\Delta T)^{2/3}$ where ΔT = temperature at ground (5 ft) minus temperature at 600 ft.

$\log_e W$ where W = wind velocity averaged between ground and 600 ft.

The absolute value of wind component was used throughout, and regression coefficients were computed separately for upwind and downwind sound propagation corresponding to the two directions of dive passes for each day's flight. Regression coefficients were computed for all distance intervals referred to 300 feet.

The above weather parameter functions were chosen primarily to give the best expected correlation with the attenuation within shadow zones. They are based on the following theoretical considerations. The formation of sound shadows by upward refraction of rays from a low elevation source has been described in the literature and is illustrated in Fig. 10. The fact that some sound can be observed in the shadow zone is due to diffraction from the shadow boundary and to scattering into the shadow zone from turbulent regions between the source and the shadow boundary. An expression for the total attenuation, A_{Sh} (not including molecular absorption, A_H), has been

derived, as follows[2]:

$$A_{Sh} = 10 \log \frac{I_o}{I_{Sh}} = 10 \log \frac{I_o}{I_D + I_S} \qquad (11)$$

where I_o = relative intensity of sound entering shadow at boundary at receiver height (5 ft)

$$= \frac{(2fW)^2 + A}{d_o^2}$$

I_D = intensity of sound diffracted into shadow region

$$= \frac{A}{dd_o} \exp. \left[-2K (a + \beta \cos \phi)^{2/3} f^{1/3} (d-d_o)\right]$$

I_S = intensity of sound scattered into shadow region

$$= \frac{(fW)^2}{(d-d_o/2)^2}$$

d_o = horizontal distance from source to shadow boundary at receiver height

d = horizontal distance from source to receiver, assumed equal to slant distance

f = frequency, cps

W = wind velocity, ft/sec

A, K = experimental constants

α = sound velocity gradient due to temperature gradient at receiver height, sec^{-1}

= -1.07 x temperature gradient*, °F/ft at 68°F

$\beta \cos \phi$ = gradient of wind component in opposite direction to sound propagation at receiver height, sec^{-1}

$$= \frac{d(W \cos \phi)}{dz}$$

For a given source and receiver height, the distance, d_o, from source to shadow boundary varies as $(\alpha + \beta \cos \phi)^{-1/2}$. Representative computed plots of shadow attenuation as a function of source to receiver distance, d, and wind velocity, W, taken from Reference 2, are shown in Fig. 11, in which the wind-sound angle is assumed to be 180° and the temperature gradient zero. The wind gradient is also assumed proportional to wind velocity at a given height. Beginning at the shadow boundary, the diffracted intensity, I_D, is by far the larger component of sound in the shadow, but drops off very rapidly both inversely and exponentially with distance. The higher the wind velocity (that is, the larger the gradient), the closer is the shadow boundary to the source and the more rapidly the diffracted intensity drops off. At greater distances the scattered intensity becomes the major component. It drops off at a rate approaching the inverse square law and the intensity increases with the square of the wind velocity. In selecting weather parameter functions for the regression computations of the dive pass data, it was expected that the average attenuation for upwind propagation at the lowest elevations would show a curve with distance indicating shadow attenuation and would have a shape approximating an average of the curves computed from the foregoing theory. The functions, $(W \cos \phi)^{2/3}$ and $(\Delta T)^{2/3}$, were chosen to apply to the diffraction region and the function, $\log_e W$, pertains to the scattering region. The function, $W \cos \phi$, was also included for comparison with the 2/3 power. The wind velocity component, $W \cos \phi$, was substituted for the gradient, $\beta \cos \phi$, because they have been shown experimentally to be closely proportional at a given height. Similarly, the temperature difference, ΔT, was used in place of the sound velocity gradient due to temperature because they are nearly proportional for the temperature range observed. Since the quantities, $(\Delta T)^{2/3}$ and $(W \cos \phi)^{2/3}$, are related exponentially to the diffracted intensity they are taken as being proportional to the attenuation in decibels. Strictly speaking, the attenuation is proportional to the function, $(k\Delta T + W \cos \phi)^{2/3}$, where k is some constant, rather than to each term separately to the 2/3 power. However, the average values and ranges of ΔT and $W \cos \phi$ obtained in the study are such that their sum to the 2/3 power is very closely

* In accordance with meteorological terminology, a temperature decreasing with height is considered to have a positive gradient, but the corresponding decrease of sound velocity is considered as a negative gradient.

proportional to either term to the 2/3 power. To simplify the regression computations, therefore, the terms were treated as separate variables. Since the scattered intensity is proportional to W^2, the log of W was used to compute the regression of scattered attenuation in db on wind velocity, the exponent being absorbed in the proportionality. Also, in order for the observed values of attenuation with respect to temperature gradient, ΔT, to be fitted by a linear, monatonic curve against $(\Delta T)^{2/3}$ as the abscissa, the values of ΔT were mostly negative (temperature at flight altitude higher than ground), so that this requirement was fairly well satisfied.

Simple rather than multiple regression coefficients were computed for the above weather parameter functions because the choice of functions made it desirable to show the relation of attenuation to each parameter individually rather than to their combination*. If a series of parameters used as independent variables are completely independent of each other, then the regression coefficient for each parameter will have the same value whether it is computed as a simple regression coefficient or as one of a series of multiple regression coefficients as defined by Eq. (4). However, if the parameters have a high correlation with each other, as, for example, $\log_e W$ and $W \cos \phi$, or especially $W \cos \phi$ and $(W \cos \phi)^{2/3}$, then the values of the multiple regression coefficients computed for these parameters will differ from the corresponding simple regression coefficients according to the degree of correlation between the parameters. Simple regression coefficients, however, have the same value for a given parameter, regardless of its dependence on any other parameter. A regression equation of the form of Eq. (4) using simple rather than multiple regression coefficients is valid for predicting the value of attenuation from known values of weather parameters only if the parameters are completely independent of each other[3].

Wind-Sound Angle

In the previous program it was observed quite consistently that attenuations were greater when the sound was propagated with the wind (downwind) from the 14.5° and 30° source elevations than against the wind. This is the opposite of the effect observed for ground-to-ground propagation. In order to study in more detail the effect of wind direction on attenuation, selected level recorder charts for the circular passes were divided into sections corresponding to octants of the circle and the average level in each octant was read from the chart. These octant levels and their variations from the mean level of each circular pass were tabulated as functions of absolute wind direction, relative wind-sound angle, wind velocity, frequency, site location, ground cover, and season of the year.

* The simple regression coefficient indicates the variation of attenuation with respect to a given weather parameter when all other parameters are held constant, and is therefore equivalent to the partial derivative with respect to that parameter.

SECTION IV

RESULTS

The dependence of sound attenuation on weather was evaluated by the different analyses discussed in Section III. The principal results are given in this section.

RANGE OF WEATHER CONDITIONS

The range of the weather parameters is given in Table II (Appendix A) and plotted in Fig. 12. The number of observations has been plotted as a function of the individual weather parameters. It will be seen that substantial differences between the Arizona and Illinois data exist in the humidity and the humidity function as well as the wind and wind gradient. It appears that strong winds were very rare in Arizona and the absolute humidity there was usually considerably lower than at the Illinois site. In comparing the two locations it should be noted that the Arizona data refers to the winter months and the Illinois data to summer and early fall. The negative mean values of temperature gradient appearing in the table indicate a predominance of temperature inversions at the lower altitudes, that is, higher temperatures at flight altitude than at ground. This resulted from the comparatively large number of measurements taken near the beginning and end of the day, particularly in Arizona, when inversions typically occur.

The distribution of the humidity function, H, Fig. 12, is of particular interest. It is seen that, although the range of this function is very wide, the mean value given in Table II is comparatively small. A few very large values occurred in Arizona. In Illinois H was always small during this period.

MEAN VALUES OF ATTENUATION

Circle and Overhead Passes - Source Elevation 14.5° to 90°

Table III (Appendix A) gives the attenuation, $\bar{A}_a$, in octave bands averaged over all the different weather conditions for the circle and overhead passes - approximately 100 readings. Each of the original readings for the circle passes was itself averaged by eye over two complete circles. For the overhead passes each reading was the average of the four overhead passes (Table I). Also included in Table III are values of average residual attenuation, $\bar{A}_o = \bar{A}_a - \bar{A}_H$. The average humidity attenuation, $\bar{A}_H$, was computed from the average value of the humidity function, H, given in Table II and the regression coefficients relating attenuation to the humidity function at each frequency, as determined experimentally from the circle pass and overhead data. This determination is explained in the following section. The method of deriving $\bar{A}_o$ for the dive pass data differs from the above in that values of A_H were computed individually for each flight and deducted from the corresponding A_a. The resulting $\bar{A}_o$ values were then averaged. However, the average residual attenuations, $\bar{A}_o$, for the two sets of data should be comparable for the same conditions of distance and source elevation.

Table III also lists the standard deviation, σ_d, of the atmospheric attenuation, A_a. These values indicate the spread of the measured attenuations due to all weather variables, including humidity, as well as to experimental error of measurement and chance unknown factors. For frequencies below 300 cps the effect of humidity is negligible, and the listed values of σ_d apply equally to the atmospheric attenuation, A_a, and the residual attenuation, A_o.

One of the purposes of the work reported in this volume was to check the repeatability of data obtained in the previous year's program, as reported in Part I. This may be done by comparing the average attenuations for the circle and overhead passes for the two years. The data are not exactly comparable for the reason that the average weather conditions were not the same for the two years. A comparison of the mean values of the more important parameters is given in Table IV* (Appendix A). From this it is seen that, with the possible exception of temperature gradient, the overall mean values for the two years are quite similar. Since the effect of absolute humidity is considerably greater than any of the other parameters, as will be shown in a following section, the values of average atmospheric attenuation, $\bar{A}_a$, contained in Part I were converted to average residual attenuation, $\bar{A}_o = \bar{A}_a - \bar{A}_H$, in the same manner as the corresponding data given in Table III of this report. The resulting values for the two years, with humidity effects eliminated, are plotted in direct comparison in Fig. 13. The distance intervals as abscissæ are shown on a linear rather than a logarithmic scale, the zero point of each interval representing the nearest distance to the source for the indicated source elevation. For example, zero on the distance scale corresponds to 600 feet for the 90° passes and 2400 feet for the 14.5° passes. It is seen that all of the data for both years and for all source elevations from 14.5° to 90° can be represented as a linear function of attenuation against distance within plus or minus 1 db for each frequency, up to a distance interval of 5000 feet. The 14.5° data at the largest distance interval is subject to question because of the unfavorable signal-to-noise ratio. There is a consistent tendency for the attenuations for the second year to be larger at distances near the source than for the first year. The second year's data, in fact, is better represented as proportional to the log of the distance than to the distance directly. There is no immediate explanation for this trend, but it might be associated with the rather marked difference in average temperature profile between the two years and its effect on the constancy of sound power output of the source. However, the general agreement of the two years' data is close enough, for practical purposes, that this difference may be neglected. If the residual attenuation is assumed to be due primarily to scattering by air turbulence, a linear rather than logarithmic relation between attenuation and distance would be more reasonable. However, since turbulence of the size or scale contributing most to sound scattering tends to decrease with altitude, the slope of the curve would not be expected to remain constant.

* In Part I the absolute humidity is given as 2.64 grains/cu. ft. A conversion factor of 2.3 gives the value of 6.1 gm/m^3 listed in Table IV.

Straight lines have been fitted by eye to the data in Fig. 13. For the two frequencies, 150-300 and 300-600, where the humidity attenuation, A_H, is negligible, the slope of the lines is the same as shown in Part I, since the same line fits the combined two years' data as well as either year alone. At the two higher frequencies, the slopes are smaller than those given in Part I, because of the correction for humidity attenuation. The slopes of the lines, expressed as average residual attenuation coefficients, $\overline{\alpha}_o$, in db per 1000 ft., are plotted against the 1/3 power of the frequency in Fig. 14. It is seen that this plot is represented very closely by a straight line having the equation:

$$\overline{\alpha}_o = 0.11\, f^{1/3} \quad \text{db/1000 ft} \tag{12}$$

where f is the mean frequency of an octave band.

Another purpose of the second year's program was to compare propagation characteristics at the Illinois and Arizona sites where both the climate and the ground cover differed widely. The important weather parameters are compared in Table II and Fig. 12. Since it was expected that the large difference in absolute humidity would account for most of the difference in attenuation at high frequencies, this parameter was eliminated as before by computing the average residual attenuation, $\overline{A}_o$, for the two sites separately for the second year's program. As noted before, these two sets of data correspond, respectively, to the summer months in Illinois and the winter months in Arizona. The data are plotted in Fig. 15 in the same manner as in Fig. 13. The straight lines shown in these plots are drawn with the same slope as in the previous figures containing all of the data for the two years. There is somewhat more scatter in the Illinois-Arizona comparison, due to the smaller number of cases, and at the lower frequencies there appears to be somewhat higher attenuation for the Illinois summer than for the Arizona winter. However, the lines shown fit the data about as well as any others that could be drawn by eye. For practical purposes, therefore, the residual attenuation may be considered to be essentially independent of general climate and ground cover, and to have an average value dependent only on frequency.

Dive Passes - Source Elevation 2° to 15°

Table V (Appendix A) lists the mean values, $\overline{A}_o$, and standard deviation, σ_{A_o}, of the residual attenuation for the dive passes. The culling out of data subject to ambient noise interference resulted in a reduced number of cases at the farthest distances from the source, and a bias of the averages toward small attenuations. In the table, those averages which are based on less than 80 per cent of the number of cases at the closest distance, namely the 425-300 ft. interval, are indicated by a line, and are considered subject to question.

The average residual attenuations for the dive passes are plotted in Figs. 16, A to D. In these charts the 5°, 10°, and 15° average attenuations are lumped together and only the maximum and minimum values occurring at each distance are plotted. The 2° attenuations are plotted individually. Upwind

and downwind data are separated throughout. For source elevations of 5° to 15° there is no pronounced variation of attenuation with angle and no large difference between upwind and downwind propagation. For the higher frequencies the 2° downwind attenuations also fall within the range of attenuations for the higher angles and are not plotted separately. At the lower frequencies the downwind attenuations for the 5° to 15° angles tend to be slightly higher than the upwind values. The attenuations for the 2° elevation, however, are higher at all frequencies for upwind than for downwind propagation and higher than for any greater source elevation. The very large values and steep rises of attenuation at the higher frequencies are clearly due to shadow effects.

CORRELATION OF ATTENUATION WITH WEATHER VARIABLES

Circle and Overhead Passes

Regression coefficients, m, which best fit the equation:

$$A = \bar{A} + m_T (T-\bar{T}) + m_g (g-\bar{g}) + m_H (H-\bar{H}) + m_W (W-\bar{W}) + m_G (G-\bar{G})$$

are plotted as a function of distance in Figs. 17 to 21. An indication of the order of magnitude of the various parameters is indicated by a dotted line marked $1/\sigma$ which is the value of the regression coefficient which, when multiplied by the standard deviation of the corresponding weather parameter, will produce 1 db change of attenuation. It may be observed, as in the previous study, that the regression coefficients tend to be small, usually accounting for less than 1 db change in attenuation. The observed standard deviation in attenuation of 2 to 6 db, as given in Table III, may therefore be attributed only in part to dependence on the weather parameters, the remaining variation being due to experimental error and to unknown meteorological factors.

Where there is an indication of a possible dependence of the regression coefficient on distance, a straight line is fitted by eye to the plotted points so that zero attenuation corresponds to zero distance. This was done only for the temperature and humidity function, as shown in Figs. 17 and 21. For the other weather parameters, namely, temperature gradient, wind velocity, and wind velocity gradient, the regression coefficient scattered excessively. This scatter, particularly when both positive and negative coefficients appear, indicates either that the weather parameter in question actually has no influence on the attenuation, or if so that its influence is so small as to be completely obscured by the random experimental error in the measurement of the attenuation or by the comparatively larger effects of other parameters.

Figure 21 indicates that m_H varies linearly with distance and increases systematically with frequency. A plot of m_H/f^2 (where f is the geometric mean frequency of an octave band in kilocycles) against distance is shown in Fig. 22. From this it is possible to describe the effect of humidity with a single number, where a slope of 0.1 was selected as giving the best

fit by eye. Thus,

$$m_H = 0.1\,(d_2-d_1)\,f^2$$

or

$$a_H = HM_H$$

$$a_H = 0.1\left(\frac{T+45}{h^2}\right) f^2 \quad \text{db/1000 ft} \tag{13}$$

Equation (13) was used to compute the humidity attenuation, $A_H = a_H\,(d_2-d_1)$, which was deducted from the gross attenuation, A_a, to give the residual attenuation, A_o, for both the dive passes and the circle and overhead passes.

For comparison, a line with slope 0.15, the theoretical value of k in Eq. (8), is included in Fig. 22 *. The experimental data will fit this theoretical slope if a value of frequency is chosen which is approximately 0.8 times the geometric mean frequency of each octave band. This correction appears reasonable, since the attenuation measured in an octave band will be weighted toward that end of the frequency range at which the smaller attenuations occur.

Dive Passes

Simple regression coefficients, b, computed for each of the four weather parameters defined in Section III are listed in Table VI (Appendix A). The standard deviation, σ_P, of each parameter is given at the head of the corresponding column, together with values of $1/\sigma_P$. Regression coefficients smaller than $1/\sigma_P$ indicate that the standard deviation of the corresponding weather parameter will produce less than 1 db change in attenuation. As in Table V, the line across each set of data indicates the distance beyond which the number of cases falls below 20 per cent of the maximum. Values below this line become increasingly questionable.

Upwind Propagation

The variation in residual attenuation, A_o, with weather for the 2° and 5° upwind dive passes is plotted in terms of standard deviation, σ_{A_o}, against distance and frequency in Figs. 23 and 24. For both 2° and 5° elevations and for all frequencies, the spread in attenuation increases sharply with distance up to 1200 to 1700 ft. and thereafter remains constant or diminishes slightly. The maximum value of σ_{A_o} is ± 12 to 13 db, occurring at a distance of 1200 ft. and at frequencies from 300 to 2400 cps for the 2° elevation and in the 1200-2400 octave band for the 5° elevation. The spread in attenuation increases slightly with frequency for the 2° elevation and shows a stronger

* Reference 1, pp 13, 14, 152.

dependence for 5°, although a regular trend is not apparent in either case. The spread in attenuation is essentially the same at both angles for high frequencies, but at low frequencies is less for the 5° elevation than for 2°.

Regression coefficients for the 2° and 5° upwind dive passes are plotted against distance in Figs. 25 to 34. For the 10° and 15° dive passes the regression coefficients were almost all smaller than $1/\sigma_P$ and are therefore not plotted. In these charts the regression coefficients, instead of being plotted directly, are each multiplied by the corresponding value of σ_P. This product, $b\sigma_P$, termed "normalized regression coefficient" gives directly in decibels the change in attenuation attributable to the standard deviation of the indicated weather parameter. The standard deviation, σ_{A_o}, of the attenuation is also plotted on each chart for reference. The ratio of $b\sigma_P$ to σ_{A_o} is equal to the correlation coefficient, r, between the attenuation, A_o, and the corresponding weather parameter and indicates how much of the total observed variation in attenuation can be accounted for by its dependence on the variation in each weather parameter over its observed range. By plotting the normalized regression coefficients for all four weather parameters on the same chart, the relative influence of the parameters on the attenuation can be directly determined by inspection.

The regression coefficients for the three wind parameters are plotted with the same sign as computed, which was generally positive. In most cases, the regression coefficients for the temperature gradient parameter, $(\Delta T)^{2/3}$, were of opposite sign to the wind parameters. Where attenuation is due to shadow effects, a negative slope of attenuation with respect to this parameter is to be expected because decreasing negative values of temperature gradient, corresponding to decreasing positive values of $(\Delta T)^{2/3}$, produce increasing attenuation. As noted before, the observed values of ΔT were predominantly negative. In order to permit ready comparison of the $(\Delta T)^{2/3}$ regression coefficients with the others on each chart, they are plotted with reversed sign throughout. To take account of the general case where both positive and negative temperature gradients are encountered, the regression coefficients for $(\Delta T)^{2/3}$ should be considered as positive with respect to changes in ΔT in the positive direction, where a positive temperature gradient is defined as a decrease in temperature with height.

The temperature gradient parameter, $(\Delta T)^{2/3}$, and the three wind parameters show strong correlations with the attenuation for all distances up to the limit set by 80 per cent of the total cases. The normalized regression coefficient values, $b\sigma_P$, for $W\cos\phi$ and $(W\cos\phi)^{2/3}$ are almost identical throughout, as would be expected from the nearly linear relationship between the two functions over the range in question*. The simpler function, $W\cos\phi$, may, therefore, be used in place of the 2/3 power for predicting the effect of wind component on attenuation. The computed correlation coefficients

* Occasional marked differences are due to the fact that the plotted values of $b\sigma_P$ were computed from a constant value of σ_P for each parameter based on the maximum number of cases (84), while the regression coefficients were computed from a varying number of cases depending on the attenuation data available for each distance and frequency.

of .18 and .20, respectively, between the temperature gradient parameter, $(\Delta T)^{2/3}$, and the two remaining wind parameters, $W \cos \phi$ and $\log_e W$, indicate that, while temperature gradient is not completely independent of wind, as assumed, they are sufficiently independent that their contributions to the total observed spread in attenuation may be considered to be additive. Thus, for example, a value of $b\sigma_p$ of 6 db for the $W \cos \phi$ parameter and 5 db for the $(\Delta T)^{2/3}$ parameter may be considered together to account almost entirely for an observed standard deviation in attenuation, σ_{A_o}, of 12 db. Where the sum of the $b\sigma_p$ values for the temperature gradient and the larger of the two wind parameter values is considerably less than the observed spread in attenuation, the excess can be attributed either to (1) random errors in measurement of attenuation, (2) non-linearity between attenuation and either or both of the parameters in question, or (3) the effects on attenuation of other parameters (such as ground reflection, turbulent scattering, etc.) which are related very indirectly or not at all to those under consideration.

The correlations between attenuation and the two wind parameters, $W \cos \phi$ and $\log_e W$, are of the same order, as would be indicated by the computed intercorrelation of .63 between the two wind parameters, and are in general somewhat larger than the correlation between attenuation and temperature gradient.

The highest correlation between attenuation and the combined effects of wind and temperature gradient occurs for the 2° elevation at the 1200 and 1700 ft. distances, which are the same at which maximum variation in attenuation occurs. At these points, the σ of the temperature gradient parameter, $(\Delta T)^{2/3}$, accounts for 30 to 40 per cent of the spread in attenuation, σ_{A_o}, and σ of either the wind component parameter, $W \cos \phi$, or the scalar velocity parameter, $\log_e W$, accounts for 50 to 70 per cent of σ_{A_o}. Thus, the total variation in attenuation is accounted for almost entirely by the combined variation in temperature gradient and wind. Beyond 1700 ft., the correlation between attenuation and any of the parameters drops off sharply. This may be due in part to the reduced number of cases. There are no marked differences in correlation with frequency. However, with increasing frequency, correlation of the wind component parameter tends to become higher in relation to that of the scalar velocity component.

The correlations for 5° upwind propagation are similar to those for 2° except that they are generally lower for all of the parameters. The maximum combined correlations of temperature gradient and wind are about 80 per cent, occurring at 1700 to 3400 ft. in the 300-600 cps octave band. The correlation is generally more uniform with distance and does not show the sharp drop after 1700 ft. that occurs for the 2° elevation. Furthermore, the effect of the scalar wind parameter is larger than that of the wind component at all frequencies.

For upwind propagation at 10° and 15° elevations the spread in attenuation, not including the 2400-4800 cps band, σ_{A_o} varied from an average of 3 db at 425 ft. to 6 db at 4800 ft., and was largely independent of frequency. The spread in attenuation for the 2400-4800 band was considerably greater than for the other frequencies up to a distance of 850 ft., beyond

which the number of cases dropped below 80 per cent of the maximum number. However, as pointed out above, the regression coefficients for the 10° and 15° elevations accounted, with a few exceptions, for no more than 1 db of the observed spread at any distance, and the correlations were correspondingly too small to be significant.

Downwind Propagation

The standard deviations, σ_{A_o}, of the attenuation for downwind propagation at 2° and 5° source elevations are plotted against distance in Figs. 35, 36. For the 2° elevation the spread in attenuation is generally higher at all distances and frequencies than for larger angles, reaching a maximum of 6 to 10 db at 1200 ft. and beyond. There is considerable scatter between the different frequencies, with a rough trend showing an increase in σ_{A_o} with frequency. For the 5° elevation the average values of σ_{A_o} range from about 3 db at 425 ft. to 7 db at 4800 ft. There is no marked dependence on frequency except for the lowest and highest bands (75-150 cps and 2400-4800 cps), both of which show a greater spread in attenuation than the intermediate frequencies. The σ_{A_o} values for the 10° and 15° source elevation are generally similar to those for 5° and to the 10° and 15° upwind data.

The correlation between attenuation and the weather parameters is in general smaller for downwind than for upwind propagation, and in nearly all cases the normalized regression coefficient values, $b\sigma_p$, are less than 2 db. The principal exceptions occur in the case of 2° source elevations and in the lowest octave band (75-150) at all source elevations. These data are plotted in Figs. 37 to 44. The values for the parameter, $(W \cos \phi)^{2/3}$, are very close to those for $W \cos \phi$ and are, therefore, omitted from the plots. Where the regression coefficients are mostly negative, the negative curve of $\pm \sigma_{A_o}$ is plotted for comparison. For the 2° elevation the data in the 75-150 bands are quite similar to the corresponding data for upwind propagation. The regression coefficients for the scalar wind velocity and the temperature gradient parameters show a strong correlation with the attenuation up to the limit of the valid data at 1700 ft., and their combined values account for 75 to 80 per cent of the observed standard deviation in attenuation, σ_{A_o}, at all distances. The maximum effects of the standard deviations, σ_p, of the two parameters are 4 and 3 db, respectively, at 1200 ft. At all other frequencies the correlations and the regression coefficients are generally small, with the exception of the 600-1200 band, where the scalar wind parameter accounts for 4 db of the 9 db spread in attenuation at 1700 ft.

The plots for the 75-150 bands indicate that the regression coefficients for all three parameters follow a definite and regular trend from positive to negative with increasing source elevation angle. This is illustrated in more detail in Fig. 45. The magnitude of the regression coefficients, $b\sigma_p$, and the correlations at the 10° and 15° elevations are about the same, but of opposite sign, as for 2°, namely, a maximum effect of a single parameter of about 4 db and the combined effect of wind and temperature gradient accounting for 75 to 80 per cent of the spread in attenuation. This reversal of sign would indicate that in the lowest frequency band the downwind attenuation increases with wind velocity, with wind component, and with temperature

gradient* for 2° and 5° source elevations but decreases at 10° and 15° elevations. There is an apparent similar trend in the 150-300 band for the temperature gradient parameter only, but the regression coefficients are small, the $b\sqrt{p}$ values ranging from 0 to 2 db. There is no indication of this trend at any higher frequencies, and regression coefficients are all small.

Attenuation in Shadow Zone

As noted above, the large attenuations and the high correlations of attenuation with wind component and temperature gradient for the 2° upwind passes indicate the presence of shadow attenuation. It is of interest to compare the observed values of shadow attenuation with the theoretical values given by Eq. (11). In order to use this equation it is necessary to estimate (1) the sound velocity gradients, α and $\beta \cos \phi$, due to temperature and to wind component opposite to the direction of sound propagation, respectively, (2) the horizontal distance d_0 from the source to the shadow boundary at receiver height (5 ft), and (3) the experimental constant, K. The temperature is found from meteorological data to vary approximately logarithmically rather than linearly with height up to a few hundred feet. Assuming that this relation holds between the heights at which ΔT (°F) was measured in this program, namely, 5 ft. and 600 ft., the value of α at 5 ft. was determined from the equation:

$$\alpha_5 = .045 (T_5 - T_{600}) \quad \text{sec}^{-1}$$

The wind velocity has also been found experimentally to increase approximately logarithmically with height, and the velocity gradient at a given height is roughly proportional to the velocity. Since directly comparable data for wind component at 5 ft. and some greater height was not available from the weather observations, experimental data by others[4] on both of the above relations were used to estimate the wind gradient at 5 ft. as a function of the wind velocity observed at 300 ft. from the weather balloon readings. The equations used are:

$$W_5 = 0.65 W_{300} \quad \text{ft/sec}$$

$$\beta_5 = 0.037 W_5 = 0.024 W_{300} \quad \text{sec}^{-1}$$

* As defined before, an increasing temperature gradient is interpreted as a decreasing temperature at 600 ft altitude with reference to ground temperature.

These estimated values of α_5 and $\beta_5 \cos \phi$ were used in an expression supplied by Nyborg and Mintzer* for computing the distance, d_0, from source to shadow zone as a function of source and receiver height where the sound velocity decreases logarithmically with height, as given by:

$$c_z = c_0 \left(1 - B \log_e \frac{z}{z_0}\right)$$

where

$$B = \frac{z}{c_0} \left(\alpha_z + \beta_z \cos \phi\right)$$

The calculations showed first that for the range of wind and temperature gradients encountered in this program shadow formation would not be expected to occur at all in about half of the total cases. This was due to the large proportion of negative temperature gradients which tended to outweigh the positive wind gradients, resulting in negative values of $(\alpha + \beta \cos \phi)$. For the 2° dive passes, the calculations showed further that the microphone would be expected to lie in the shadow zone for a still smaller proportion of the total cases, corresponding to the highest values of combined temperature and wind gradient. Since the attenuation rises sharply as the shadow boundary crosses the microphone, and becomes a strong function of wind and temperature gradient only in the shadow zone, there may be considerable inaccuracy in representing the relation between attenuation and either the wind or the temperature gradient by a linear function over the entire observed range of these parameters, as is done in computing the regression coefficients.

Observed values of shadow attenuation were compared with theoretical values for 2° upwind dive passes by selecting five flights made on days having large wind and temperature gradients such that the combined gradients, $(\alpha + \beta \cos \phi)$, were of about the same value in each case and would place the microphone in the shadow zone. The average value of $(\alpha_5 + \beta_5 \cos \phi)$ was 0.4.

An experimental value for K of 2.8×10^{-4} was arrived at by fitting the observed attenuation data for the five flights to the expression for attenuation of diffracted sound contained in Eq. (11). Theoretical curves of attenuation of diffracted sound versus distance from source to observation point are shown in Fig. 46 using the above values of $(\alpha_5 + \beta_5 \cos \phi)$ and K. The observed attenuations averaged for the five flights are plotted for comparison. The agreement is considered quite good in view of the experimental error in the measured attenuation data for the dive passes and the approximations involved in estimating the sound velocity gradient, $\alpha + \beta \cos \phi$. The attenuation values at 1200 ft are approximately linear with respect to the 1/3 power of the frequency, as predicted, although the slope is somewhat greater.

* Reference 1, p. 53.

The presence of a scattered component in the sound entering the shadow zone would be indicated theoretically by a leveling off of attenuation with respect to distance and by a decrease in attenuation with increasing wind velocity and frequency. The observed average residual attenuations for the 2° upwind passes do tend to become constant with distance at about 2000 ft., as shown in Fig. 16, but the effect is at least partially obscured by ambient noise. Furthermore, the observed attenuations in the leveled-off region tend to increase rather than decrease with frequency. Also, the expected inverse relation of attenuation to scalar wind velocity would result in negative regression coefficients, b_4, in this region, but they do not appear. In general, the data are not sufficiently complete or precise to indicate a well-defined scattered component distinct from the diffracted component in the shadow zone and thus to permit an adequate check of the theory.

Effect of Wind Direction for Circular Passes

The results of the detailed analysis of the circle passes by octants are summarized in Table VII. The wind-sound octant numbered 0 corresponds to downwind propagation, where the sound and wind reach the microphone from the same direction. The numbers follow the counter-clockwise pass of the airplane, octant 4 representing upwind propagation. The data are grouped first according to wind velocity as read at ground level to the nearest 5 mph. Where the before and after readings differed for a given flight, the higher was chosen. For the Arizona data, the winds were, in general, so variable during a flight and high winds so infrequent that it was impractical to try to tabulate more than the single 5 to 15 mph bracket. Where the wind direction varied before and after the flight, the "before" direction was arbitrarily chosen. Since the variation between maximum and minimum level in a circular pass increased with frequency, most of the data selected were for the 1200-2400 cps band in order to illustrate the effect most clearly and to facilitate comparisons between wind velocities, sites, etc.

The data are further sub-grouped according to source elevation angle, site, and ground cover. The first set of circle passes analyzed was for the period from July to September, 1956, at the Illinois site. Since the winds were predominantly from one direction during this period (south to west) the correlation of attenuation with absolute source direction was about as strong as with wind-sound angle. At this time, the microphone was located very close to the north edge of a field of corn which was 2 to 6 ft. high. This suggested that the directional attenuation might be due to the ground cover rather than to wind effects. This was checked by analyzing two sets of circle passes from the previous year's program at the Illinois site. In this case, the microphone was at all times well removed from the nearest boundary of corn or other crop. The first set was representative of the nine-month period from February to December, 1955, and would be generally comparable to the second year's data except for microphone position. The second set was for the winter months of December, 1955, to February, 1956. During this period, the ground on all sides was bare except for low grass and stubble, and the wind directions were more randomly distributed.

Comparison of the data from these three periods showed definitely that the attenuation was a function of wind-sound angle and not of absolute source direction nor of ground cover variations. The average results of the 1200-2400 octave band data are shown in Fig. 47, where the deviation from the mean sound pressure level of a circular pass is plotted against wind-sound angle. The Illinois data are averaged together for each of three wind velocity ranges, and all of the Arizona data are averaged together and shown separately for the indicated wind velocity range. Data corresponding to the two source elevation angles of 14.5° and 30° are averaged throughout. All of the curves show an approximately sinusoidal variation in sound level as a function of wind-sound angle, with the maximum and minimum levels occurring close to the upwind and downwind propagation directions, respectively. For the Illinois data, the difference between maximum and minimum values is closely proportional to the wind velocity reaching an average value of about 8 db for 20 to 25 mph winds. However, the average variation for the Arizona passes is much less than for the Illinois passes of corresponding wind velocity. This is possibly due to the smaller number of cases available from Arizona and the variability of the winds there. In comparing octant analyses of individual circle passes between the two sites, it was noted that a well-defined sine curve did not appear as frequently in Arizona as in Illinois, but, where it did appear, the phase and amplitude of the curve was comparable to that of the Illinois curves at corresponding wind speeds.

Throughout all of the analyses there was no significant difference between the 14.5° and 30° source elevations for the same source-to-microphone distance of 2400 ft. Although fewer cases were available for comparison at larger distances, there was no apparent change with distance.

For all of the Illinois data from the summer of 1956, octant analyses were carried out for the 150-300 cps band in addition to the 1200-2400 cps band. A rough sinusoidal pattern was apparent, but with amplitudes much smaller than for the higher frequency, and with the maximum level occurring 90° in the counter-clockwise direction beyond the upwind source position. The difference between maximum and minimum levels was on the average less than 2 db for all passes and wind velocities, with the exception of Pass 8 (14.5° at 2400 ft.) with 20 to 25 mph winds, where the average difference was 3.5 db.

The question remained as to whether the variation in sound level with wind-sound angle was an atmospheric effect or whether the airplane in traversing the circle pass varied its sound output with respect to the microphone with changing attitude to a considerably greater extent than was apparent from earlier check tests. This was investigated by selecting a number of 15° dive passes from the Illinois program for which the wind direction was within $\pm$ 45° of the east-west line of the dive, and comparing directly the upwind and downwind sound levels. The average difference in airplane attitude to the microphone between upwind and downwind source directions would be considerably less for a given scalar wind velocity for the selected dive passes than for the corresponding circle passes, and the difference in sound output with respect to the microphone would be correspondingly less. The results of this comparison, averaged for eight flights with 10 to 15 mph winds and for four flights with 20 to 25 mph winds,

are shown in Fig. 48. It is seen that the sound levels propagated upwind differ by only 1 to 3 db from the downwind levels and are consistently lower than the downwind values instead of higher as in the case of the circle passes of the same source elevation, and that the difference is independent of wind velocity. This would appear to rule out any differences in propagation due to wind direction as the cause of the observed sound level maxima and minima in the circle passes, leaving as the most probable explanation changes in the directivity of the source due to changing attitude around the pass. The fact that the variations increase with frequency and with wind velocity supports this explanation.

SECTION V

PREDICTION OF ATTENUATION

In the preceding discussion in which attenuation was defined, it was pointed out that the rate of attenuation, α_o (in excess of square law and humidity attenuation), is not necessarily constant over the entire distance between the source and the observation point. In order to make accurate predictions of total atmospheric attenuation as a function of weather variables, it is desirable to know the shape of the attenuation-distance curve between the source and a point close enough to the observation point that the effects of atmospheric attenuation may be considered negligible. For the circle and overhead passes, the minimum distance varied from 600 ft. for 90° source elevation to 2400 ft. for 14.5° elevation. The minimum distance for the dive passes was 300 ft. throughout. It is possible to refer all of the data, at least approximately, to a common reference distance of 300 ft. by combining the 14.5° circle pass data with the 15° dive pass data. This is done in Fig. 49. The dotted lines and numbered points represent the residual attenuation, A_o, for the dive passes averaged for upwind and downwind and for the 5°, 10°, and 15° source elevations. The average attenuation for the three angles was found to be usually within 1 db of the 15° data alone. The solid lines are drawn with the slopes shown in Fig. 13 for the average of all of the circle and overhead pass data from 14.5° to 90°. Within the accuracy of determination, the 14.5° data has a slope which is not essentially different from the average slope for all elevation angles from 14.5° to 90°. These lines start at a distance of 2400 ft., which is the minimum for the 14.5° circle passes, and are adjusted vertically to fit the 15° dive pass data. The two sets of data overlap very satisfactorily and form a continuous attenuation curve from 300 to 5000 ft. for this particular source elevation. It is seen that the rate of attenuation has an initially high value near the ground and decreases to a constant rate at a distance of about 2400 ft. The vertical positions of the linear attenuation curves for the 30° and 90° source elevations cannot be established directly on these plots from the existing data, since there are no data for the common 300 ft. distance for these elevations. However, if it is assumed that the variation in attenuation rate near the ground for a given frequency, as observed for the 15° data, is a function of altitude alone, and not of the vertical angle of sound propagation, then the

vertical positions of the 30° and 90° curves may be located fairly accurately. This has been done in Fig. 50 in which the linear portions of all of the attenuation curves are considered as beginning at an altitude of 600 ft., which is the altitude corresponding to the minimum distance in both the 30° and 90° passes. It is seen that the possible error in locating the curves by the above assumption is usually less than 1 or 2 db. For the 75-150 band, the linear portions are shown with slopes extrapolated from the data for the 150 to 2400 cps frequency range, as given by the curve of Fig. 14.

The complete curve of average residual attenuation, $\bar{A}_o$, against distance from source to ground, for source elevations from 15° to 90°, may therefore be represented approximately by two sections, as shown in Fig. 51. The linear portion begins at a distance, d', from the source corresponding to an altitude of roughly 600 ft. and has a slope which is proportional to the 1/3 power of the frequency. The initial curved portion rises steeply to a value, $\bar{A}_o'$, at which the linear portion begins. For the 15° source elevation data, the value of $\bar{A}_o'$ varies approximately linearly with frequency for the range of 300 to 2400 cps. For the 75-150 band, $\bar{A}_o'$ is considerably higher. Approximate values of $\bar{A}_o'$ and d', as read from the curves of Fig. 50, are given in Table VIII.

Table VIII

Source Elevation Angle, Degrees	d' ft.	$\bar{A}_o'$, db, in octave frequency band 75 / 150	150 / 300	300 / 600	600 / 1200	1200 / 2400
15	2400	9	4	5	9	14
20	1800	7	3	4	7	10
30	1200	4	2	2	4	6
90	600	1	1	1	1	2

The average residual attenuation, $\bar{A}_o$, at any distance, d, from source to ground observation point which is greater than d' is then given by:

$$\bar{A}_o = \bar{A}_o' + \bar{a}_o (d - d')$$

Values of average attenuation rate, $\bar{a}_o$, read from the straight line of Fig. 14 and Eq. (12) are given in Table IX.

Table IX

Octave Frequency Band cps	$\bar{a}_o$ db/1000 ft.
75- 150	0.5
150- 300	0.65
300- 600	0.8
600-1200	1.05
1200-2400	1.3
2400-4800	1.65

The average values, $\bar{A}_o$, $\bar{A}_o'$, and $\bar{a}_o$, are based on the average of the particular range of weather conditions observed in this study. In making a prediction of attenuation from a given set of weather measurements, the regression coefficients relating deviations in attenuation from the average to deviations in weather variables from the average are utilized. For the linear part of the residual attenuation curve, represented by $\bar{a}_o (d - d')$, the correlation between attenuation and any of the four weather parameters which were measured, namely, wind, wind gradient, temperature, and temperature gradient, was found to be statistically insignificant, as pointed out previously. It is preferable, therefore, to consider these attenuations as having a constant average value given by Eq. (12) or the curve of Fig. 14, but subject to a scatter due to unknown or unmeasured factors. This scatter includes the standard deviations of attenuation at each frequency, distance, and elevation, as given in Table III, and also the errors in curve fitting in Figs. 13 and 14. These various deviations may be represented by an estimated overall standard deviation of residual attenuation in the linear range of $\pm$ 3 db which applies with reasonable accuracy to all distances up to 5000 ft., to all frequencies, and to all source elevations from 15° to 90°.

The value of A_o' for the 15° source elevation similarly shows very little dependence on any of the wind and temperature gradient parameters used in the dive pass analysis. Although the standard deviation of A_o' is 4 to 6 db in the frequency range from 150 to 2400 cps, the combined effects of wind and temperature gradient account for no more than about 1.5 db of this deviation. For these frequencies, therefore, the average values of A_o' given in Table VIII may be used for prediction purposes, subject to a standard deviation due to unknown causes which may be taken as $\pm$ 5 db for the 15° source elevation. The deviation would probably be less for higher source elevations. In the lowest octave band (75-150 cps) the standard deviation of A_o' for downwind propagation is 10 db, of which 3 or 4 db can be attributed to the combined effects of temperature gradient and wind velocity.

The above procedure for predicting attenuation may be extended to include source elevations down to 5°, using the same values of $\bar{A}_o'$ and d' (2400 ft) as given for 15° in Table VIII. As shown by Figs. 16 and 49, a single curve of $\bar{A}_o$ against distance, averaged for all angles from 5° to 15° and for upwind and downwind may be used within a maximum error of about 2 db. (An exception is in the 150-300 cps octave band where the upwind propagation curve for 10° lies about 5 db below the average.) The procedure

is valid up to a source distance of 5000 ft. for frequencies of 300 to 1200 cps. For higher and lower frequencies, the available data is limited to distances of about 3000 ft.

For elevations of less than 5°, the values of A_o and A_o' are influenced significantly by the measured weather variables. In applying the regression coefficients computed in the statistical analysis to the prediction of the effects of these variables, it is convenient first to convert the tabulated and plotted values to the units of measurement actually used in the weather observations, and also to convert the non-linear functions used in the regression analysis to equivalent linear approximations. This is done as follows:

Weather Parameter	Unit	Linear Approx.	Converted Regression Coefficient	Unit
$P_1 = W \cos \phi$	ft/sec	$W \cos \phi$	$k_1 = 1.5\ b_1$	db/mph
$P_2 = (\Delta T)^{2/3}$	°F 5 - 600 ft	$\Delta T \simeq -2(\Delta T)^{2/3}$	$k_2 = -0.3\ b_2$	db/°F/1000 ft
$P_3 = \log_e W$	ft/sec	$W \simeq 12.4 \log_e W$	$k_3 = 0.12\ b_3$	db/mph

The slope of the linear approximations for P_2 and P_3 are taken for the part of the curve corresponding to a range of plus and minus the standard deviation of the weather parameter. The temperature gradient, ΔT, is converted to units of °F per 1000 ft., but refers specifically to measurements taken at heights of 5 ft. and approximately 500 to 600 ft. The lower height is more critical because of the comparatively rapid change of gradient with height near the ground. The wind velocities are converted to miles per hour.

The regression equation for predicting residual attenuation, A_o, for source elevations of 2° to 15° is written:

$$A_o = \bar{A}_o + k_1 (W \cos \phi - \overline{W \cos \phi}) \text{ mph}$$

$$+ k_2 (\Delta T - \overline{\Delta T}) \text{ °F/1000 ft}$$

$$+ k_3 (W - \bar{W}) \text{ mph}$$

Inserting the average values for $W \cos \phi$, ΔT, and W obtained in the study, and the conversion factors for the regression coefficients, the above equation becomes:

$$A_o = \bar{A}_o + 1.5\, b_1 (W \cos \phi - 5.3) \text{ mph}$$

$$- 0.3\, b_2 (\Delta T + 4.5) \text{ °F/1000 ft}$$

$$+ 0.12\, b_3 (W - 9.5) \text{ mph}$$

Values of $\bar{A}_o$ as a function of frequency, distance, wind direction, and source elevation are obtained from Table V or from Fig. 16. The regression coefficient values, b_1, b_2, and b_3, are obtained from Table VI. It is to be noted that since these are simple rather than multiple regression coefficients, only one of the two wind terms should be used in the equation for a given computation. The reason for this is that since the wind component and the scalar velocity are closely interrelated, their separate effects on attenuation cannot be considered additive in a simple regression equation. However, since the temperature gradient is largely independent of wind velocity, the temperature term should be used in combination with one of the wind terms. The choice of wind terms to be used depends on which has the largest effect on attenuation. This is determined from the plotted values of normalized regression coefficients, $b\sigma_p$, given in Figs. 25 to 34 and Figs. 37 to 44. As noted previously, the temperature gradient, ΔT, is taken as positive for a temperature at ground higher than at the measuring altitude.

Attenuations predicted by the above regression equation have been compared with a number of individual observations for 2° upwind dive passes in the 300-600 cps band. These have been selected to cover a wide range of wind velocities and temperature gradients. There is fair agreement for values of A_o ranging from 0 to 8 db and, within this range, the regression equation is probably accurate to $\pm$ 3 db. However, for higher values, the observed attenuations are generally considerably smaller than the predicted values. This may result from the fact mentioned previously that, as either the wind gradient or the temperature gradient changes so that the shadow boundary crosses the microphone position, the attenuation rises more or less suddenly and cannot be properly represented as a linear function of either gradient.

The total atmospheric attenuation, A_a, is by definition the sum of the residual attenuation, A_o, and the humidity attenuation, A_H, due to molecular absorption. From Eq. (13):

$$A_H \simeq 0.1\, (f/h)^2\, (T + 45)\, (d_2 - d_1) \text{ db}$$

where

f = geometric mean frequency of octave band, kilocycles
h = absolute humidity, gm/m^3
T = temperature, °F
d_1, d_2 = distances, 1000 ft.

The total attenuation, A, including spherical divergence, is then given by:

$$A = A_o + A_H + 20 \log_{10} (d_2/d_1)$$

As discussed previously, the above expression for A_H is an approximation which holds for values of absolute humidity, h, which are more than twice the value of humidity, h_m, for which maximum molecular absorption occurs at a given frequency. For values of h less than one-half h_m, the same approximation is used except that h^2 is in the numerator. For values of h within the range, $h_m/2$ to $2h_m$, the exact formula for molecular absorption should be used. Using the experimentally determined constant based on the regression coefficients obtained in this study, as in Eq. (13), the exact formula is:

$$A_H = \frac{0.1\, f\, (T + 45)\, (d_2 - d_1)}{(h/h_m)^2 + (h_m/h)^2} \quad db \qquad (14)$$

Values of h_m, taken from Reference 1, p. 14, and of peak values of absorption, α_m, computed from Eq. (14) for values of $h=h_m$, are given for various frequencies and temperatures in Table X (Appendix A).

SECTION VI

SUMMARY AND CONCLUSIONS

The experimental program described in Part I, in which the effects of weather variables on the atmospheric propagation of sound from an elevated source to ground were statistically evaluated, has been extended to include source elevation angles below 15°, and to include a second test site, where the climate and ground cover differed appreciably from that at the first site. Some of the observations made at the first site were repeated for a check on the previous data. Reliable data from the two programs have been obtained up to an altitude of 4800 ft. and to a horizontal distance of approximately one mile, for source elevation angles of 2° to 90°. The weather variables chosen for the study have been based on data which would be obtained routinely at a typical air base. The range of weather and climatic conditions

for which measurements of propagation were obtained is believed to be wide enough to be representative of the United States as a whole.

The conclusions drawn from the combined results of the work reported in Parts I and II are as follows:

1. Those weather variables which have been found to have a statistically significant effect on sound propagation are:

Absolute humidity
Temperature
Temperature gradient
Wind velocity
Wind velocity gradient
Wind direction relative to direction of sound propagation.

2. The effects of absolute humidity and temperature may be combined into a single function which accounts for molecular absorption. For the range of absolute humidities usually encountered, the attenuation coefficient due to molecular absorption is given approximately by:

$$a_H = 0.1\,(T + 45)\,f^2/h^2 \quad \text{db/1000 ft}$$

where

T = temperature, °F
f = geometric mean of an octave frequency band, kilocycles
h = absolute humidity, gm/m^3.

For the average values of absolute humidity and temperature of 8 gm/m^3 and 60°F, respectively, obtained in the two programs, the attenuation coefficient given by this formula is approximately 2 db/1000 ft. for the 2400-4800 cps octave band.

3. Residual attenuation, obtained by deducting the attenuation due to spherical spreading and molecular absorption from the total attenuation, is essentially linear with distance above an altitude of about 500 ft. for all frequencies, for all source elevations from 5° to 90°, and for all distances from source to ground up to 5000 ft. The average residual attenuation coefficient within this region is given by:

$$\bar{a}_o = 0.11\,f^{1/3} \quad \text{db/1000 ft.}$$

where f is the geometric mean frequency of an octave band in cps. This is equivalent to approximately 1 db/1000 ft. in the 600-1200 cps band. The residual attenuation may vary by ± 3 db from the value given by the above equation, but this variation shows no significant correlation with any of the measured weather parameters, or with the change of test site.

4. The attenuation is independent of wind direction with respect to the direction of sound propagation for source elevations of 5° and higher. Results reported in Part I showed higher attenuation of sound propagated with the wind than against the wind when the airplane noise source traversed a circular path about the ground observation point. However, this effect did not appear when the same source was moving directly toward the observation point, alternately with and against the wind. Therefore, the effect previously observed has been attributed to directional characteristics of the source rather than to atmospheric causes.

5. The rate of attenuation between ground and an altitude of a few hundred feet is in general considerably greater than at higher altitudes, particularly for low angles of source elevation. The average residual attenuation for source elevations of 5° to 15° at a source distance of 2500 ft. (referred to a 300 ft. distance) ranges from 4 db for the 150-300 cps band to 14 db for the 1200-2400 cps band. The attenuation in this region has a variation of $\pm$ 5 db, but shows little or no correlation with any of the measured weather parameters.

6. For a source elevation of 2° it is possible for sound shadows to form in the presence of strong wind and temperature gradients which cause upward refraction. When the observation point is in a shadow zone, high attenuations are observed which are found to agree reasonably well with theoretical predictions. The statistical evaluation of the observed data shows on the average larger attenuations for sound propagation against the wind than with the wind at 2° source elevation and larger attenuations in either direction than for any higher source elevation. There is also a high degree of statistical correlation of attenuation with the weather parameters which determine the position of the shadow boundary, namely, temperature gradient and wind velocity component opposite to the direction of sound propagation. However, since the variation in attenuation with respect to the position of the shadow boundary is highly non-linear, the correlations do not lend themselves to accurate prediction of attenuation in individual cases.

SECTION VII

BIBLIOGRAPHY

1. Nyborg, W. L., and D. L. Mintzer, Review of Sound Propagation in the Lower Atmosphere, WADC Technical Report 54-602, Wright Air Development Center, Wright-Patterson Air Force Base, Ohio, May 1955.

2. Pridmore-Brown, D. C., and U. Ingard, Tentative Method for Calculation of the Sound Field about a Source over Ground Considering Diffraction and Scattering into Shadow Zones, NACA Technical Note 3779, 1520 H Street, N. W., Washington 25, D. C., September 1956.

3. Hoel, P. G., Introduction to Mathematical Statistics, John Wiley and Sons, Inc., New York, N. Y., 1954.

4. Bolt, Beranek, and Newman, Inc., Capabilities and Limitations Investigation of Long-Range Public Address Equipment, Final Report, Phase 4, Field Testing, Report No. 466, U. S. Army Signal Corps, 50 Moulton Street, Cambridge, Massachusetts, 1 June 1957.

FIG. 1 - GROUND VIEW OF ILLINOIS SITE

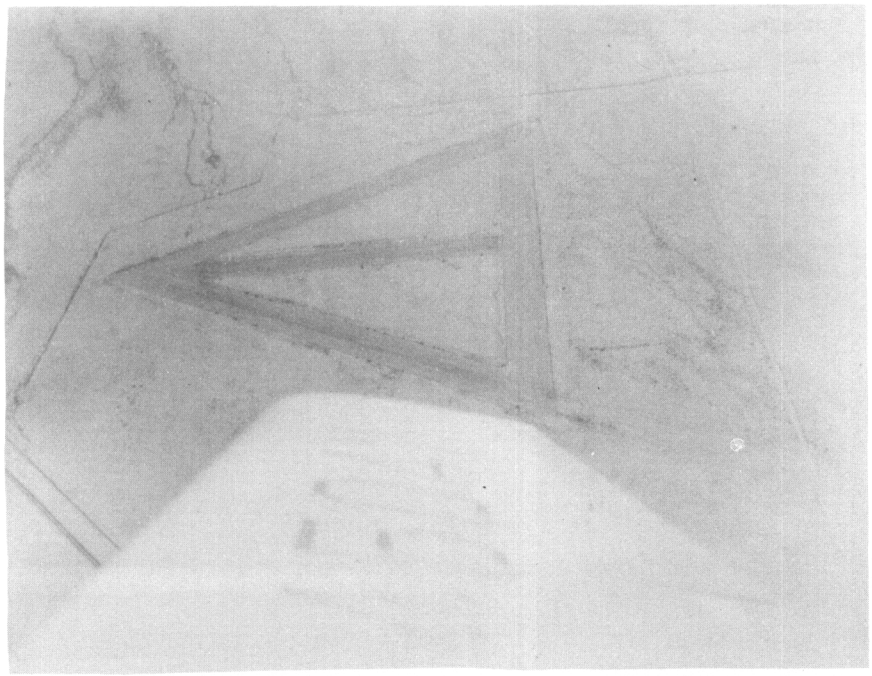

FIG. 2 - AERIAL VIEW OF ARIZONA SITE

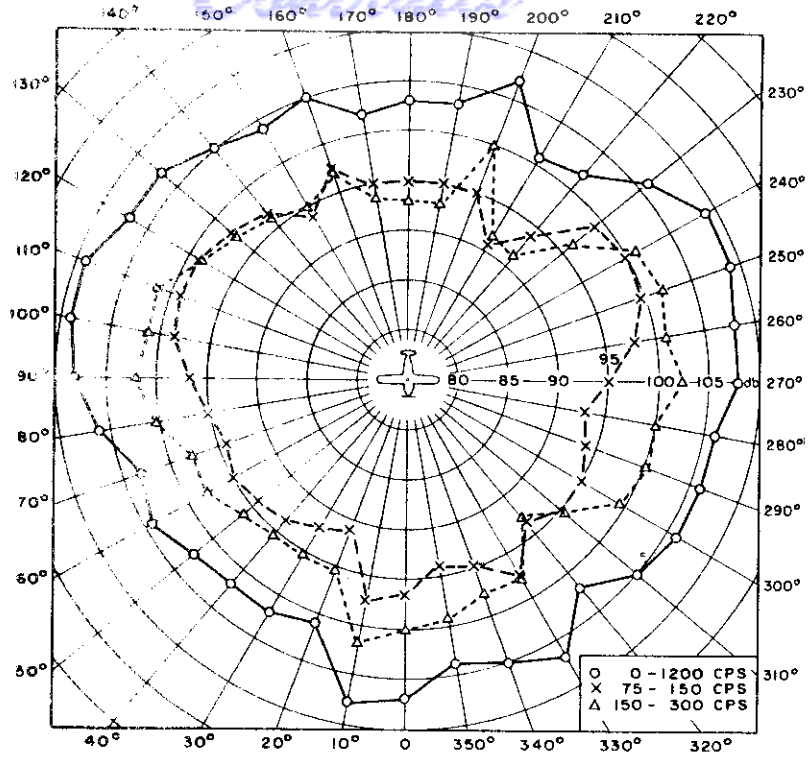

A

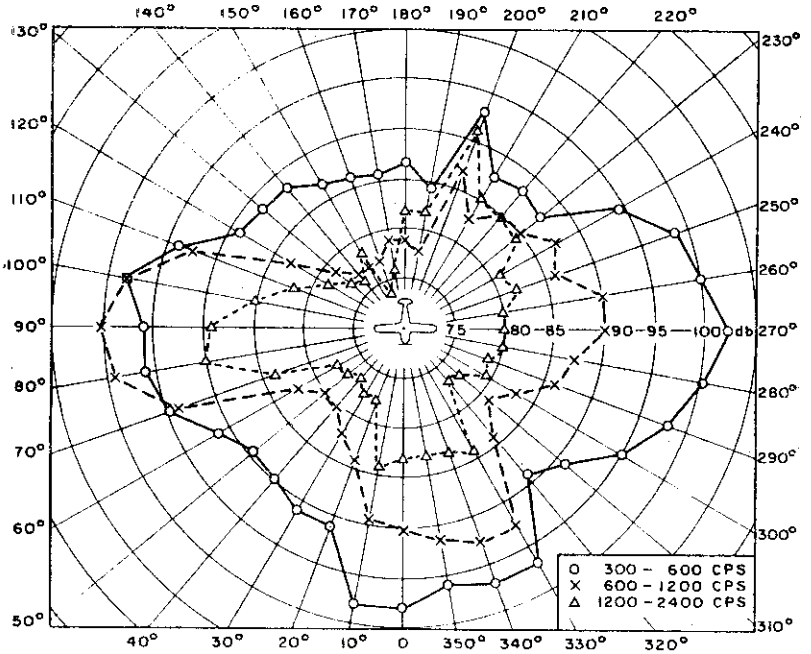

B

FIG. 3 - DIRECTIONAL SOUND LEVEL PATTERN OF AIRPLANE ON GROUND AT 50 FT. RADIUS WITH SPEED OF 2000 RPM AND 230 HP

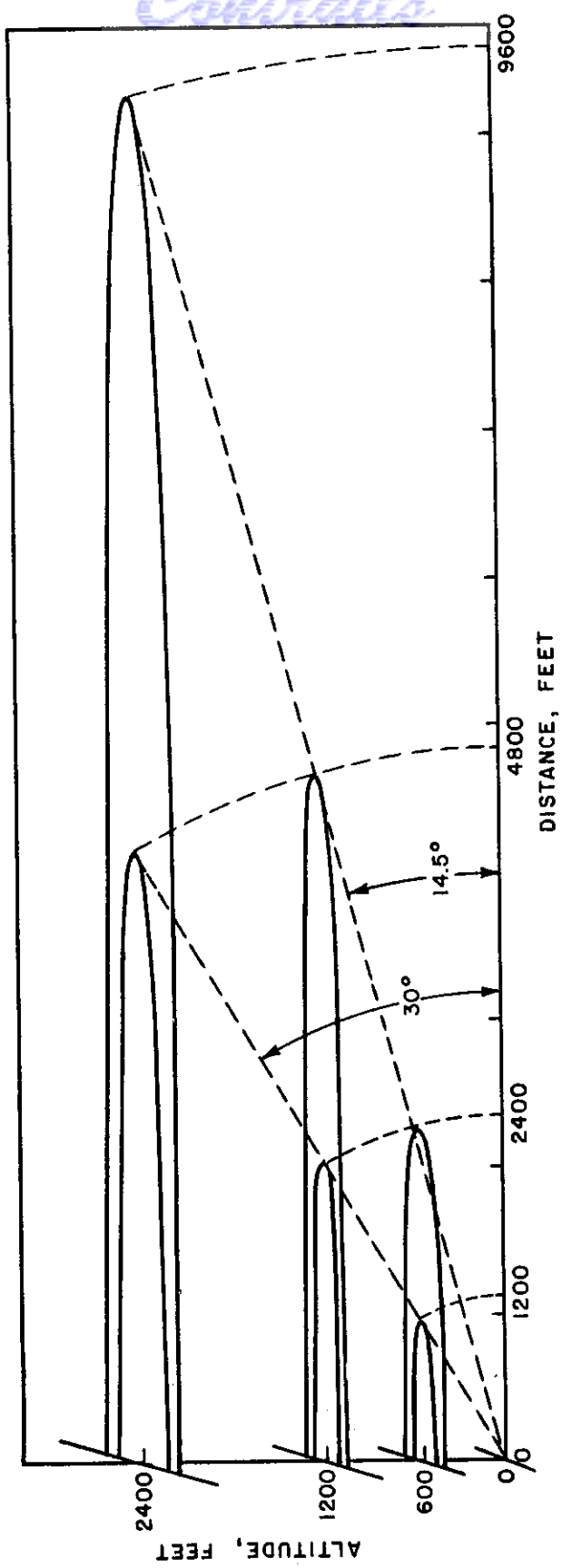

FIG. 4 - THREE-DIMENSIONAL DRAWING OF CIRCULAR AND OVERHEAD FLIGHT PROGRAM

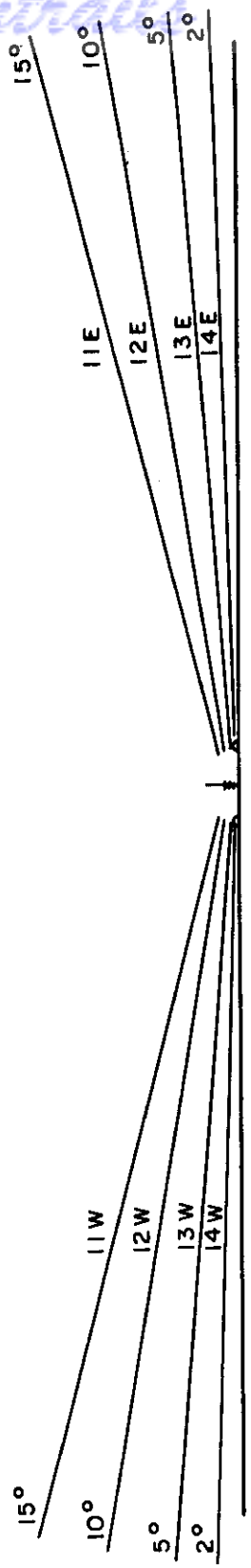

FIG. 5 - DIVE PASSES

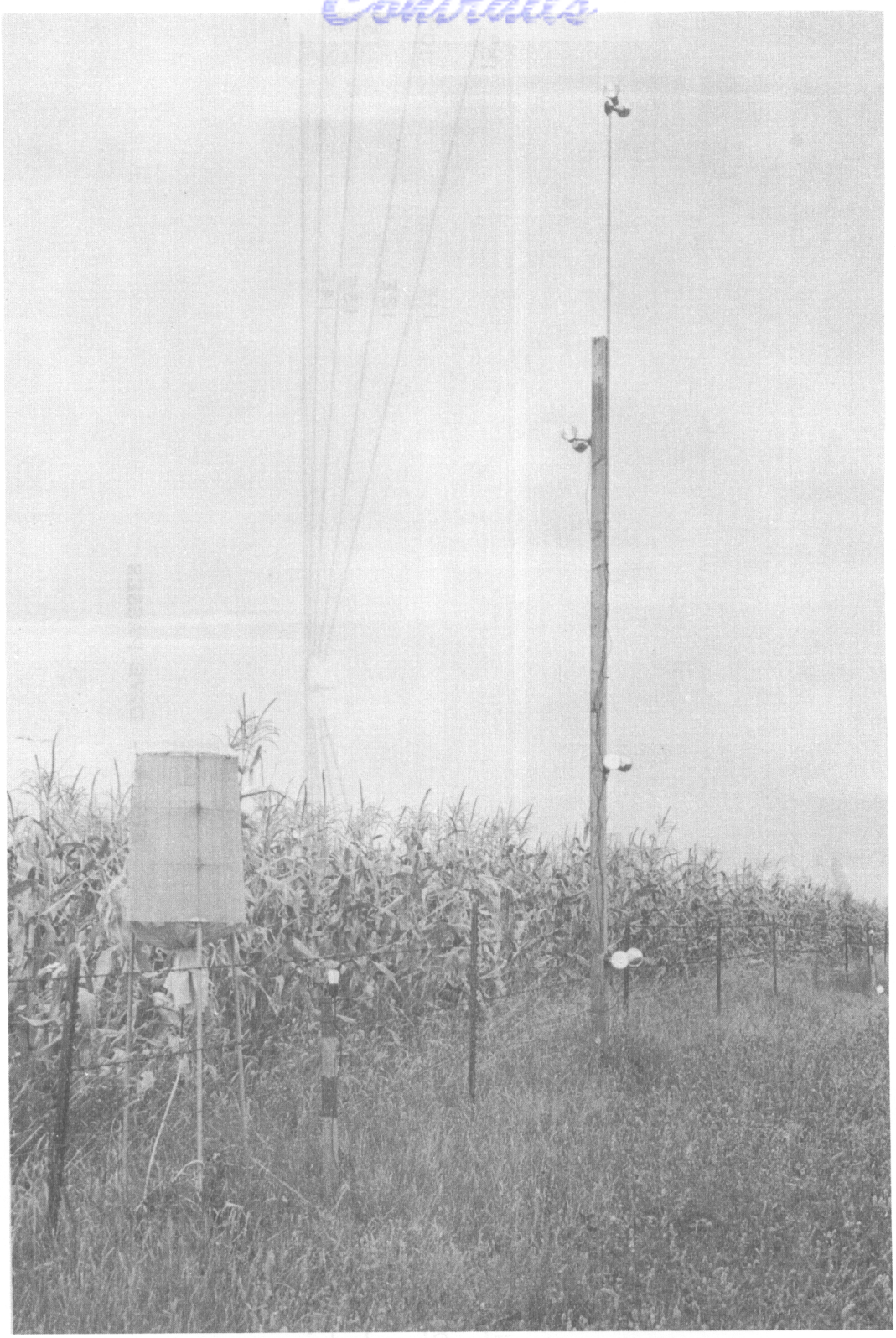

FIG. 6 - DIVE PASS GUIDE LIGHTS AND MICROPHONE

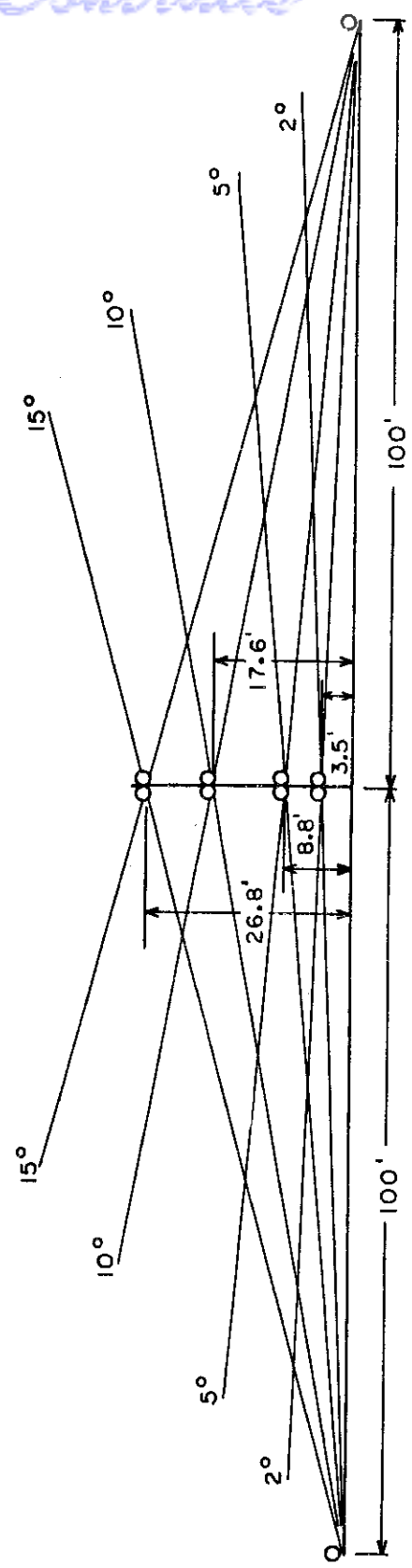

FIG. 7 - POSITION OF THE TEN LIGHTS USED TO GUIDE THE PLANE ON A PATH OF CONSTANT ELEVATION AND AZIMUTH

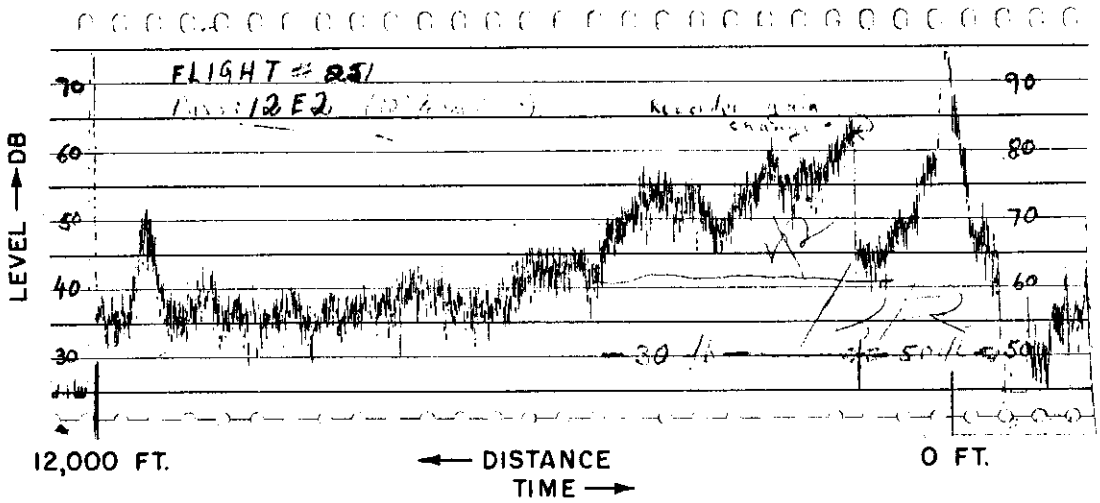

FIG. 8 - DIVE PASS RECORD

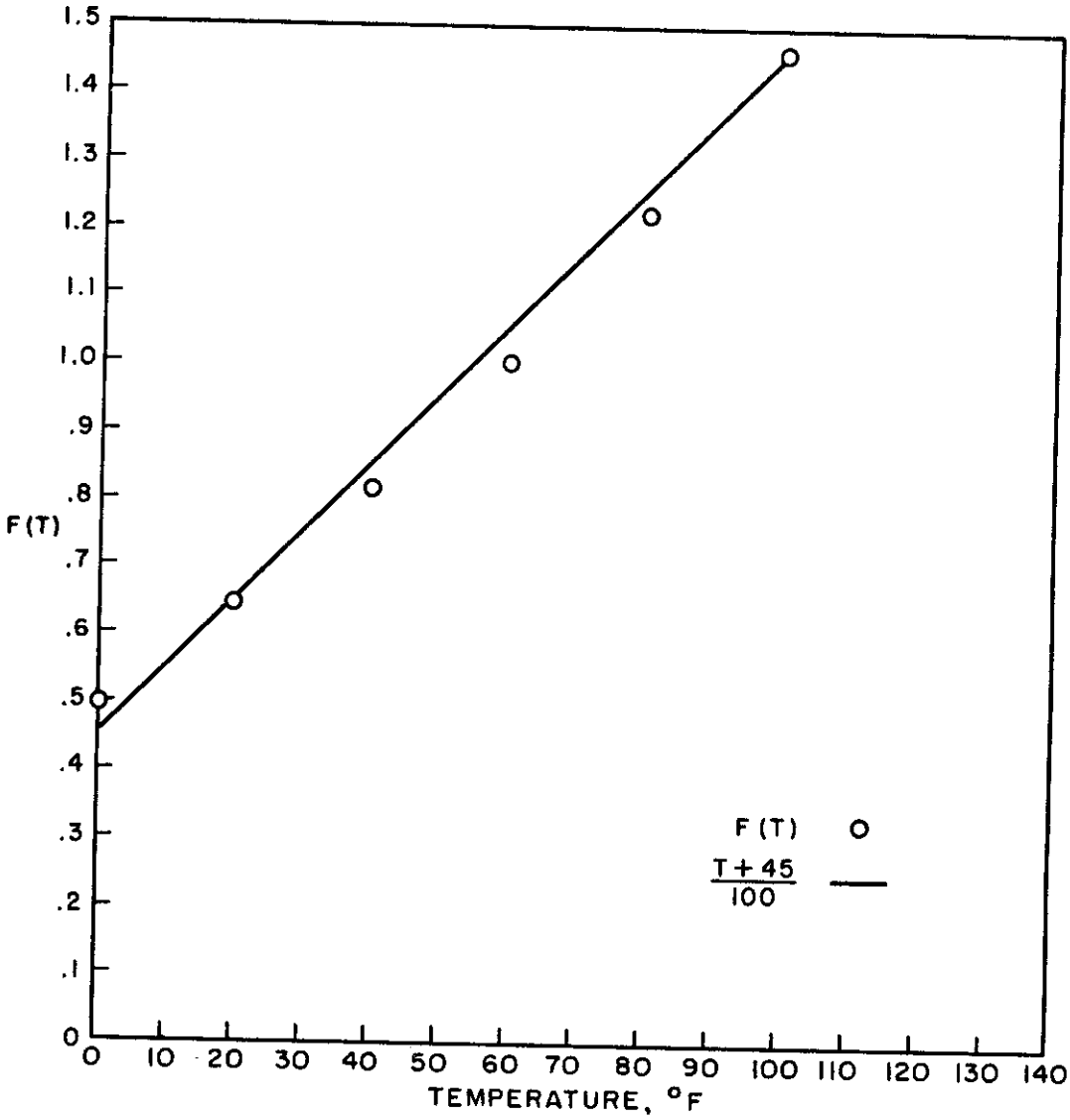

FIG. 9 - THE FORM OF THE FUNCTION F(T) COMPARED WITH THE APPROXIMATION (T + 45) / 100

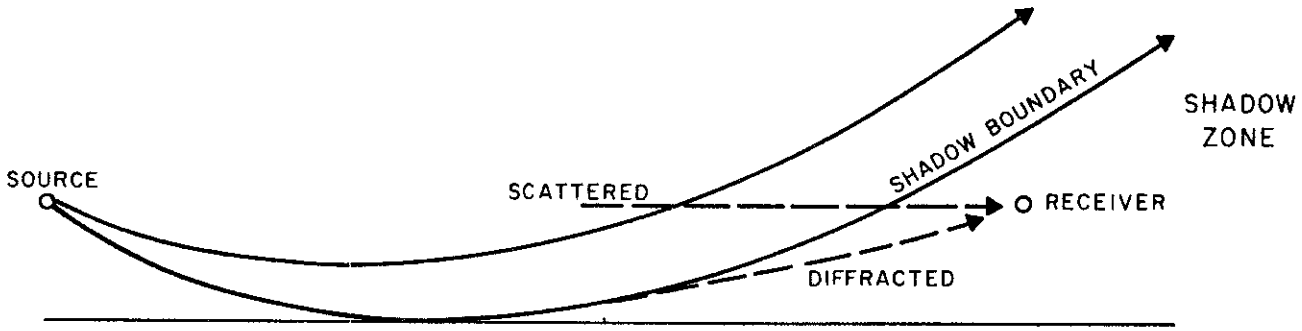

FIG. 10 - DIFFRACTION AND SCATTERING OF SOUND INTO SHADOW ZONE

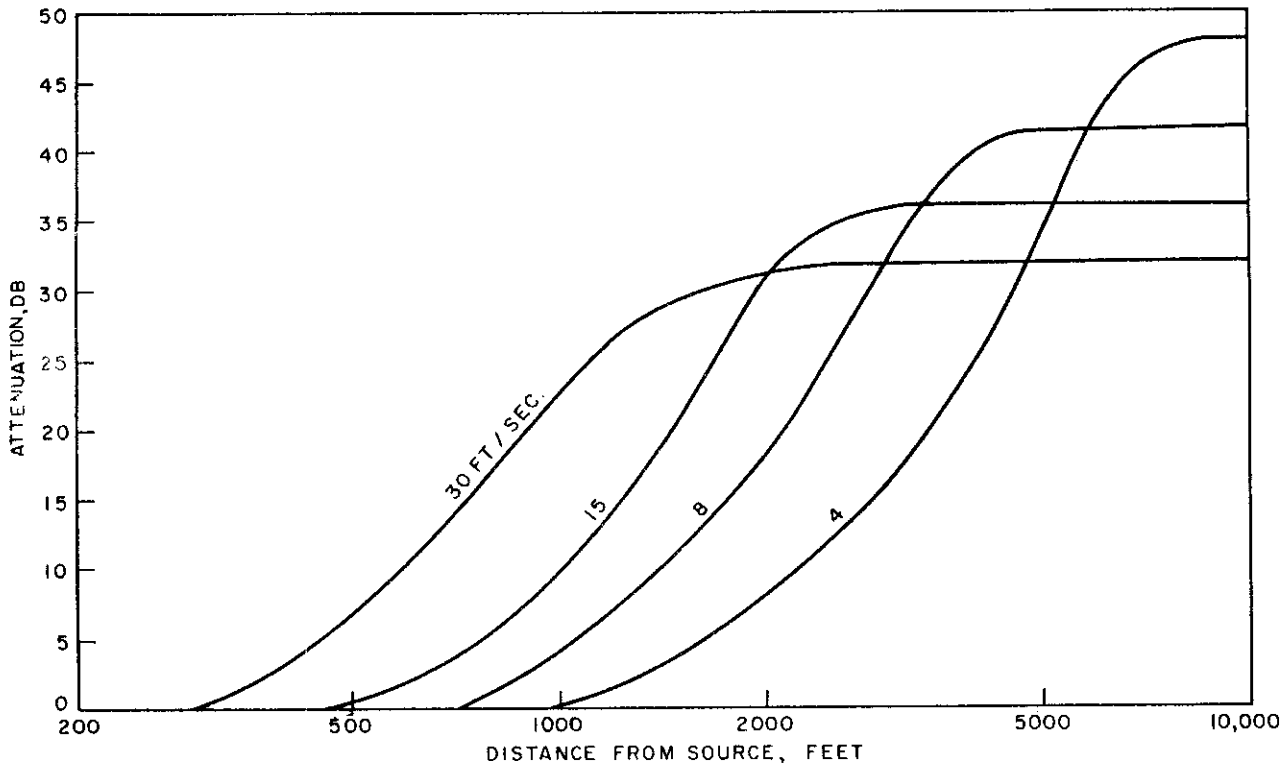

FIG. 11 - THEORETICAL ATTENUATION OF SOUND IN SHADOW ZONE AS A FUNCTION OF WIND VELOCITY AND DISTANCE FROM SOURCE. SOURCE HEIGHT, 100 FT. RECEIVER HEIGHT, 10 FT. FREQUENCY, 250 CPS. (AFTER PRIDMORE-BROWN AND INGARD)

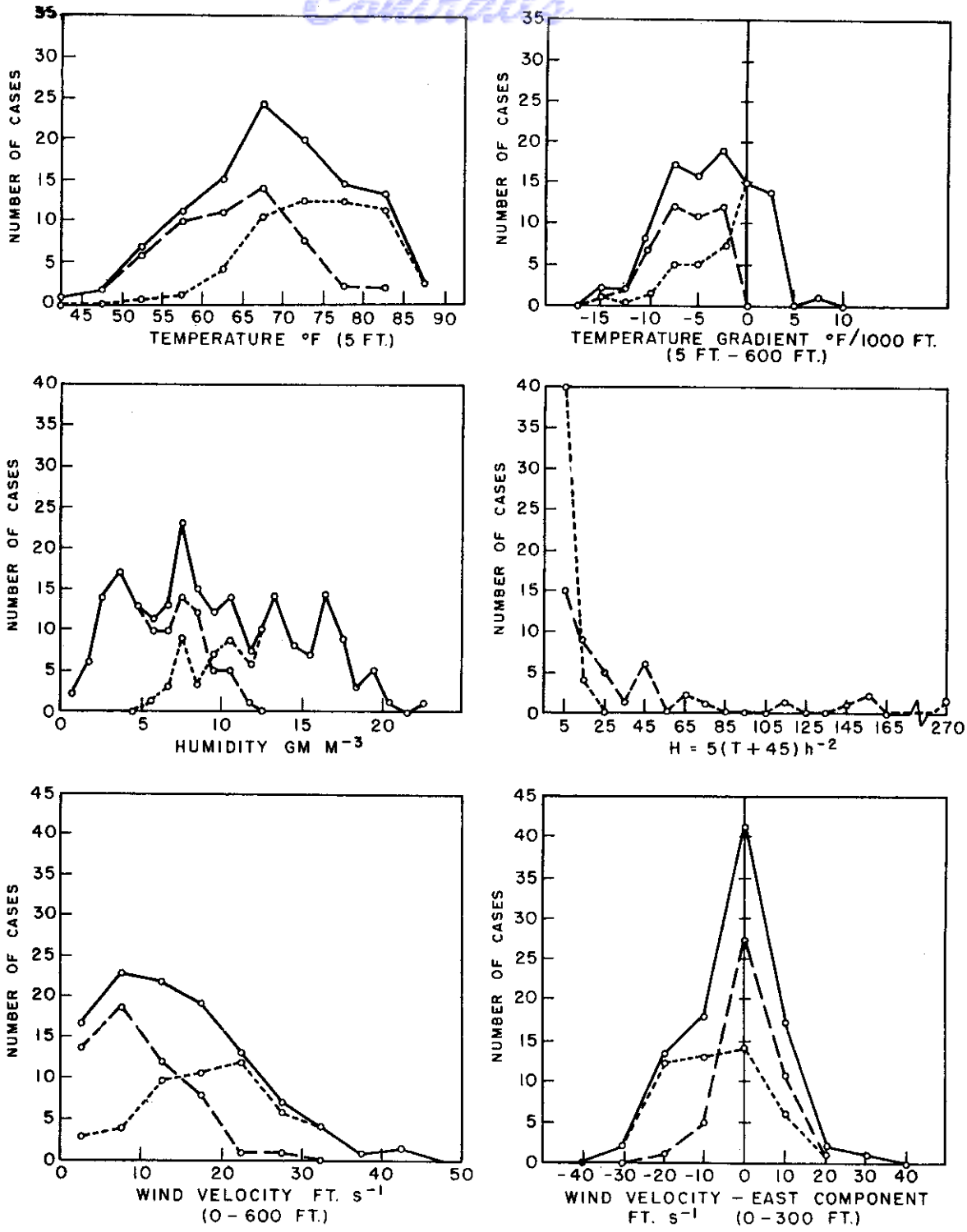

FIG. 12 - DISTRIBUTION OF WEATHER PARAMETERS

---- ILLINOIS

– – – ARIZONA

——— TOTAL

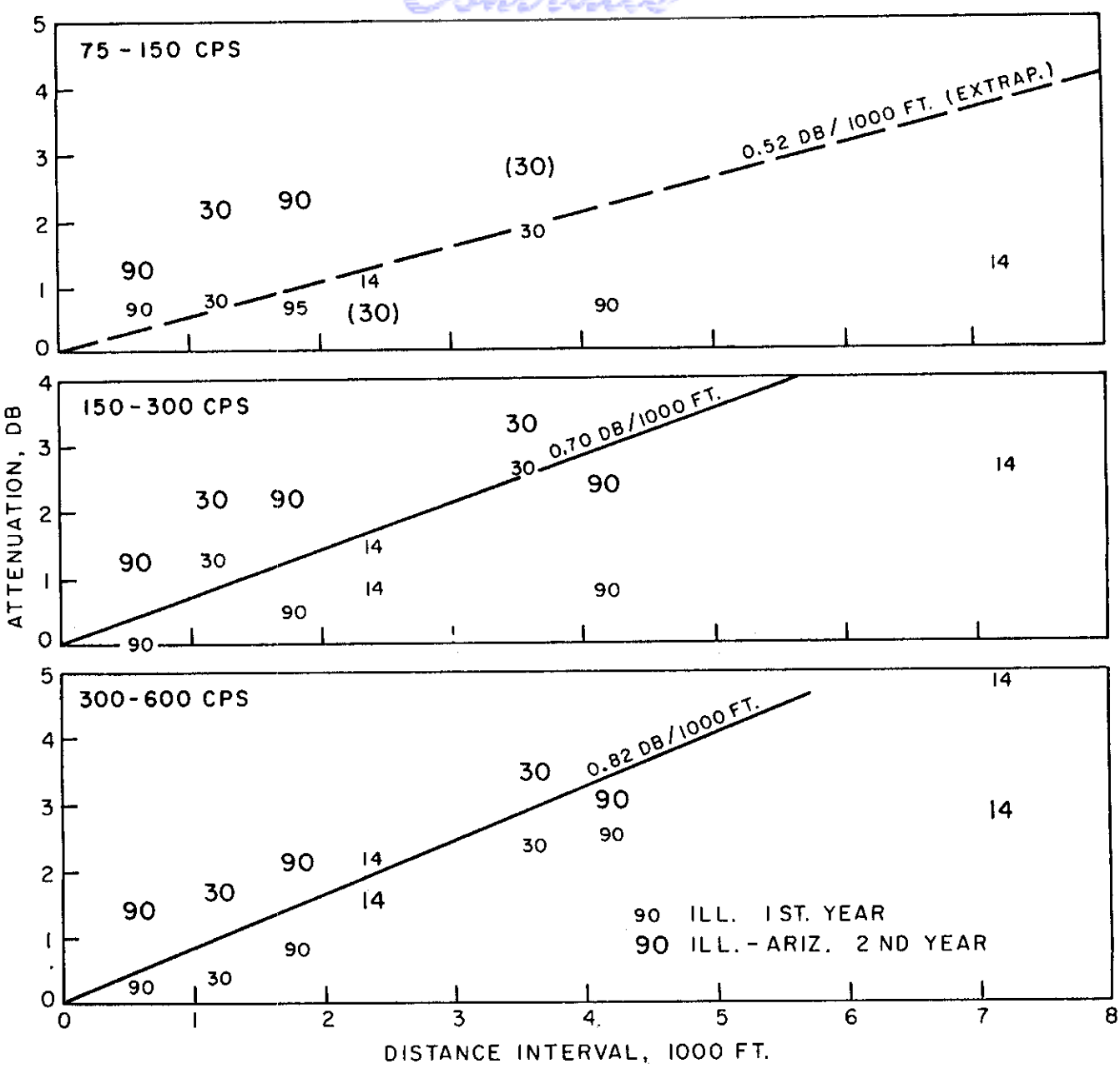

FIG. 13-A - AVERAGE RESIDUAL ATTENUATION A_o AS A FUNCTION OF DISTANCE INTERVAL FOR SOURCE ELEVATIONS OF 14.5°, 30°, AND 90°. CIRCLE PASS DATA FOR TWO YEARS. 75-600 CPS

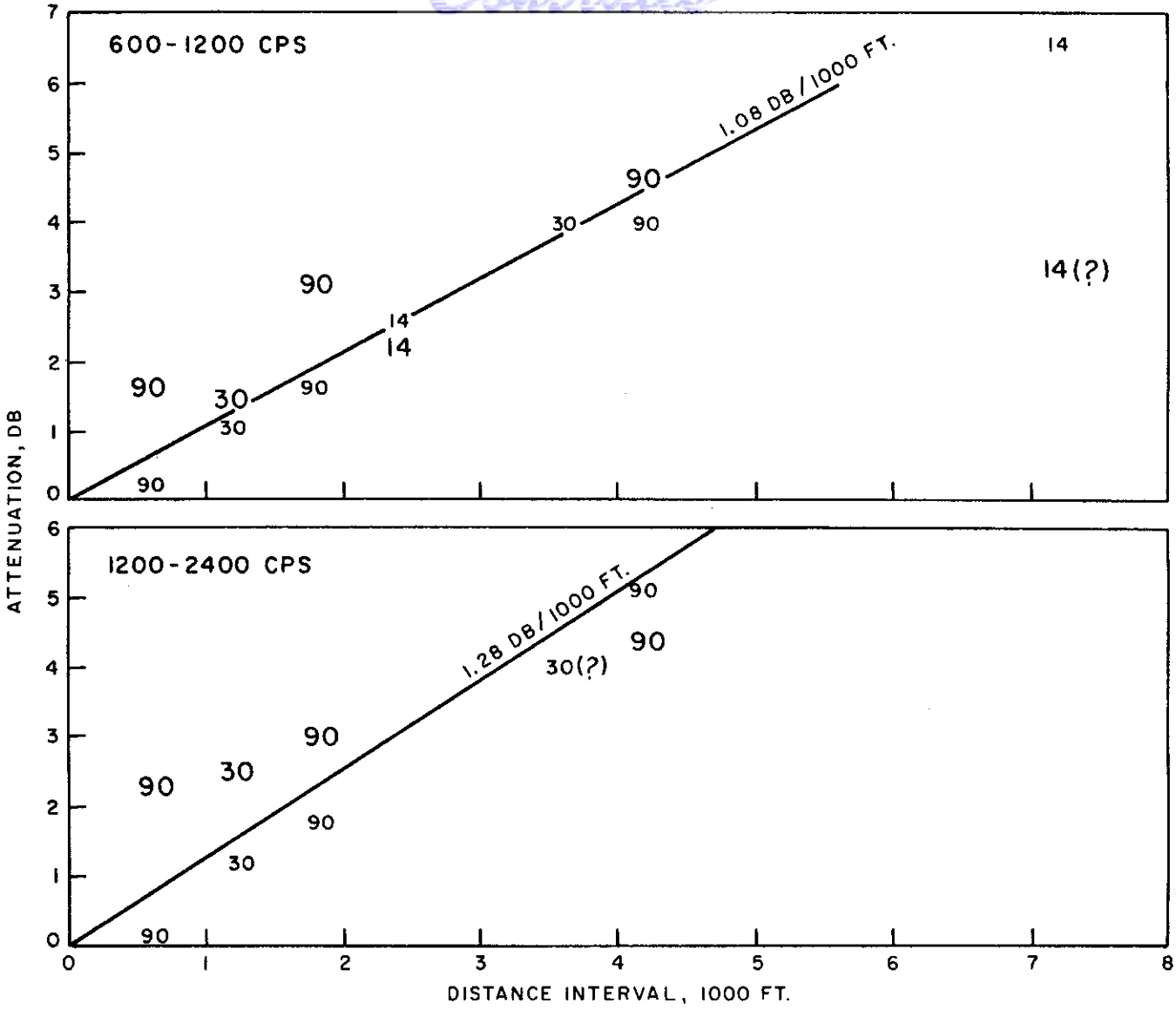

FIG. 13-B - 600-2400 CPS

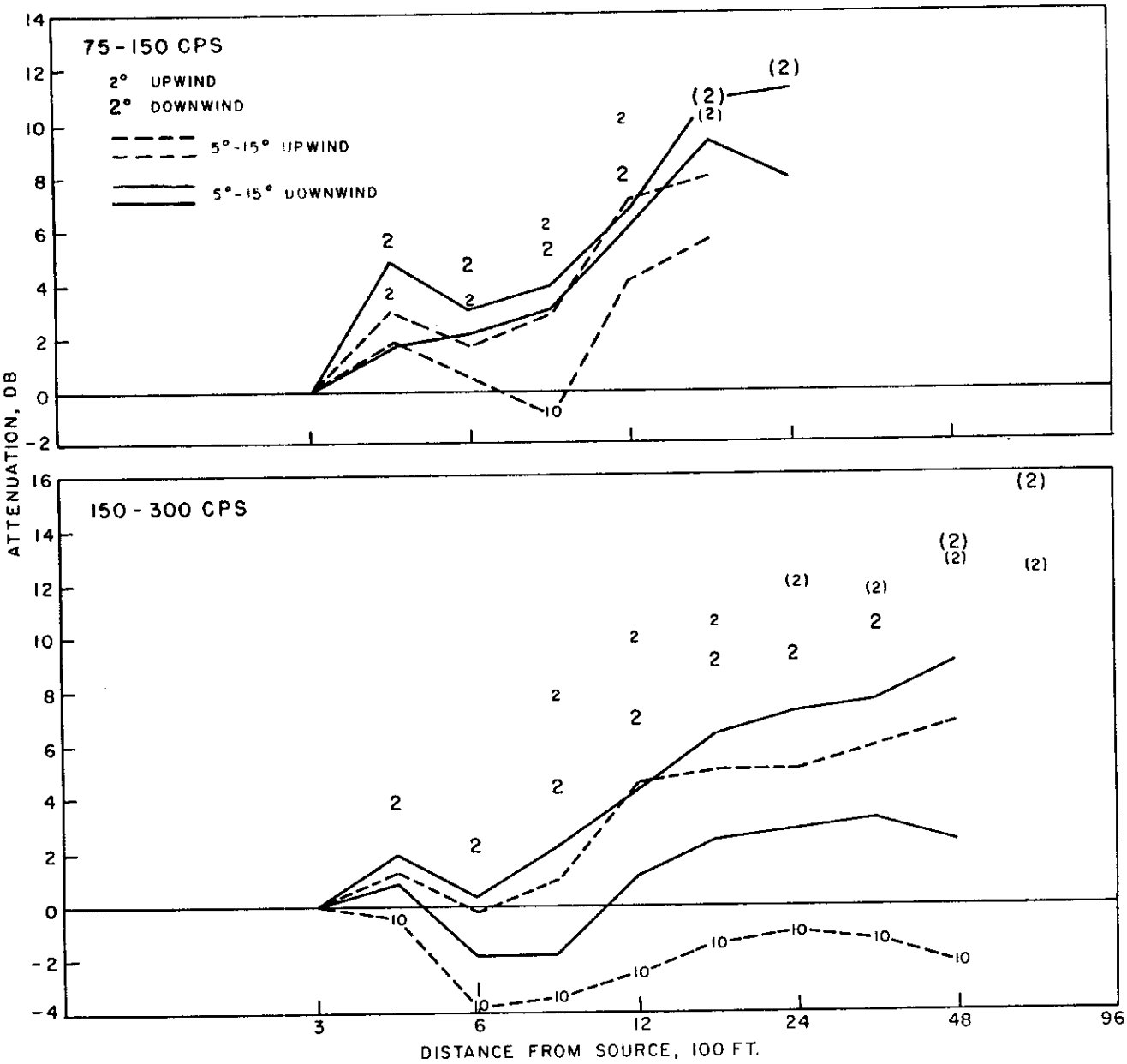

FIG. 16-A - AVERAGE RESIDUAL ATTENUATION, $\bar{A}_o$, FOR DIVE PASSES AS A FUNCTION OF DISTANCE FROM SOURCE, SOURCE ELEVATION, AND WIND DIRECTION. LINES INDICATE ENVELOPE OF AVERAGE VALUES FOR INDICATED RANGE OF SOURCE ELEVATIONS. ( ) INDICATES VALUES BASED ON LESS THAN 80 PER CENT OF TOTAL NUMBER OF CASES. 75-300 CPS.

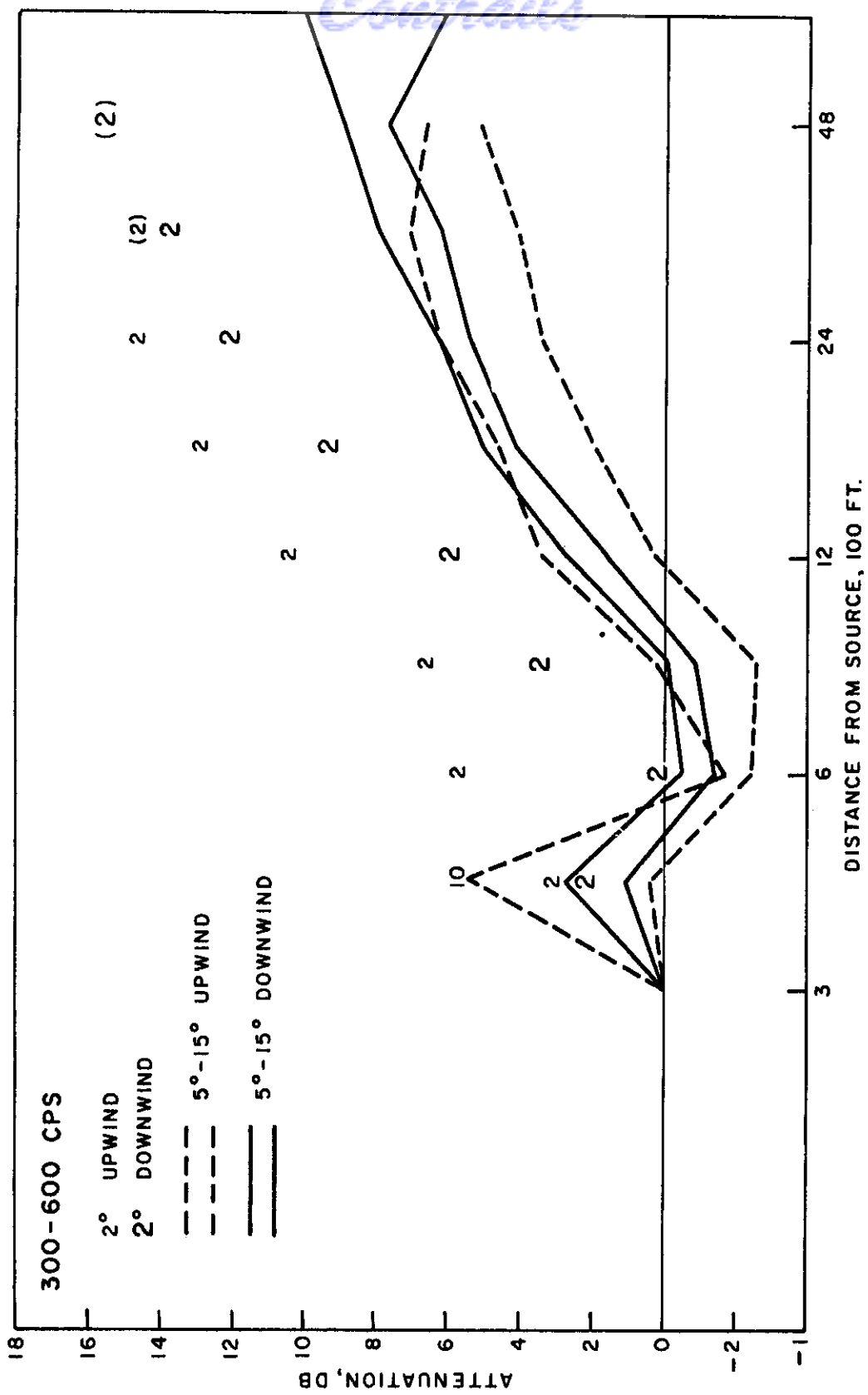

FIG. 16-B - 300-600 CPS

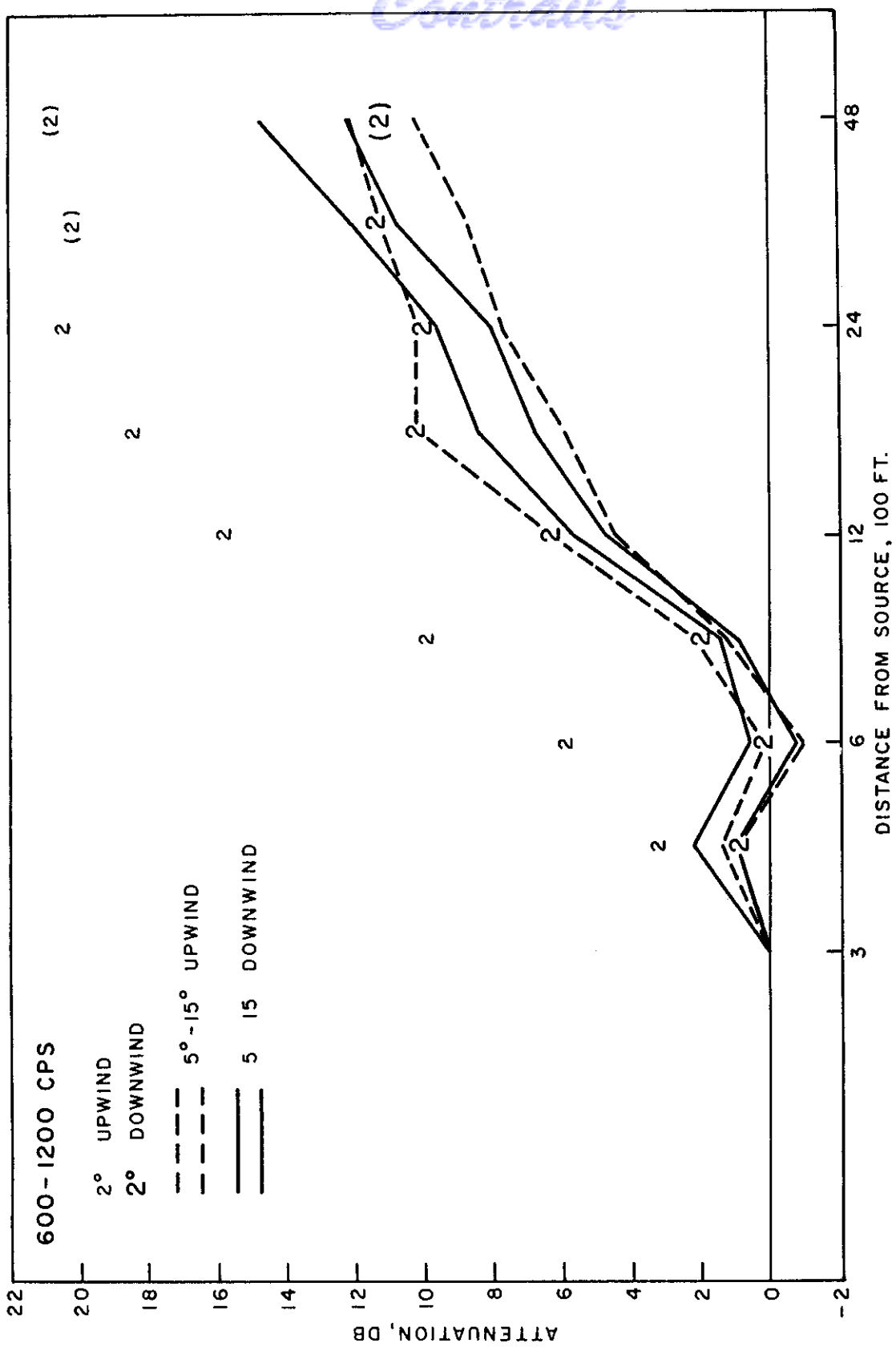

FIG. 16-C - 600-1200 CPS

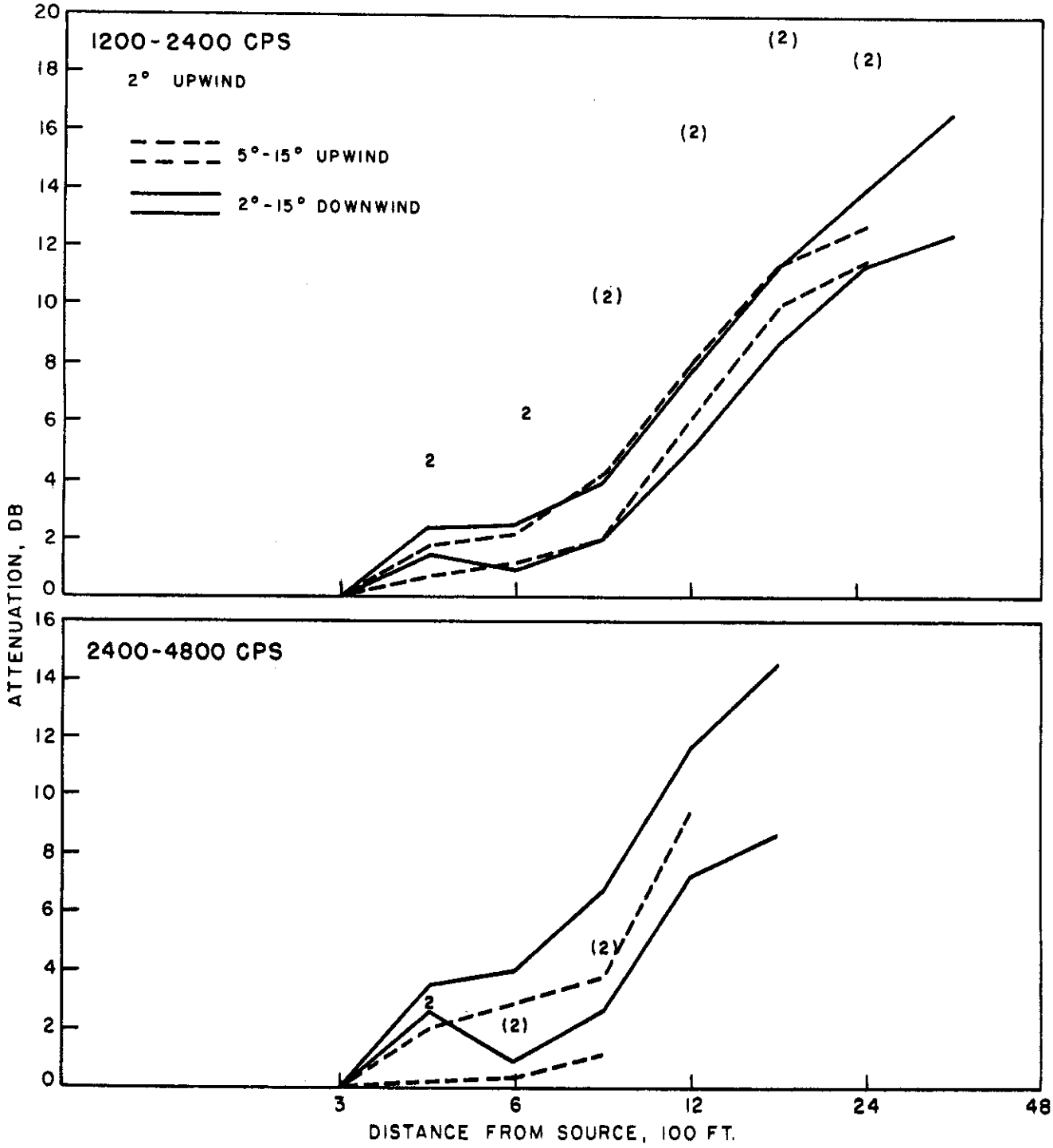

FIG. 16-D - 1200-4800 CPS

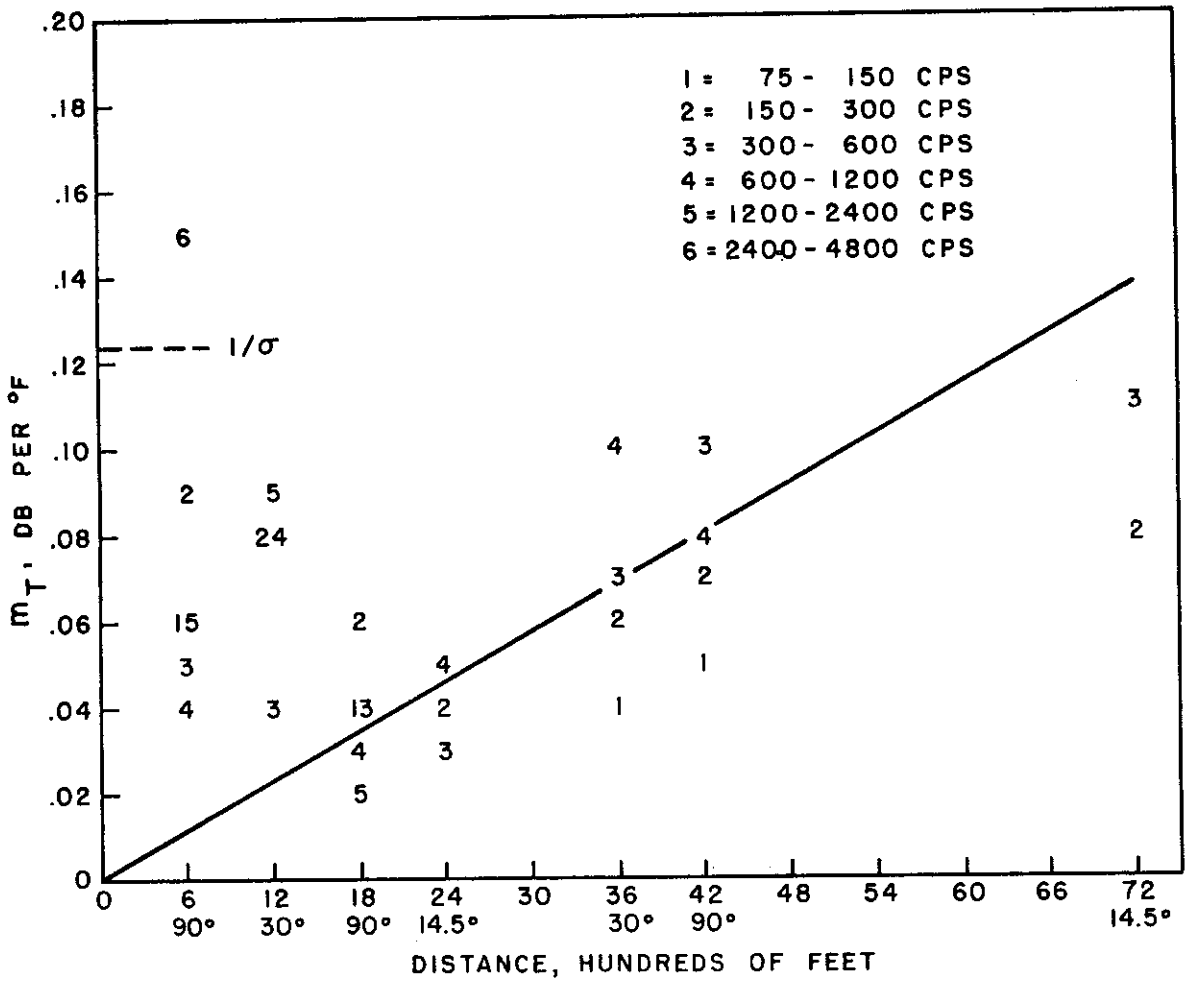

FIG. 17 - REGRESSION COEFFICIENT, m_T, OF ATTENUATION ON TEMPERATURE AS A FUNCTION OF DISTANCE AND FREQUENCY

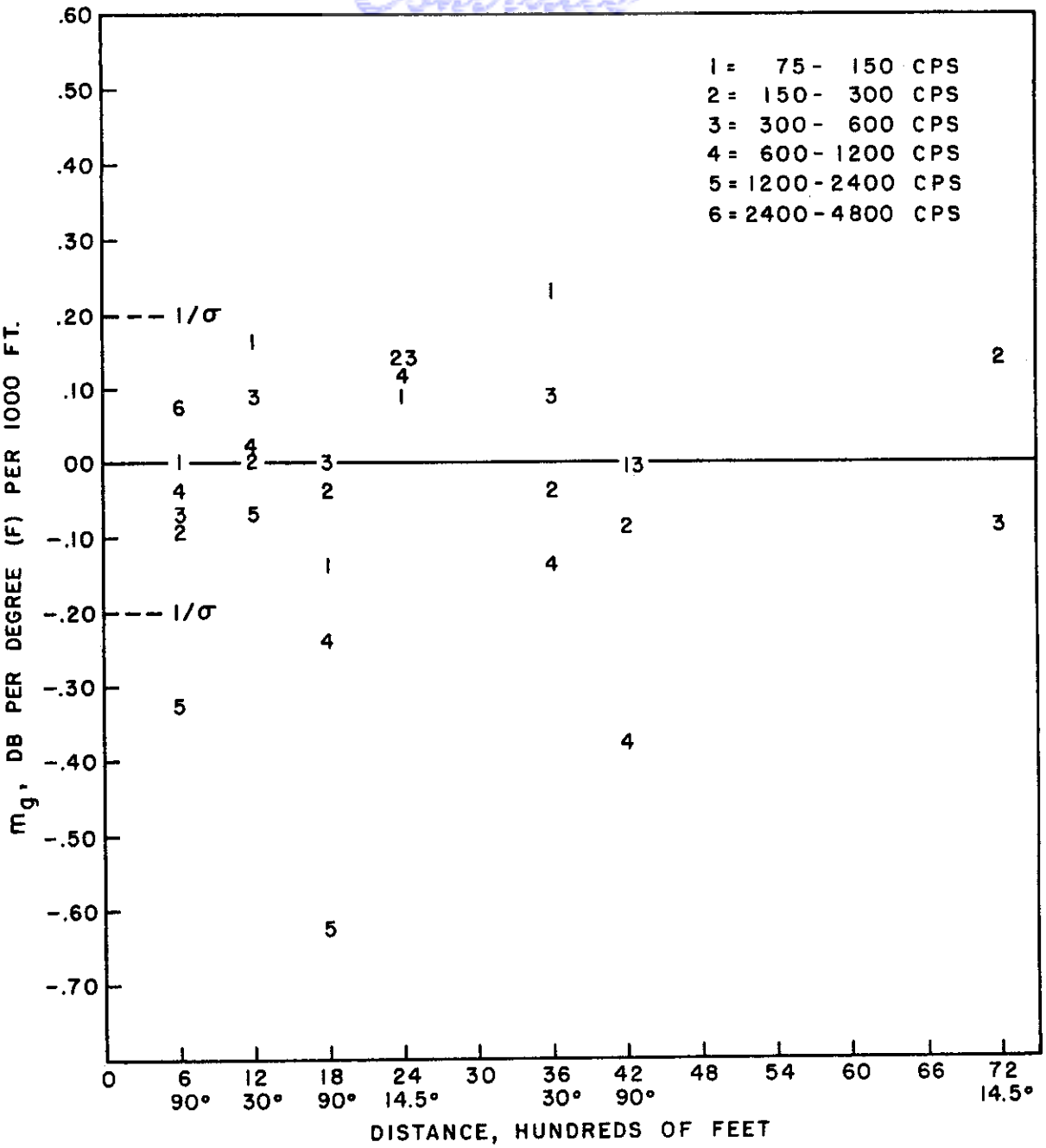

FIG. 18 - REGRESSION COEFFICIENTS, m_g, OF ATTENUATION ON TEMPERATURE GRADIENT AS A FUNCTION OF DISTANCE AND FREQUENCY

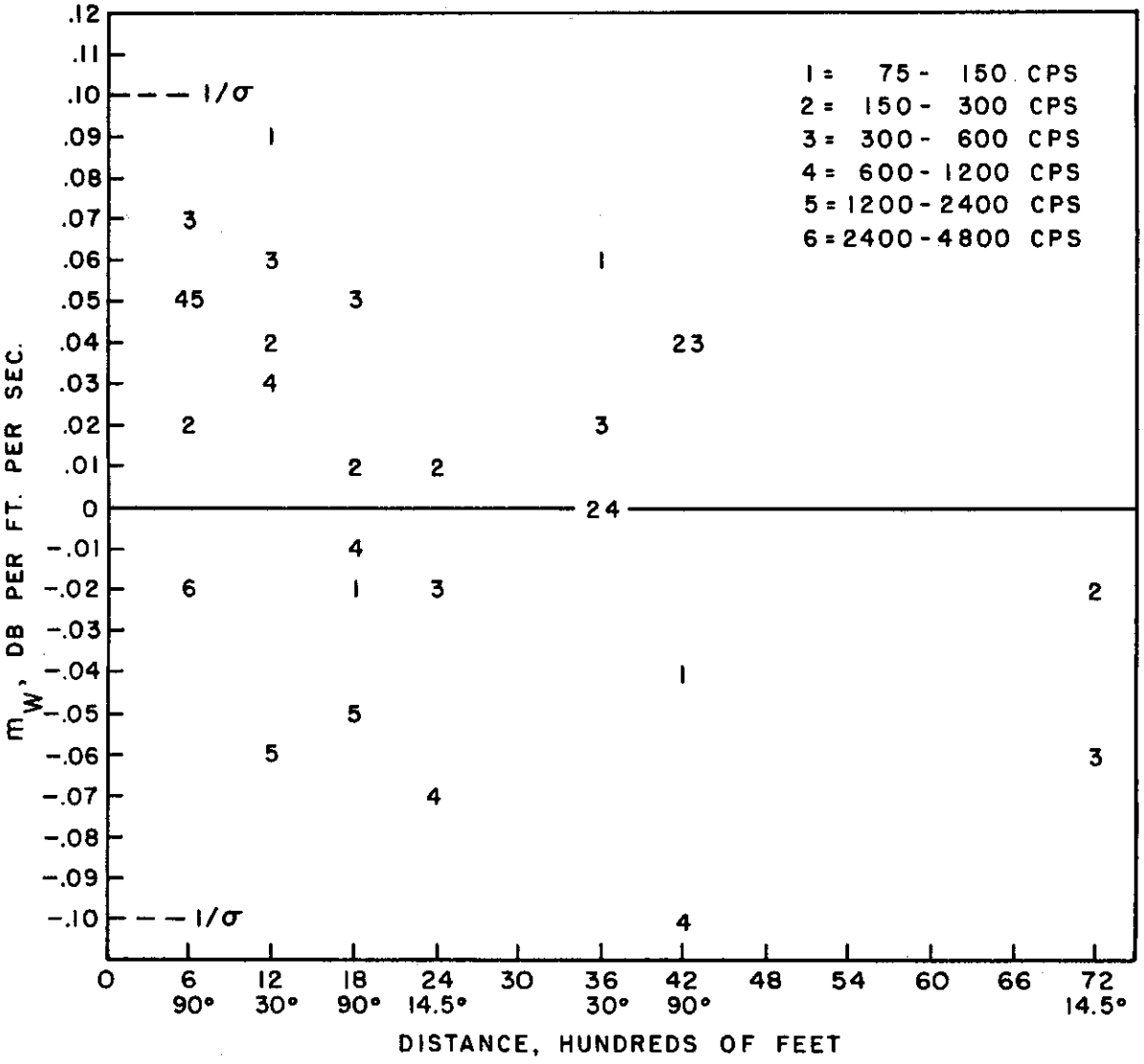

FIG. 19 - REGRESSION COEFFICIENT, m_w, OF ATTENUATION ON WIND VELOCITY AS A FUNCTION OF DISTANCE AND FREQUENCY

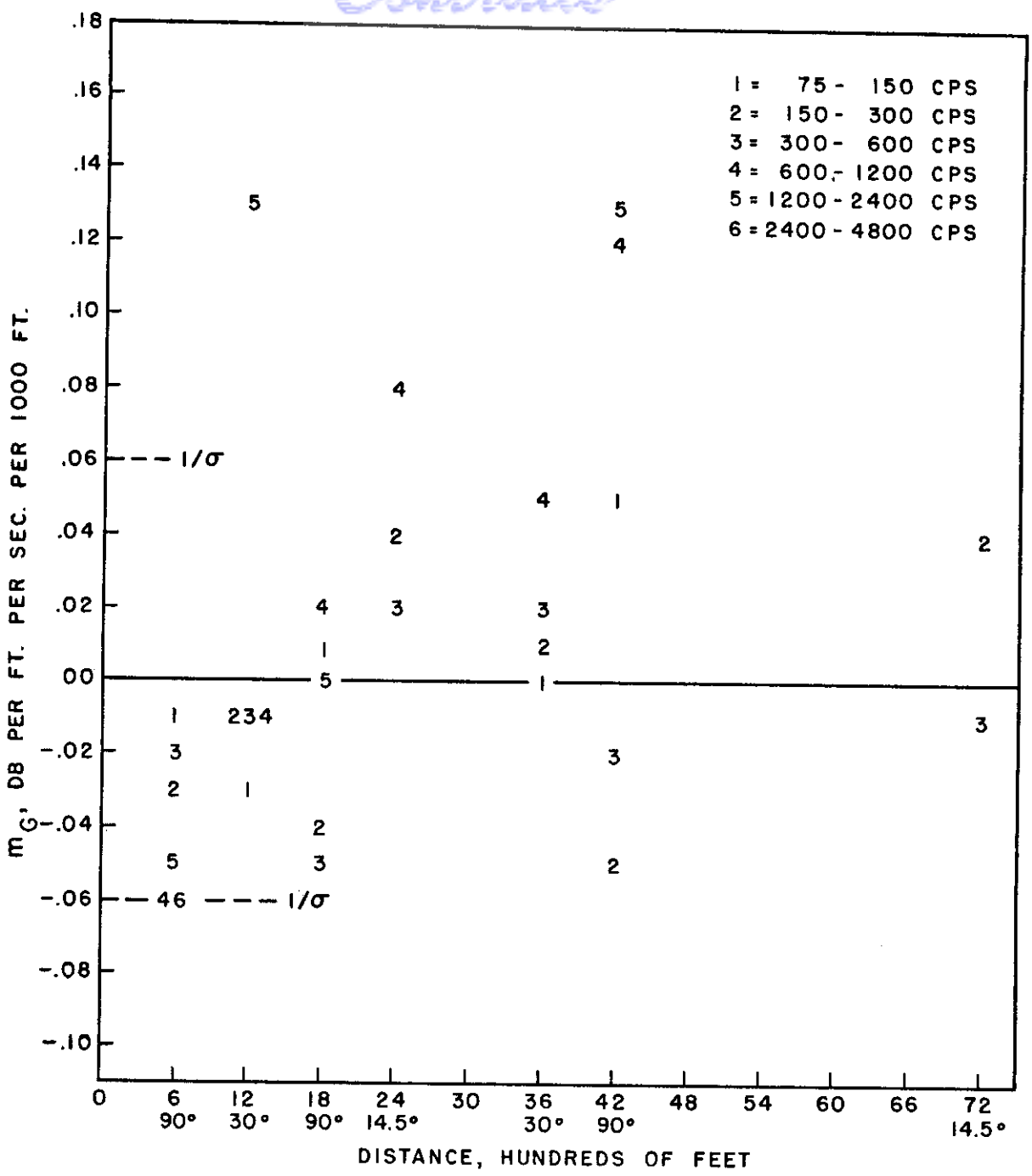

FIG. 20 - REGRESSION COEFFICIENT, m_G, OF ATTENUATION ON WIND GRADIENT AS A FUNCTION OF DISTANCE AND FREQUENCY

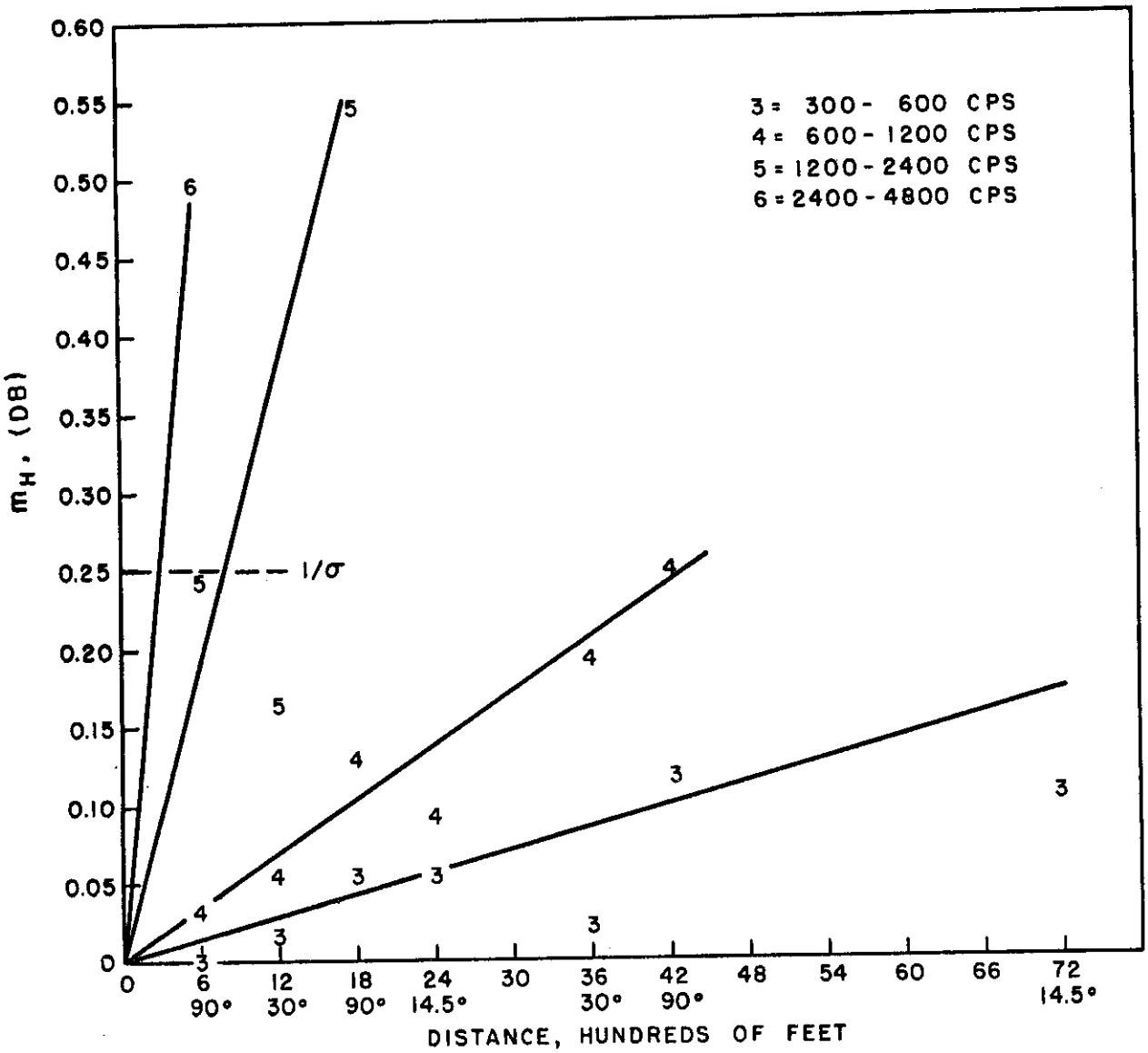

FIG. 21 - REGRESSION COEFFICIENT, m_H, OF ATTENUATION ON THE HUMIDITY FUNCTION, $H = (T + 45)/h^2$, AS A FUNCTION OF DISTANCE AND FREQUENCY. T = TEMPERATURE, ° F. h = ABSOLUTE HUMIDITY, gm/m^3.

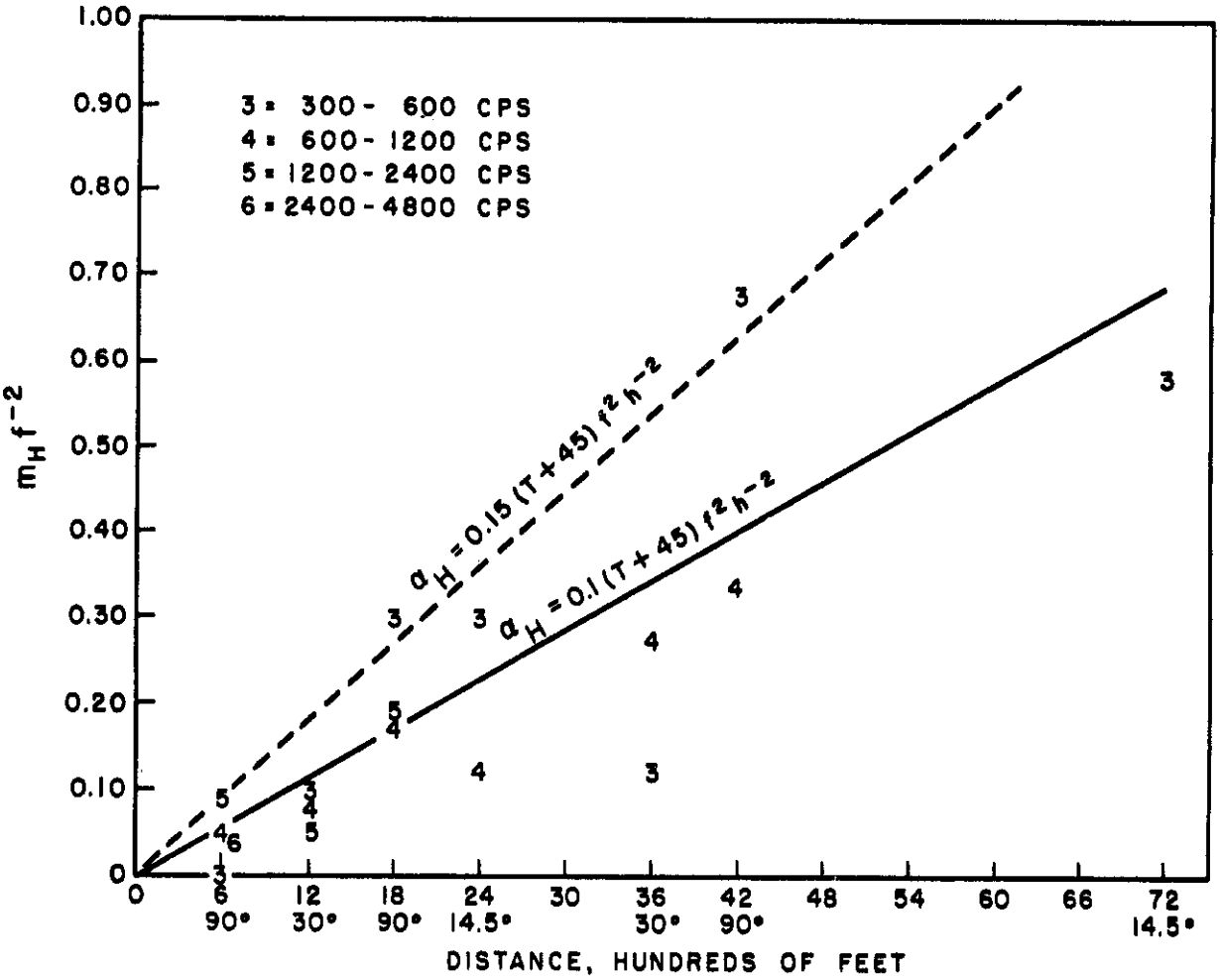

FIG. 22 - RELATION OF REGRESSION COEFFICIENT, m_H (NORMALIZED TO f^2), OF ATTENUATION ON THE HUMIDITY FUNCTION, H, TO DISTANCE AND FREQUENCY. f = FREQUENCY IN KILOCYCLES. $a_H = Hm_H$ PER 1000 FT. DISTANCE

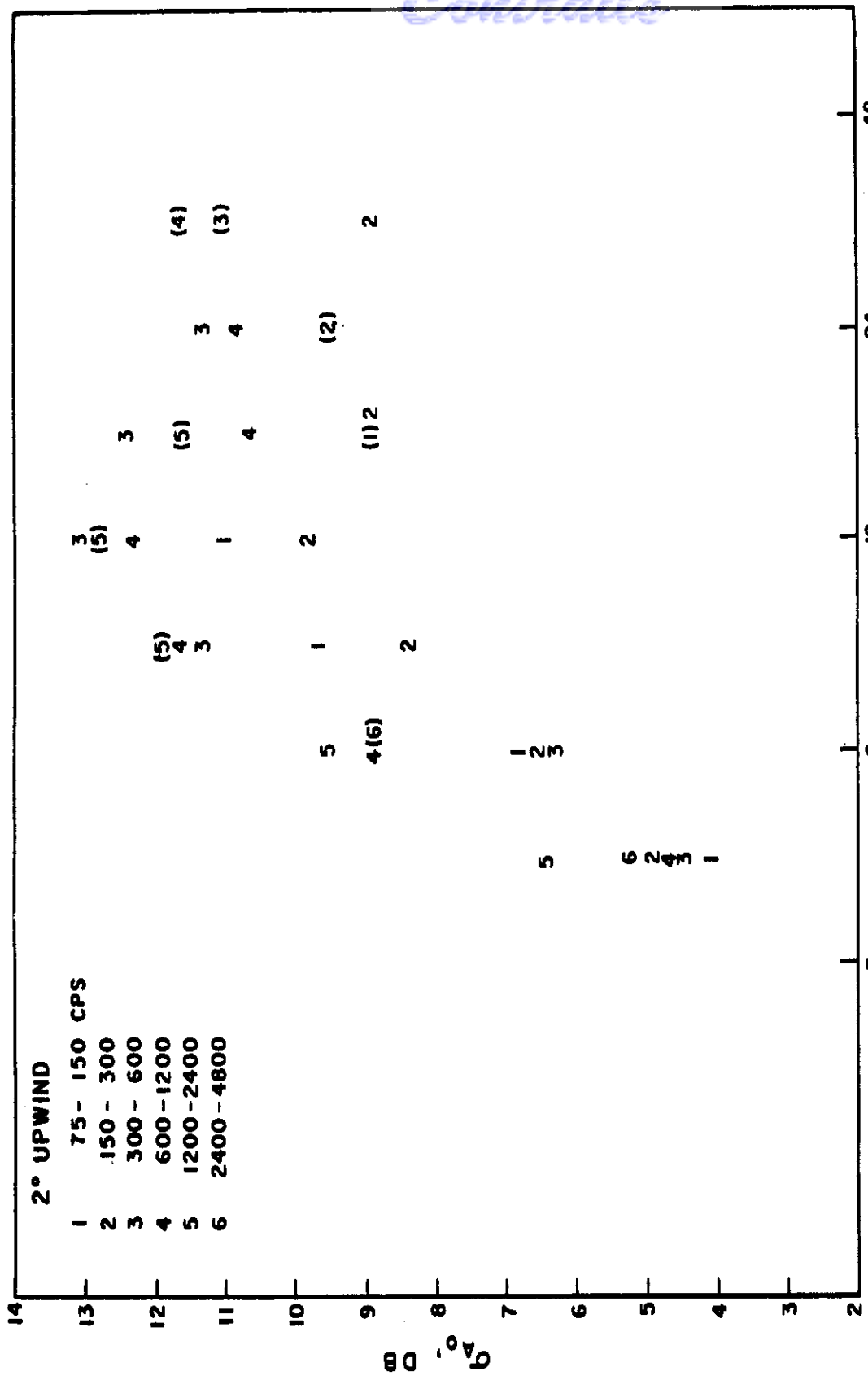

FIG. 23 – STANDARD DEVIATION, σ_{A_0}, OF RESIDUAL ATTENUATION FOR 2° UPWIND DIVE PASSES AS A FUNCTION OF DISTANCE FROM SOURCE AND FREQUENCY. VALUES BASED ON LESS THAN 80 PER CENT OF TOTAL NUMBER OF CASES INDICATED BY ( )

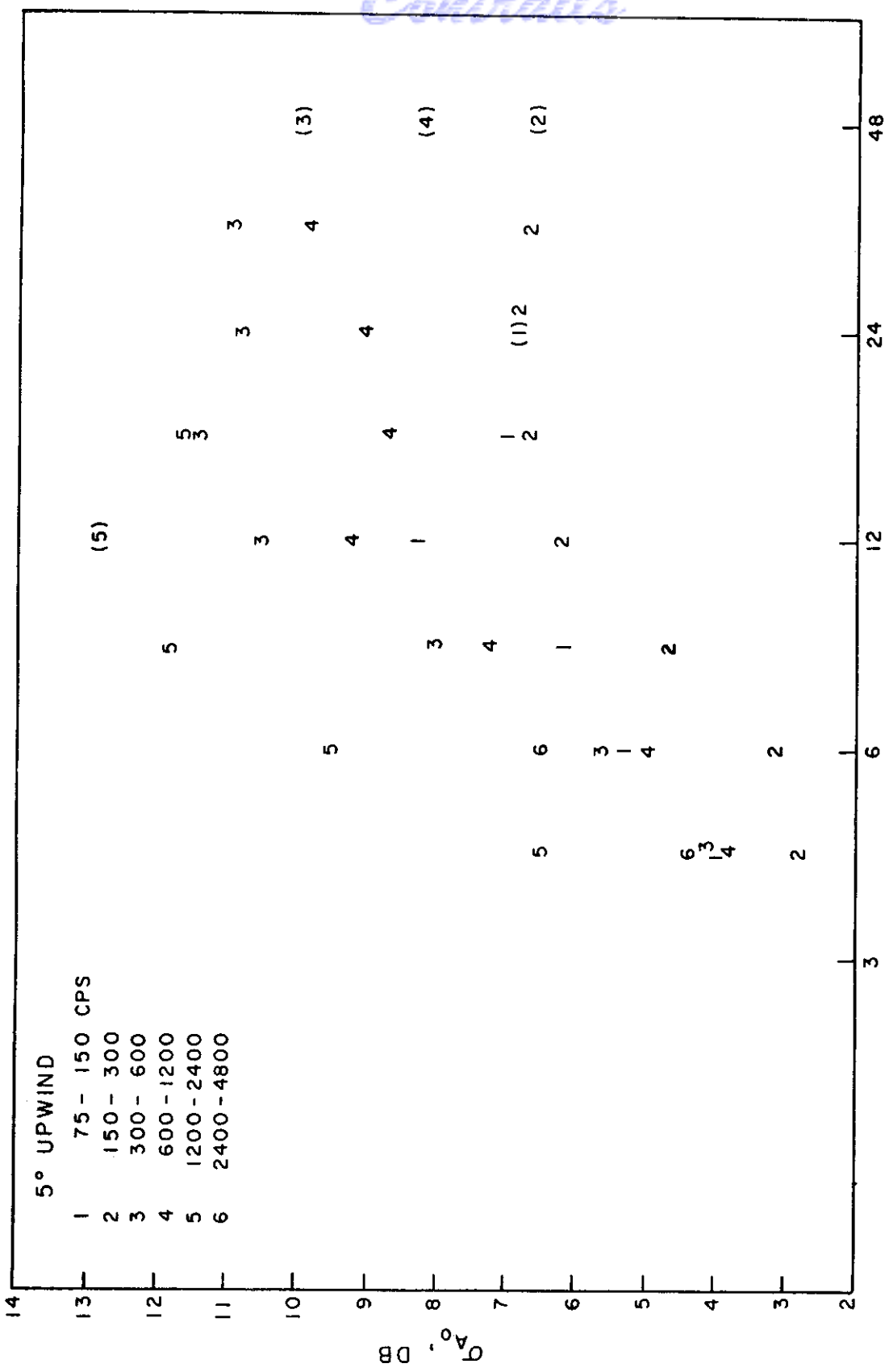

FIG. 24 - STANDARD DEVIATION, σ_{Ao}, OF RESIDUAL ATTENUATION FOR 5° UPWIND DIVE PASSES AS A FUNCTION OF DISTANCE FROM SOURCE AND FREQUENCY. VALUES BASED ON LESS THAN 80 PER CENT OF TOTAL NUMBER OF CASES INDICATED BY ( )

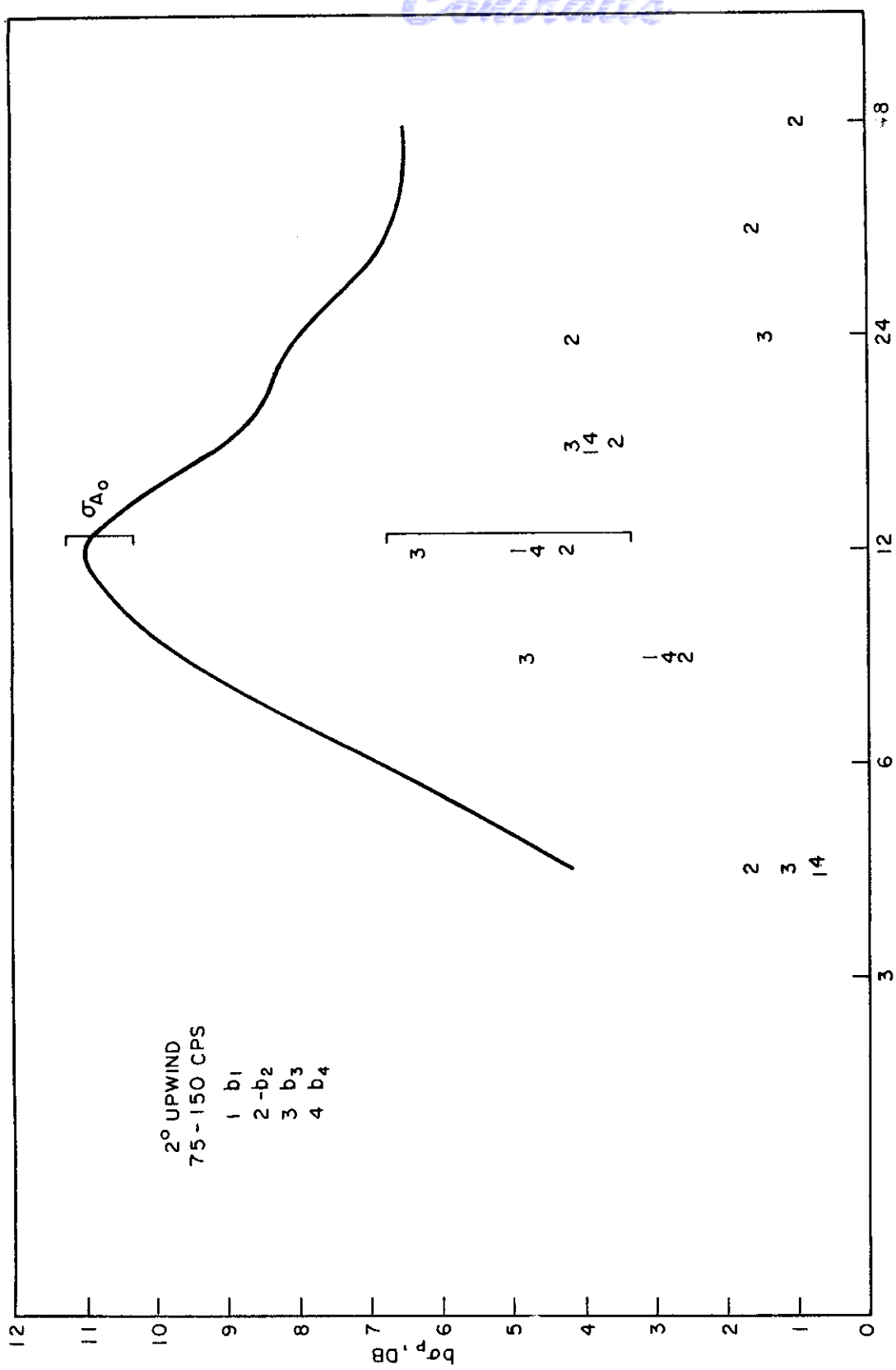

FIG. 25 - NORMALIZED SIMPLE REGRESSION COEFFICIENTS, $b\sigma_p$, OF RESIDUAL ATTENUATION WITH RESPECT TO WEATHER PARAMETERS AS A FUNCTION OF DISTANCE FROM SOURCE. POINTS TO RIGHT OF LINE ARE BASED ON LESS THAN 80 PER CENT OF TOTAL NUMBER OF CASES. 2° UPWIND, 75-150 CPS.

b_1 : $W \cos \phi$
b_2 : $(\Delta T)^{2/3}$
b_3 : $\log_e W$
b_4 : $(W \cos \phi)^{2/3}$

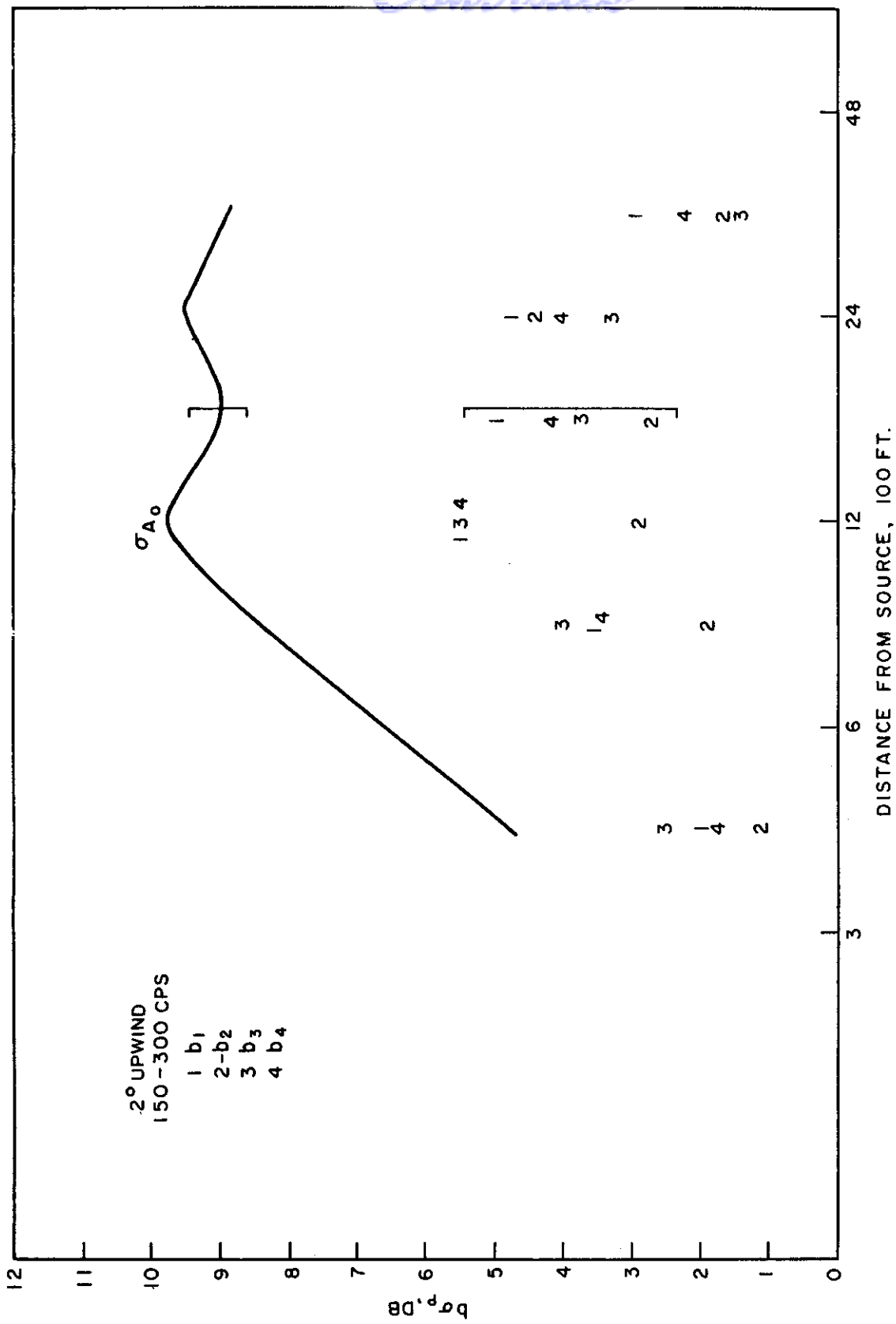

FIG. 26 - SAME AS FIG. 25, 2° UPWIND, 150-300 CPS

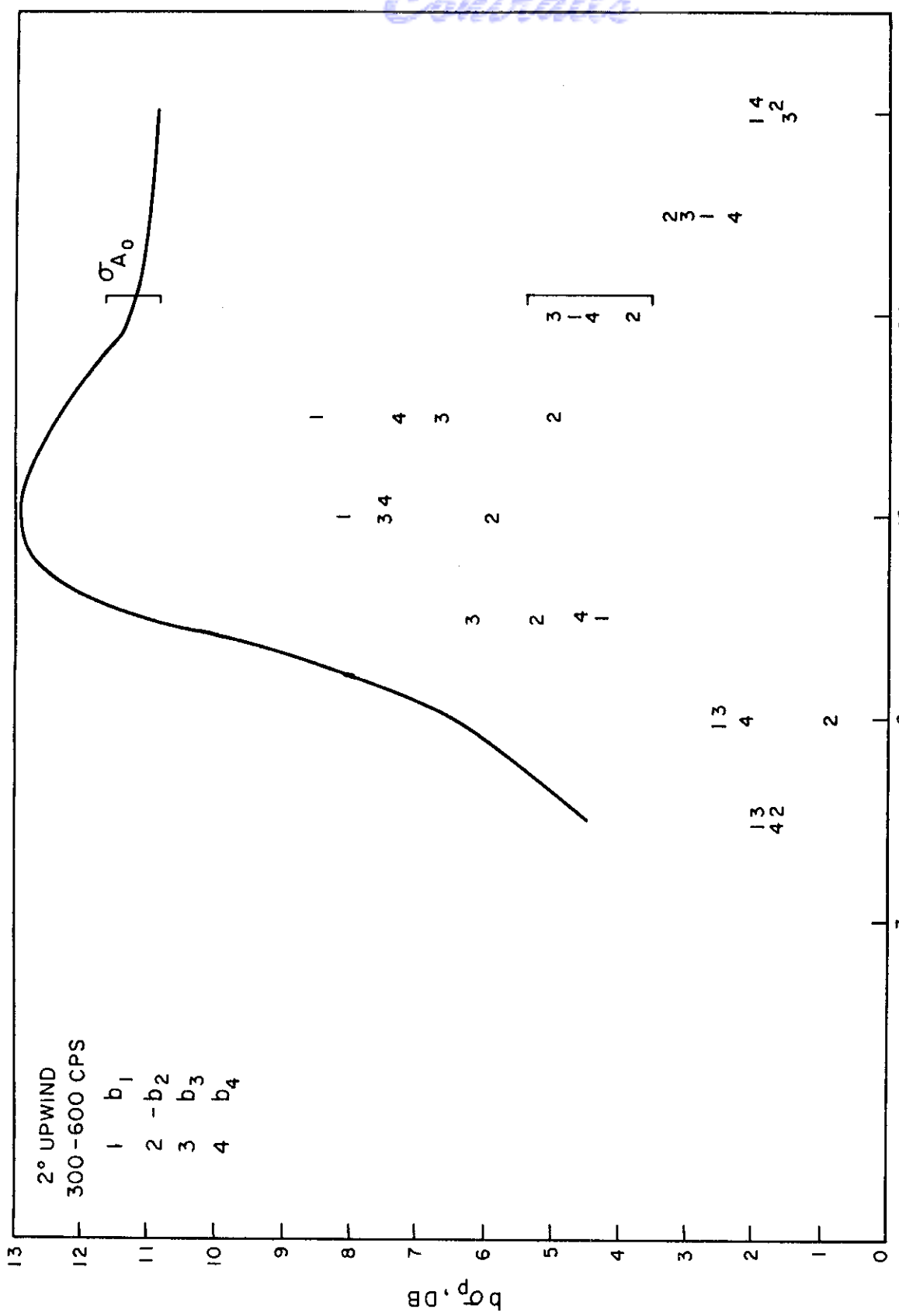

FIG. 27 - SAME AS FIG. 25, 2° UPWIND, 300-600 CPS

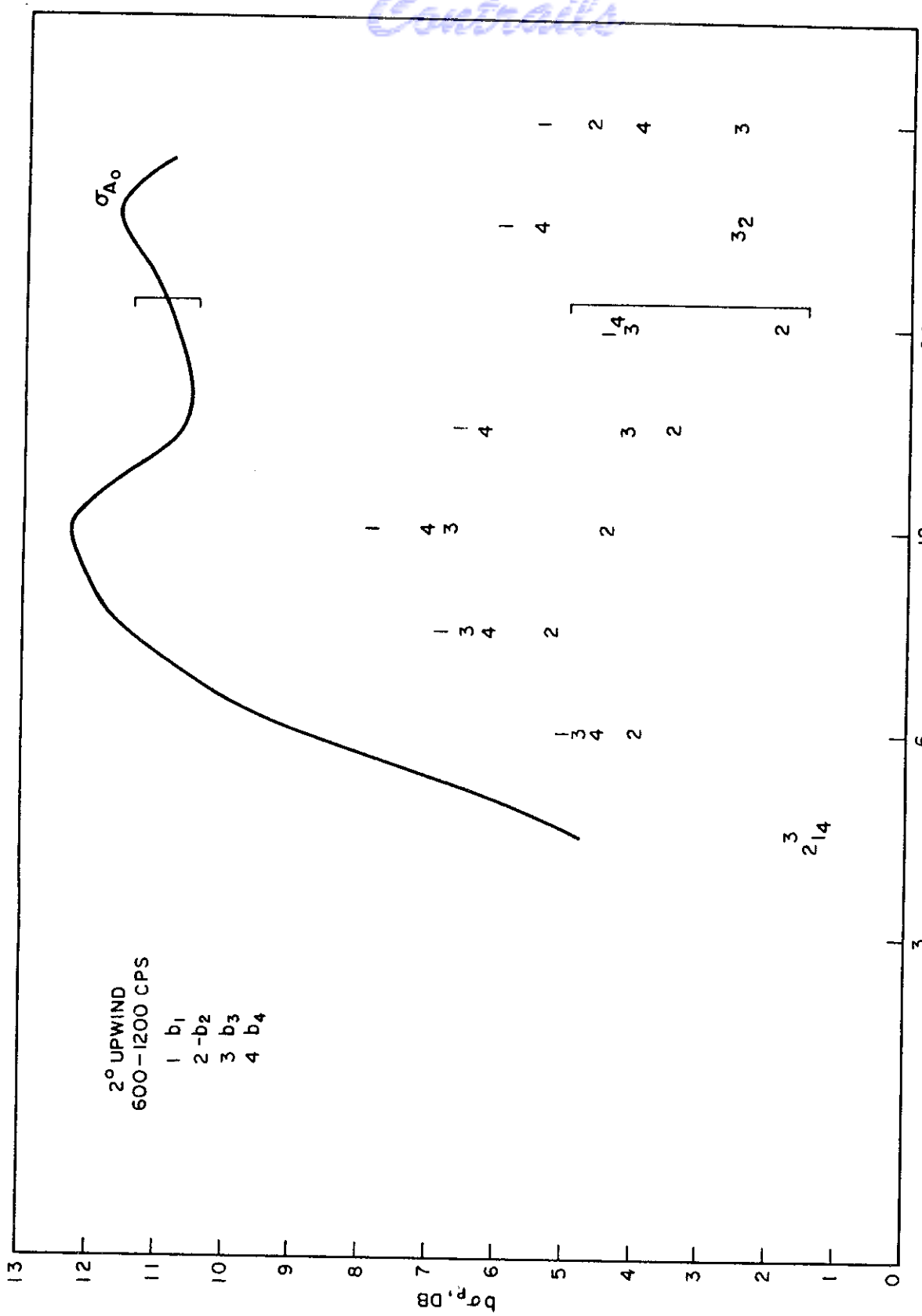

FIG. 28 - SAME AS FIG. 25, 2° UPWIND, 600-1200 CPS

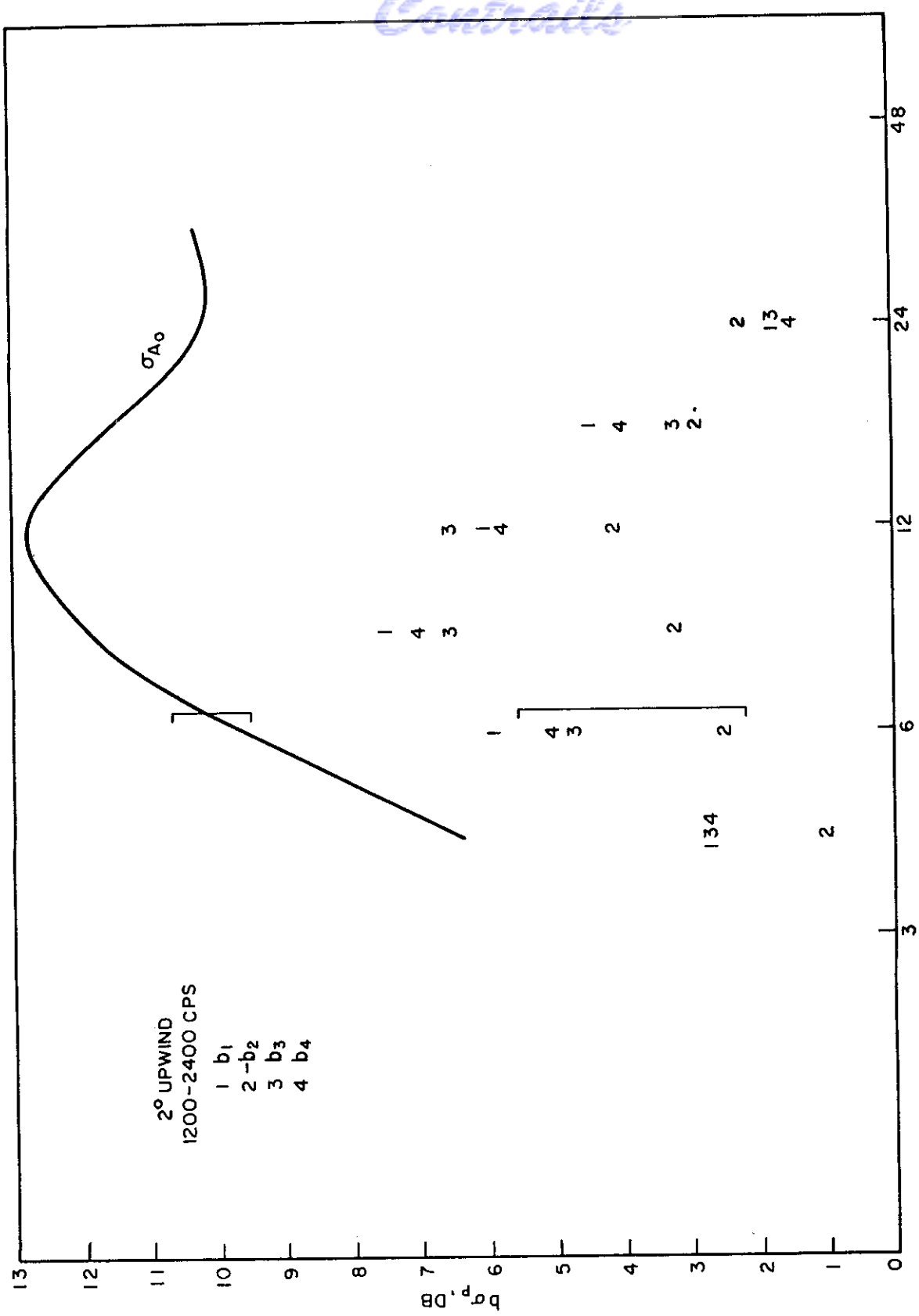

FIG. 29 - SAME AS FIG. 25, 2° UPWIND, 1200-2400 CPS

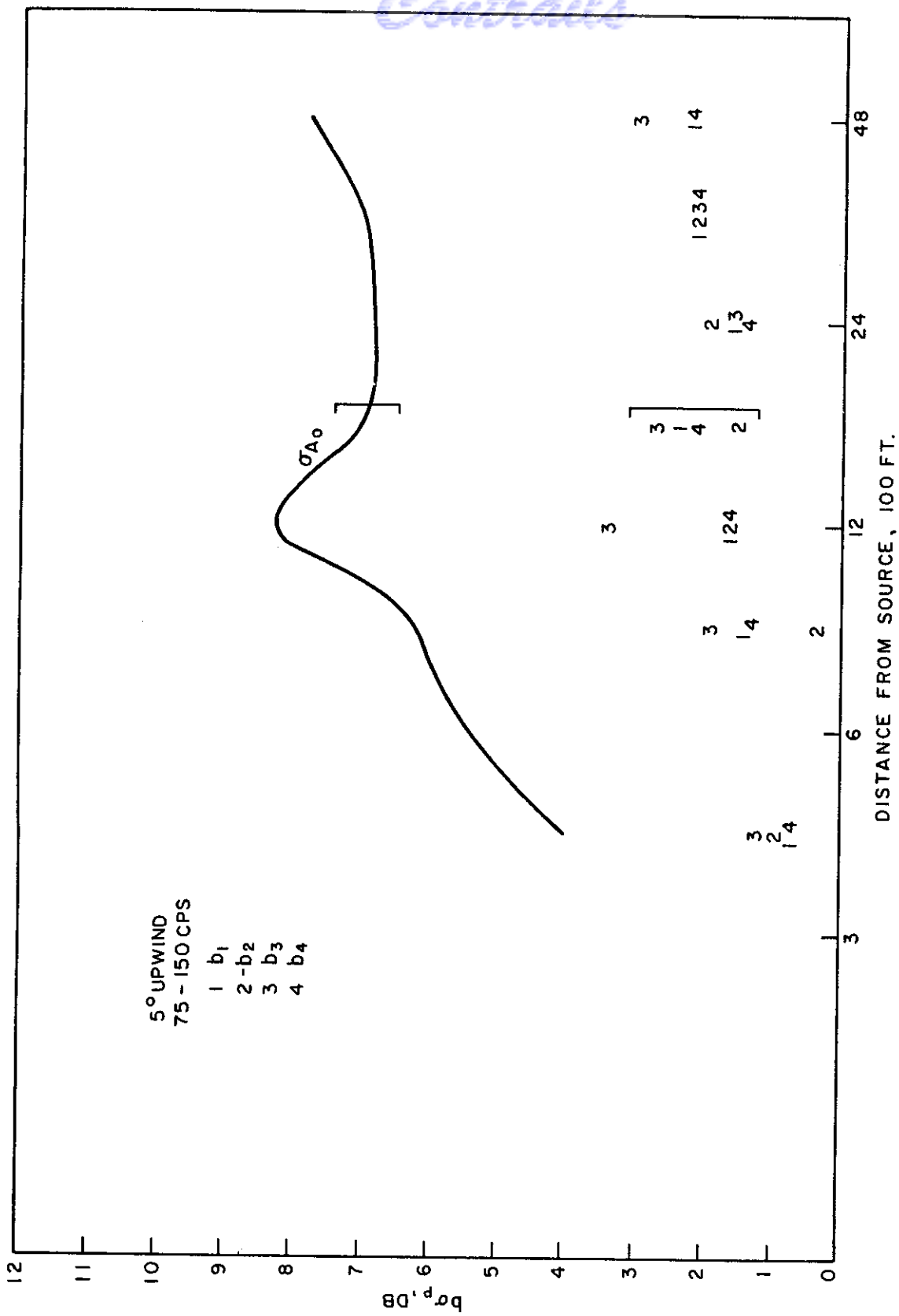

FIG. 30 - SAME AS FIG. 25, 5° UPWIND, 75-150 CPS

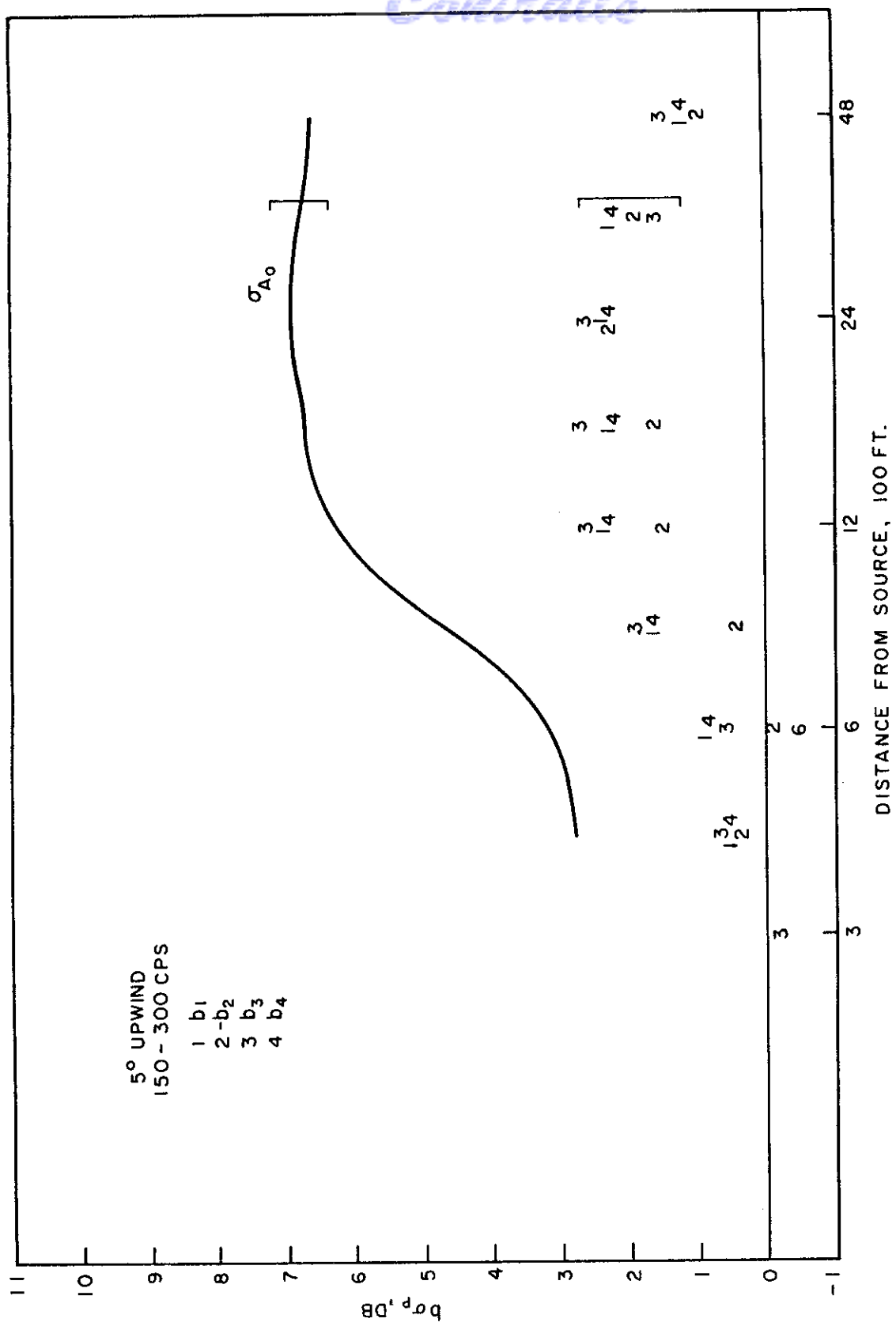

FIG. 31 - SAME AS FIG. 25, 5° UPWIND, 150-300 CPS

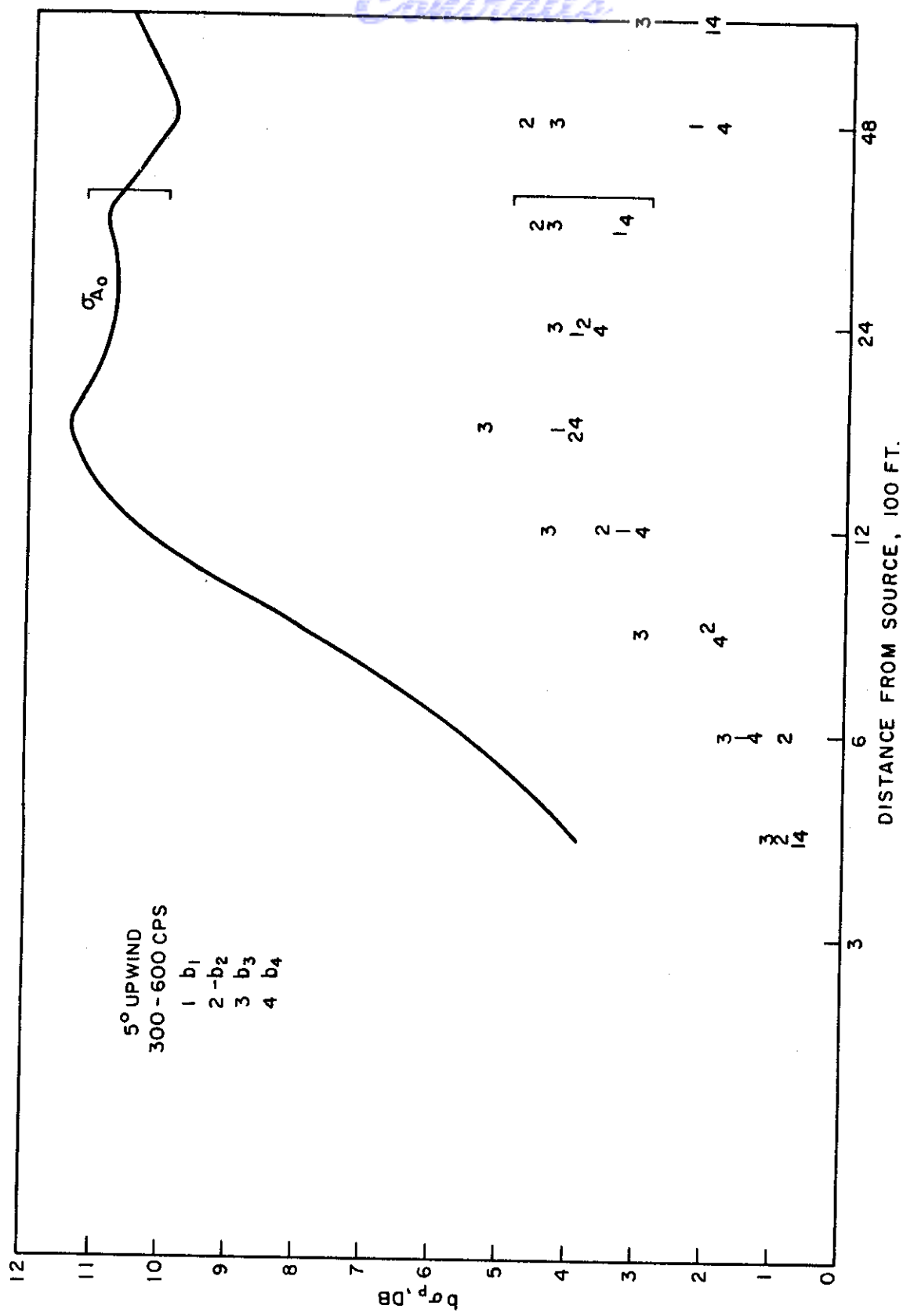

FIG. 32 - SAME AS FIG. 25, 5° UPWIND, 300-600 CPS

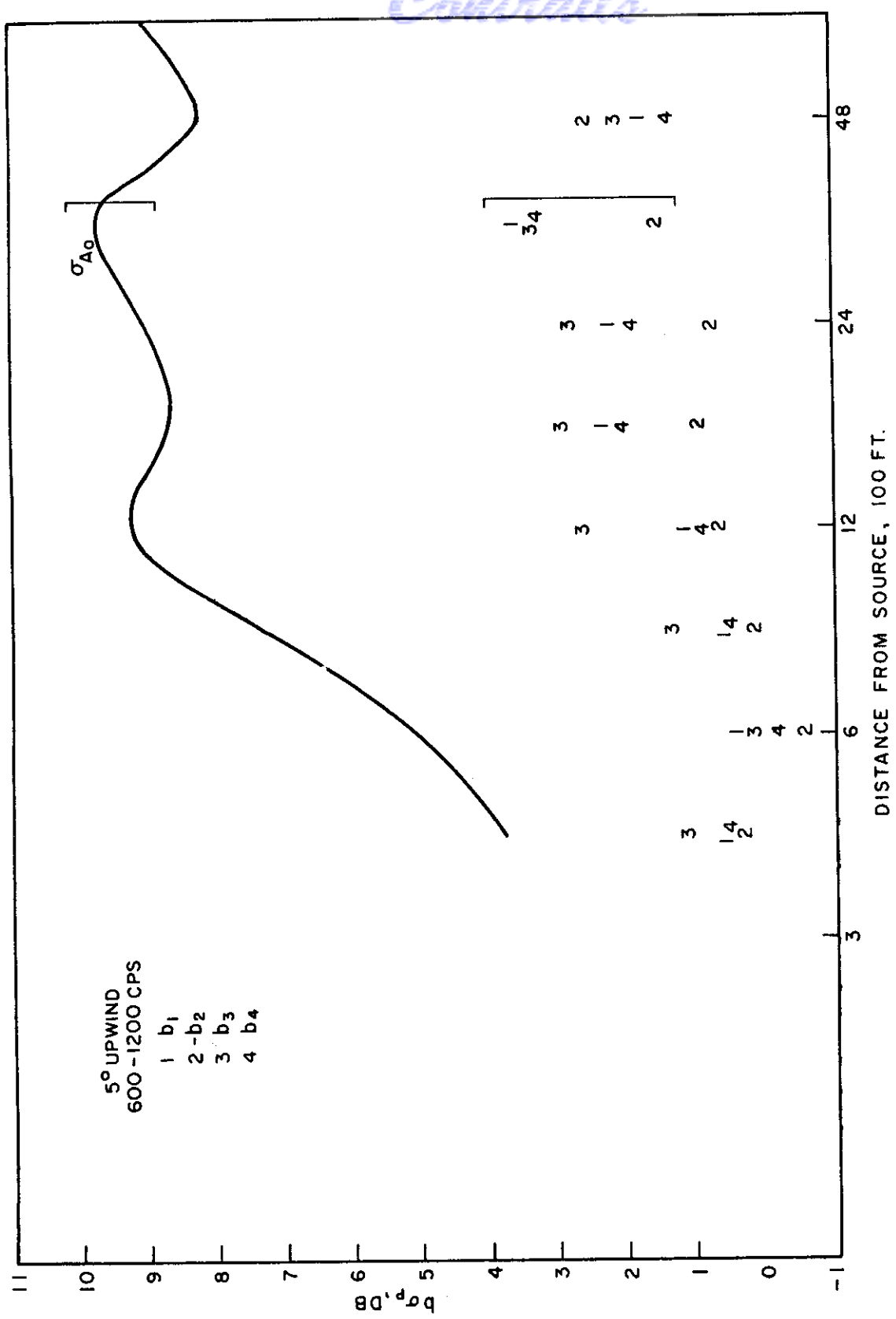

FIG. 33 - SAME AS FIG. 25, 5° UPWIND, 600-1200 CPS

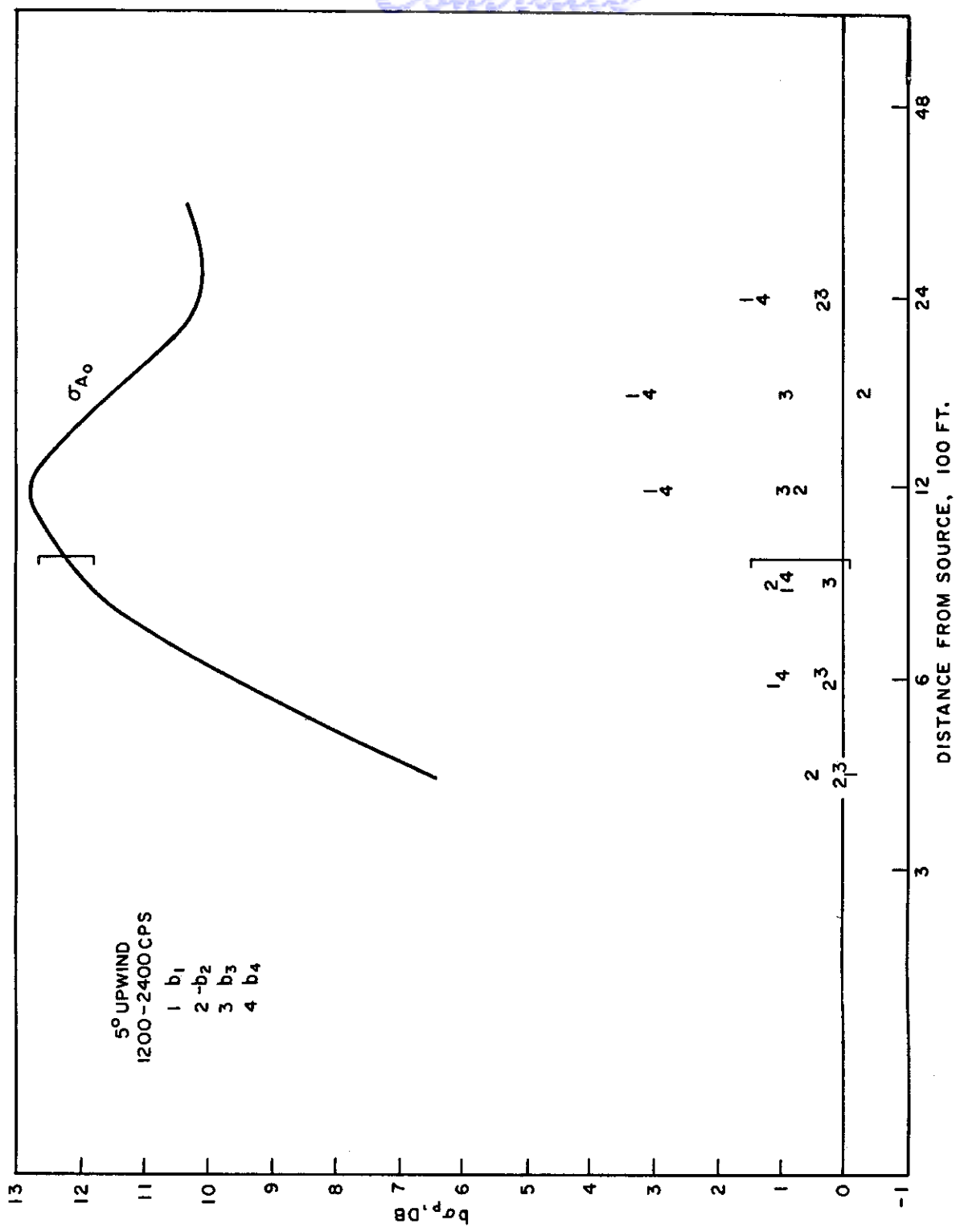

FIG. 34 - SAME AS FIG. 25, 5° UPWIND, 1200-2400 CPS

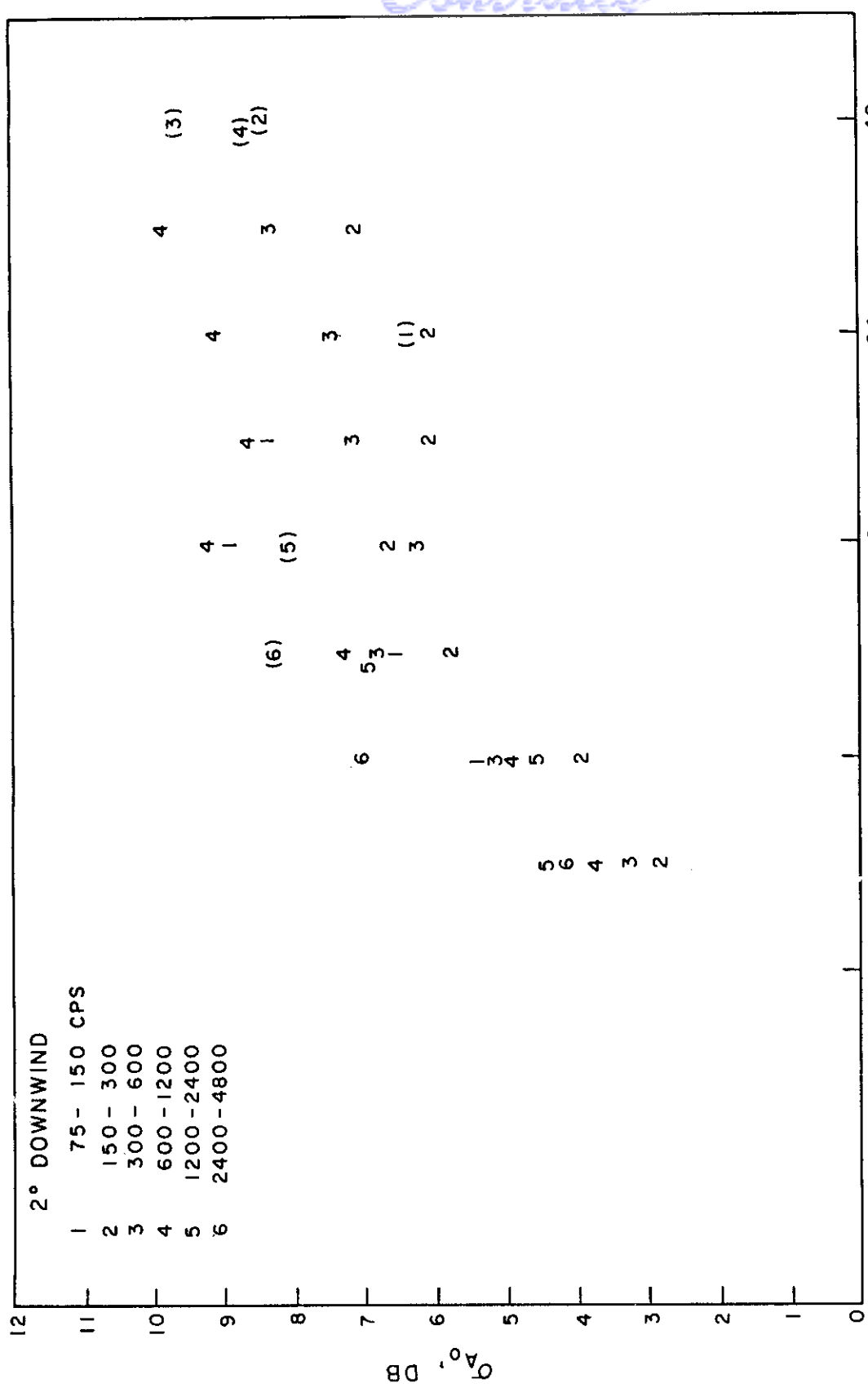

FIG. 35 - STANDARD DEVIATION, σ_{A_0}, OF RESIDUAL ATTENUATION FOR 2° DOWNWIND DIVE PASSES AS A FUNCTION OF DISTANCE FROM SOURCE AND FREQUENCY. ( ) INDICATES VALUES BASED ON LESS THAN 80 PER CENT OF TOTAL NUMBER OF CASES

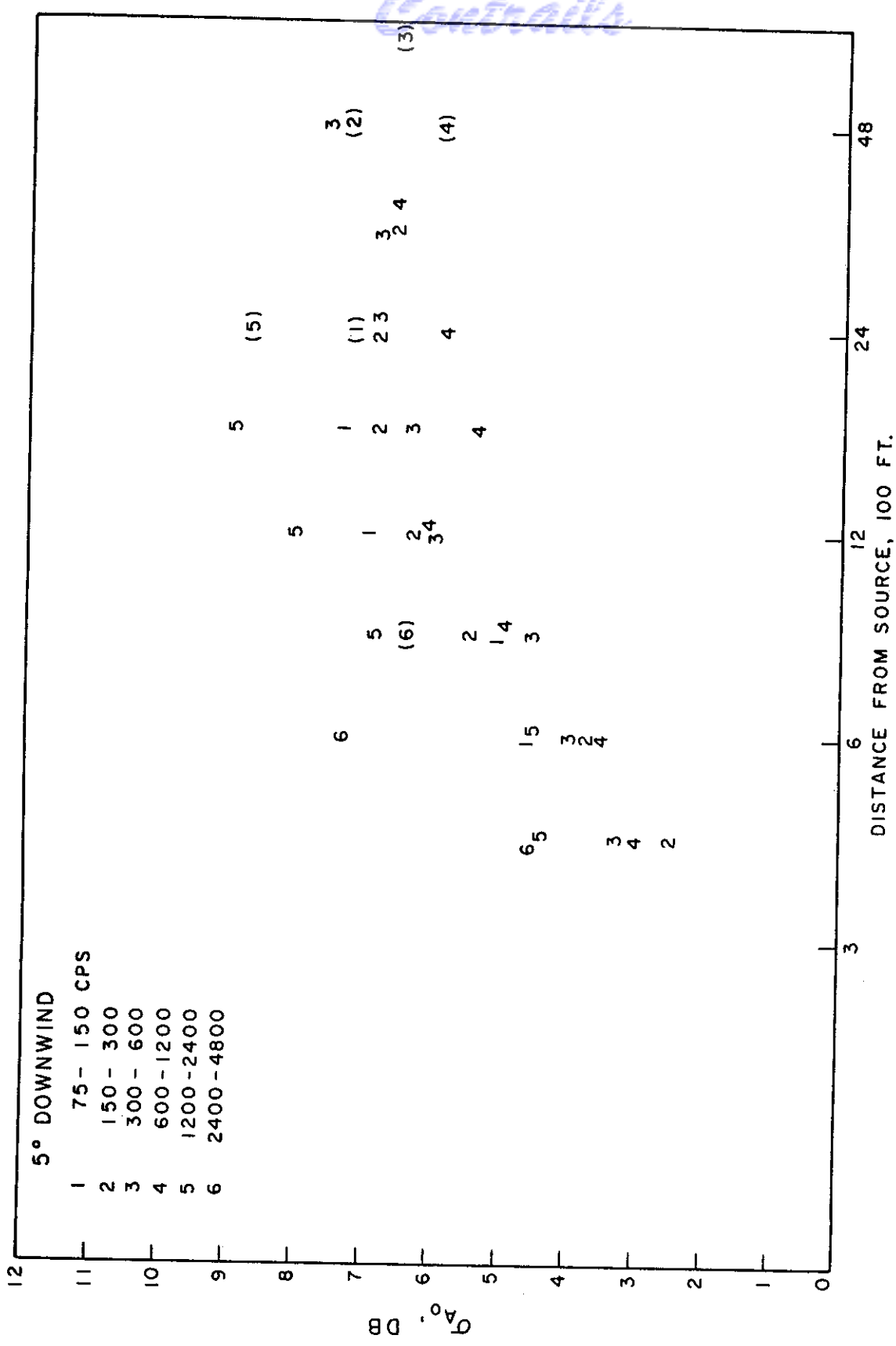

FIG. 36 - STANDARD DEVIATION, σ_{Ao}, OF RESIDUAL ATTENUATION FOR 5° DOWNWIND DIVE PASSES AS A FUNCTION OF DISTANCE FROM SOURCE AND FREQUENCY. ( ) INDICATES VALUES BASED ON LESS THAN 80 PER CENT OF TOTAL NUMBER OF CASES

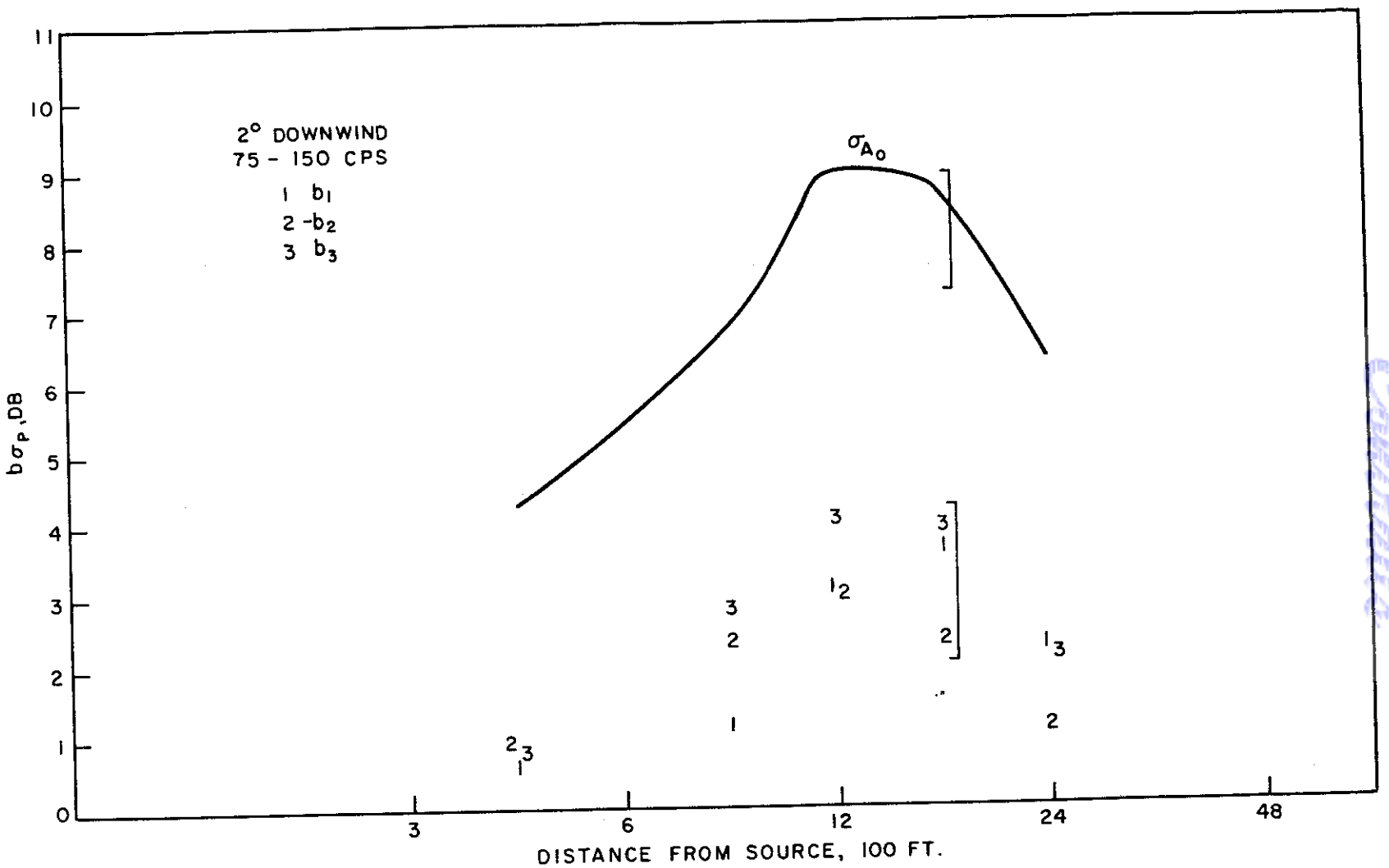

FIG. 37 - NORMALIZED SIMPLE REGRESSION COEFFICIENTS, $b\sigma_p$, OF RESIDUAL ATTENUATION WITH RESPECT TO WEATHER PARAMETERS AS A FUNCTION OF DISTANCE FROM SOURCE. POINTS TO RIGHT OF LINE ARE BASED ON LESS THAN 80 PER CENT OF TOTAL NUMBER OF CASES. 2° DOWNWIND, 75-150 CPS

b_1: $W \cos \phi$

b_2: $(\Delta T)^{2/3}$

b_3: $\log_e W$

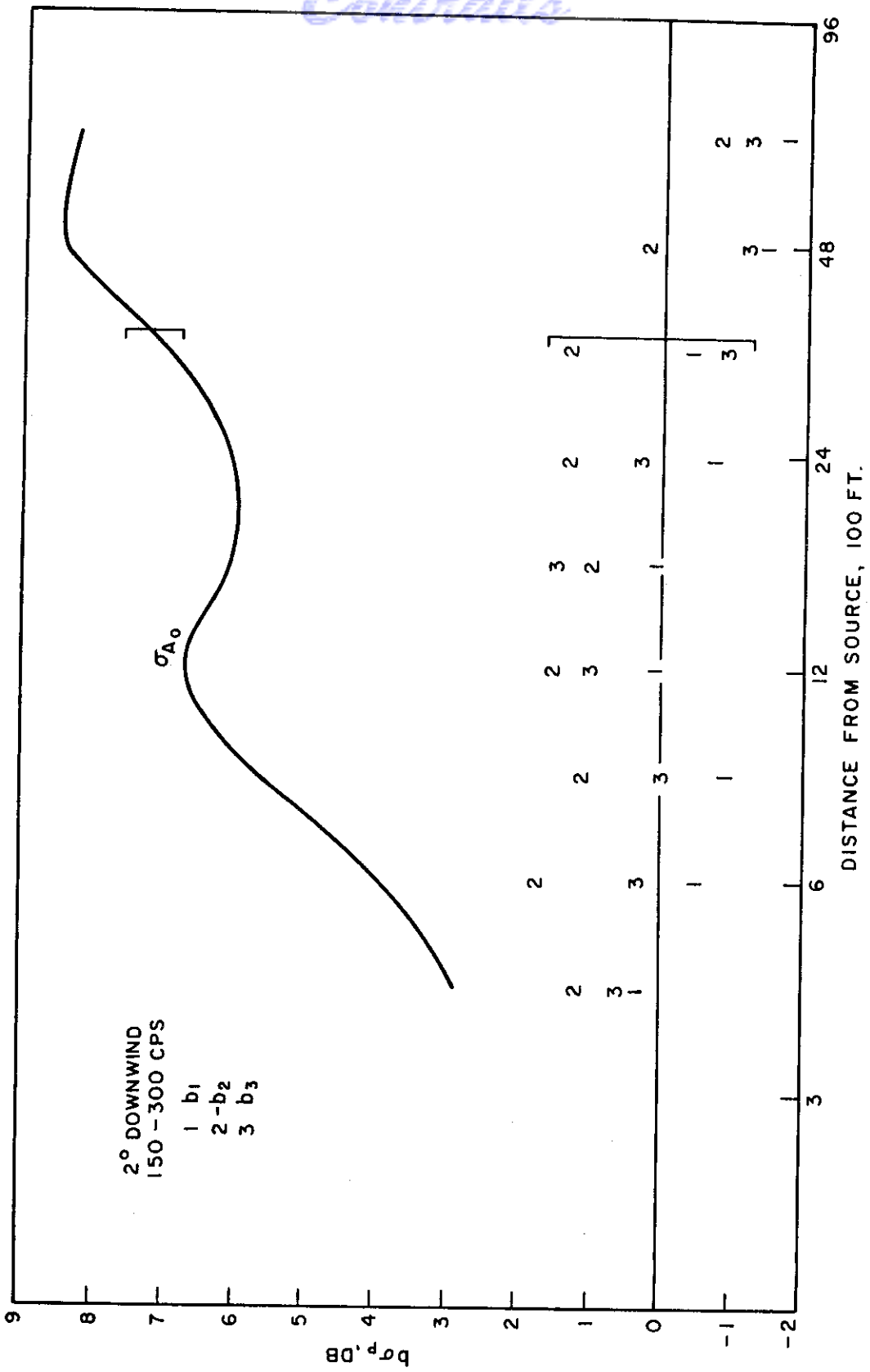

FIG. 38 - SAME AS FIG. 37, 2° DOWNWIND, 150-300 CPS

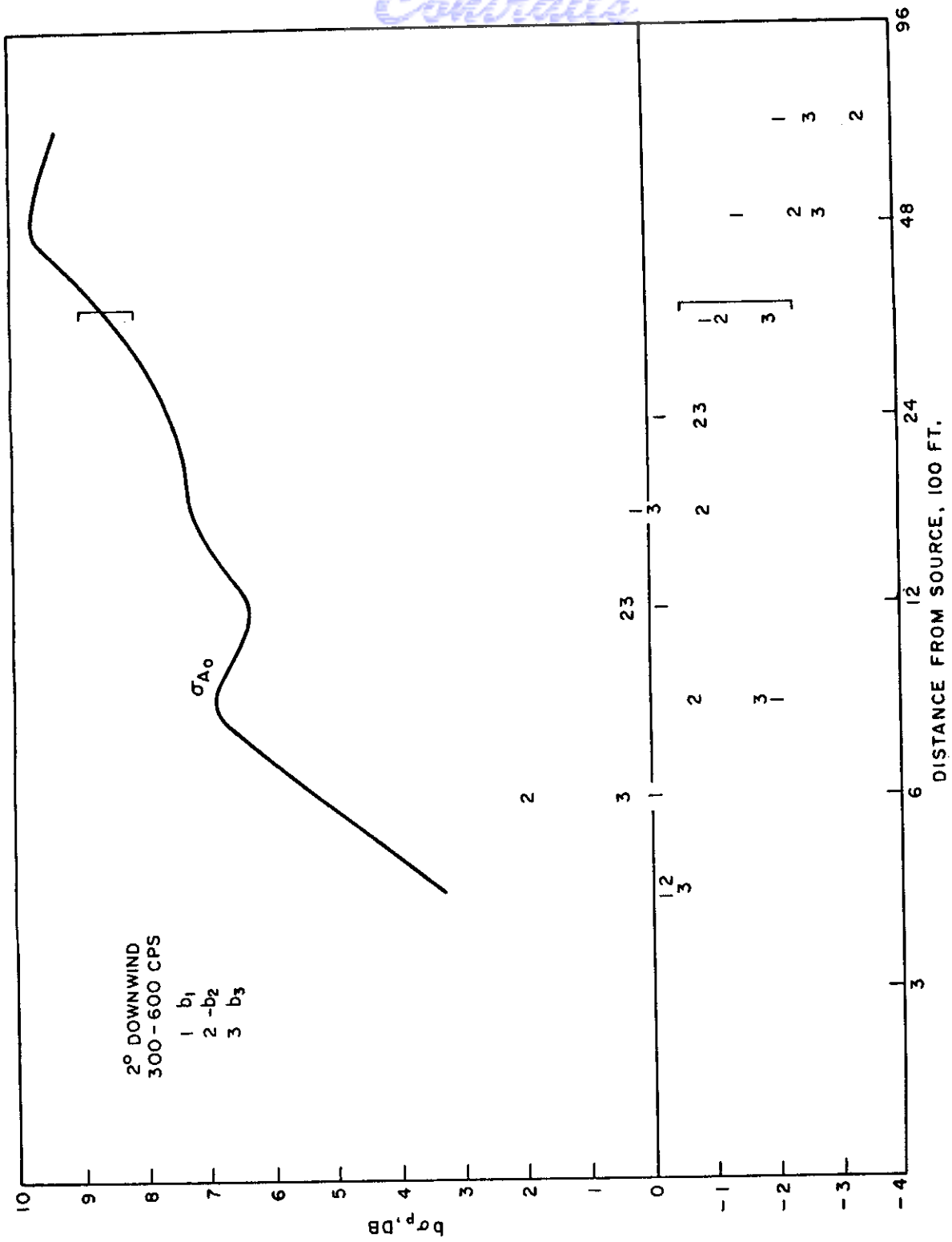

FIG. 39 - SAME AS FIG. 37, 2° DOWNWIND, 300-600 CPS

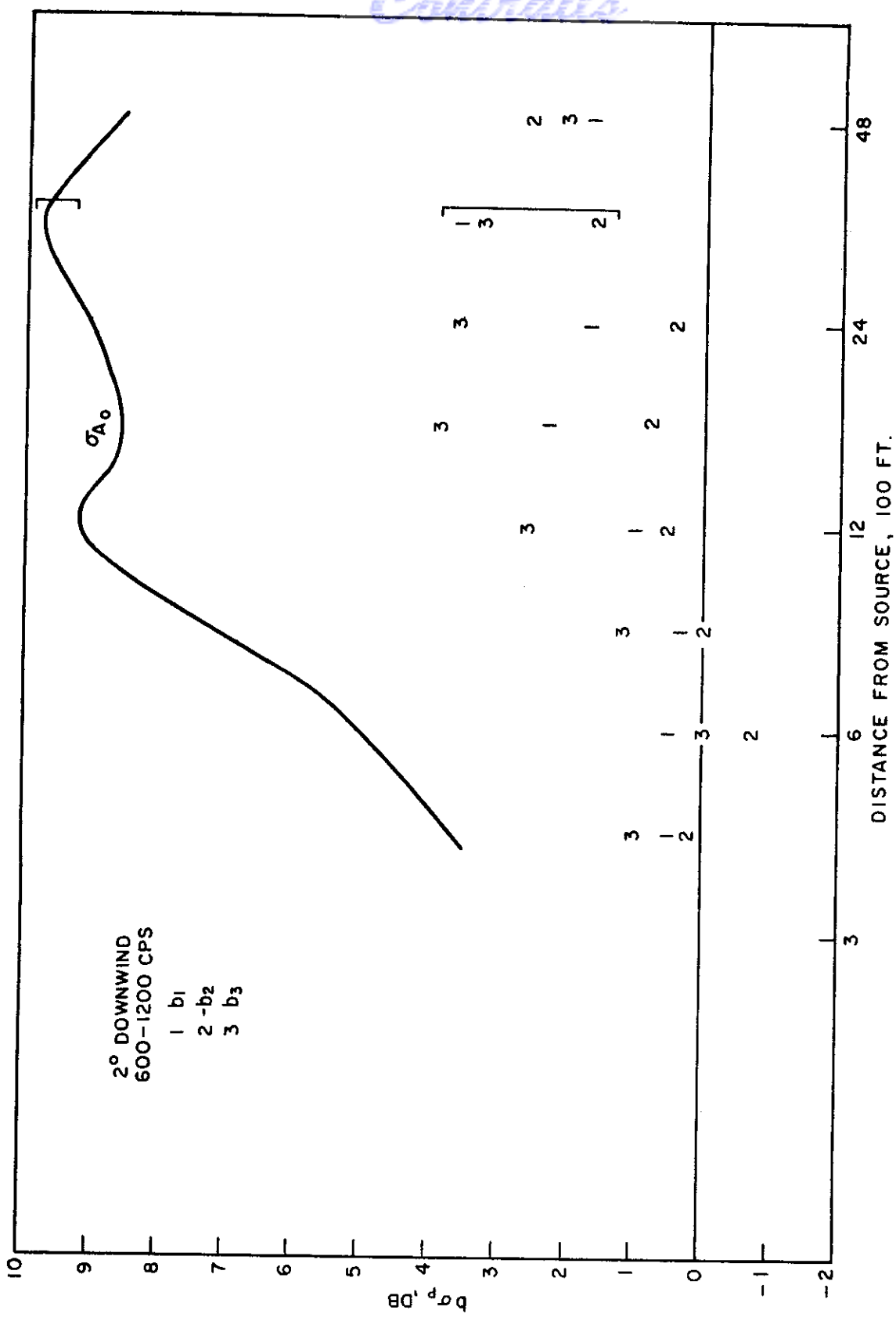

FIG. 40 - SAME AS FIG. 37, 2° DOWNWIND, 600-1200 CPS

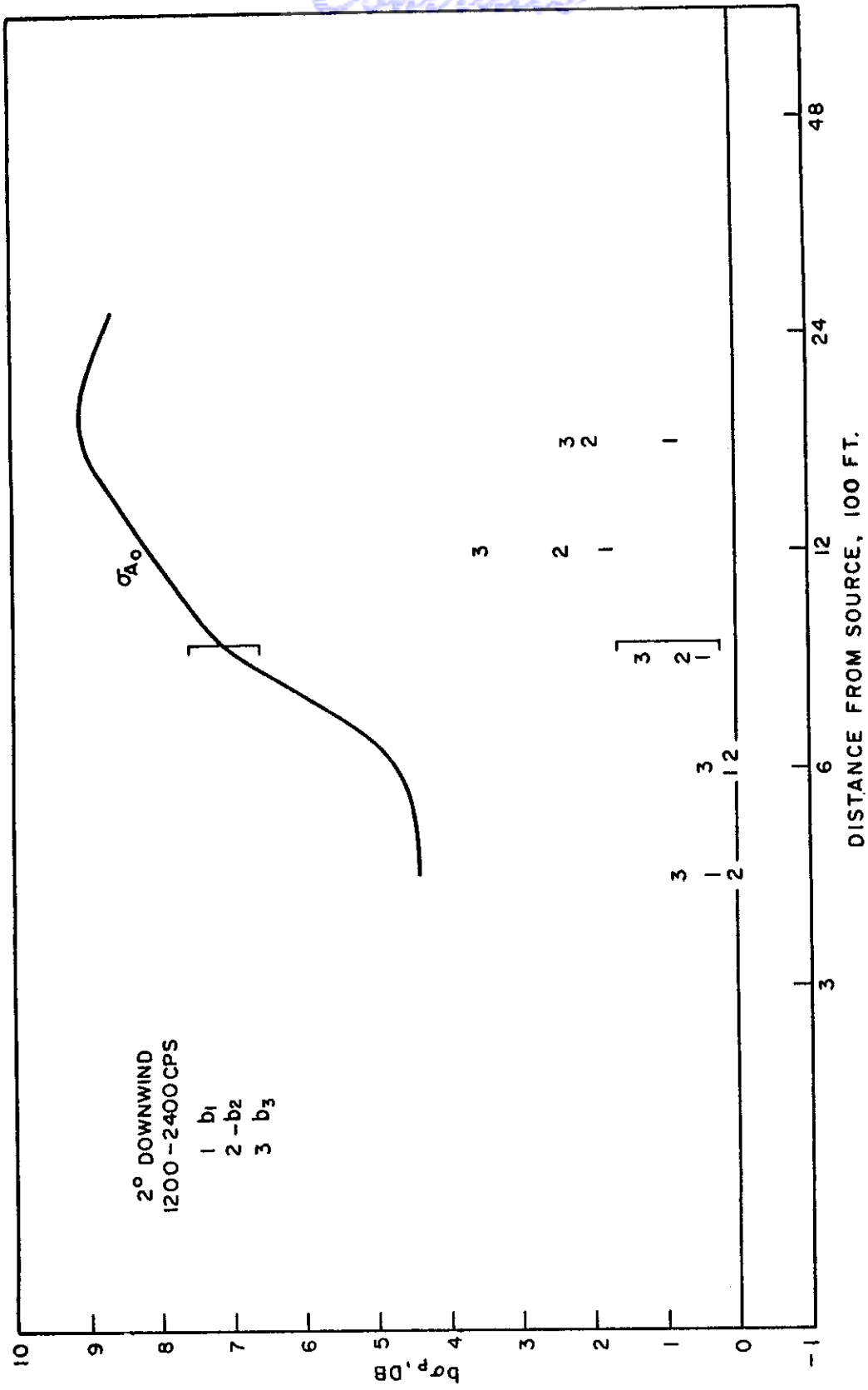

FIG. 41 - SAME AS FIG. 37, 2° DOWNWIND, 1200-2400 CPS

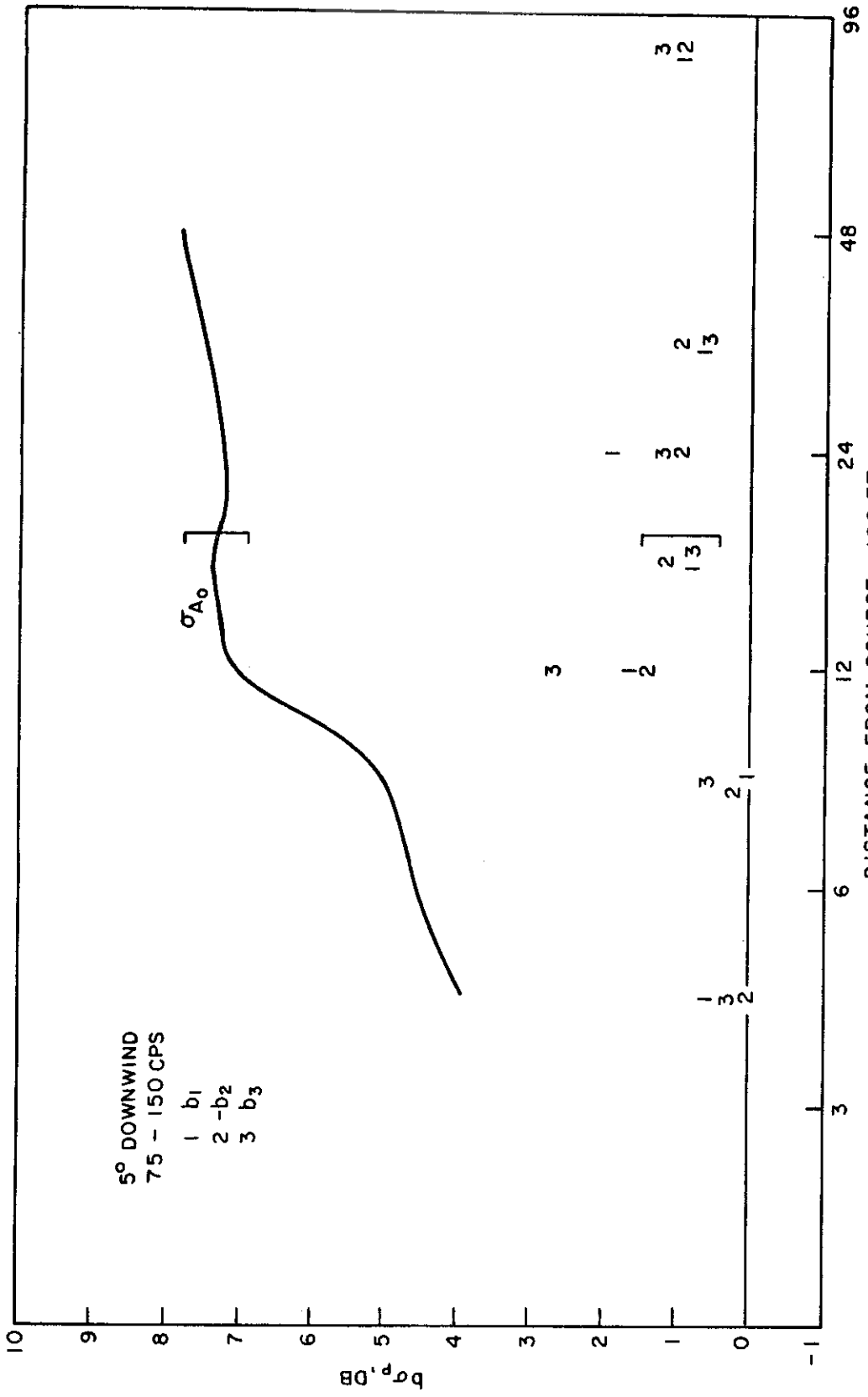

FIG. 42 - SAME AS FIG. 37, 5° DOWNWIND, 75-150 CPS

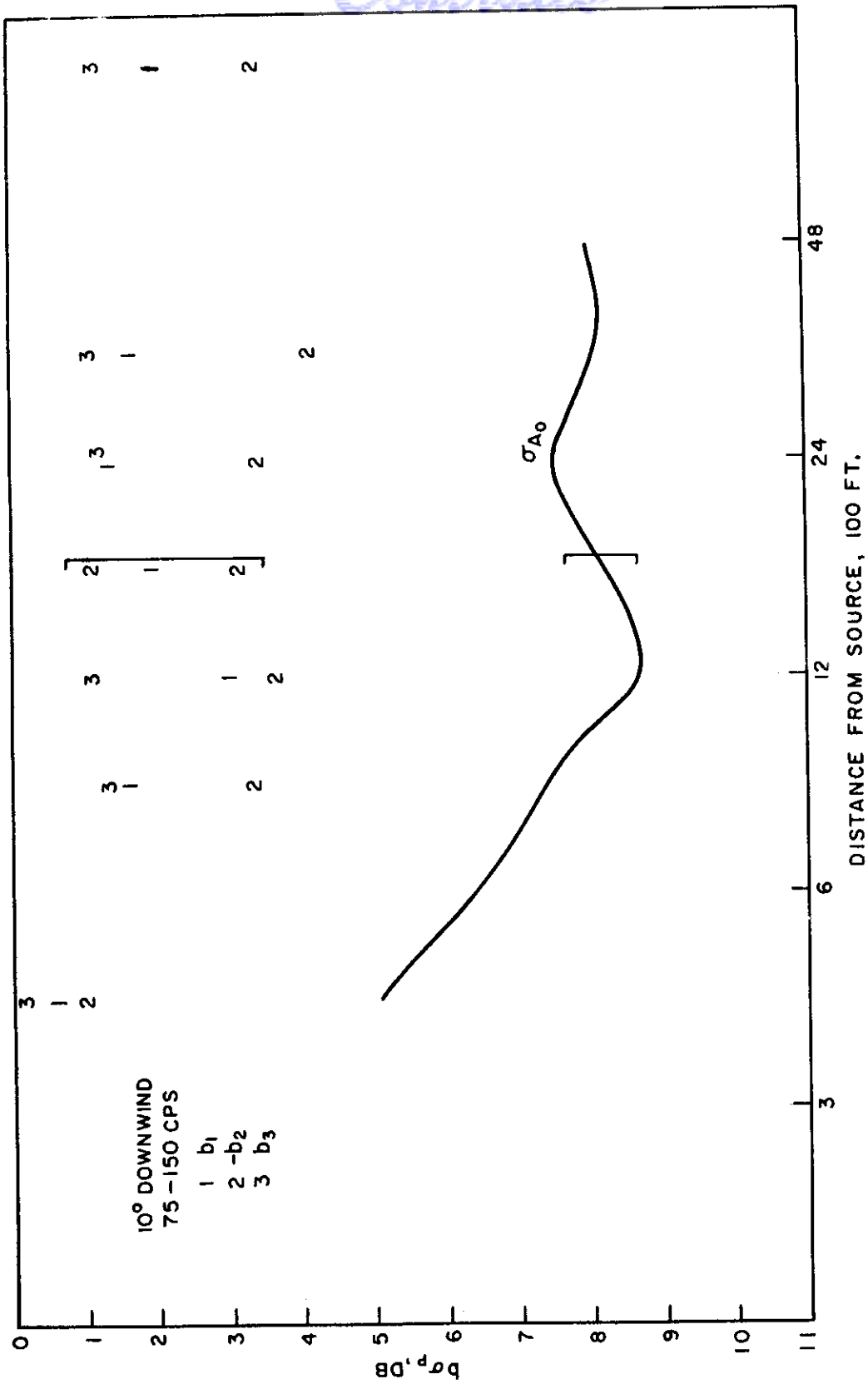

FIG. 43 - SAME AS FIG. 37, 10° DOWNWIND, 75-150 CPS

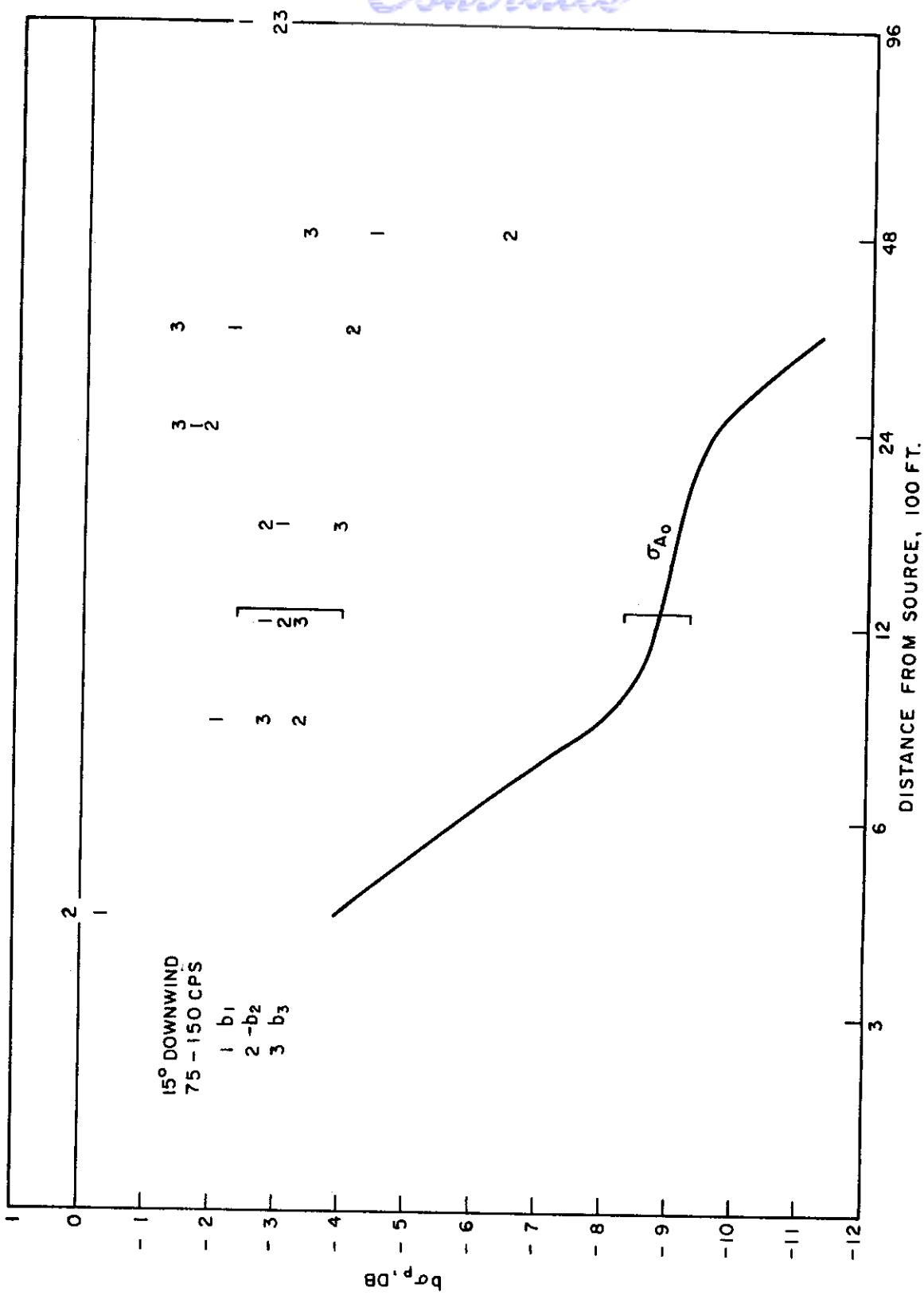

FIG. 44 - SAME AS FIG. 37, 15° DOWNWIND, 75-150 CPS

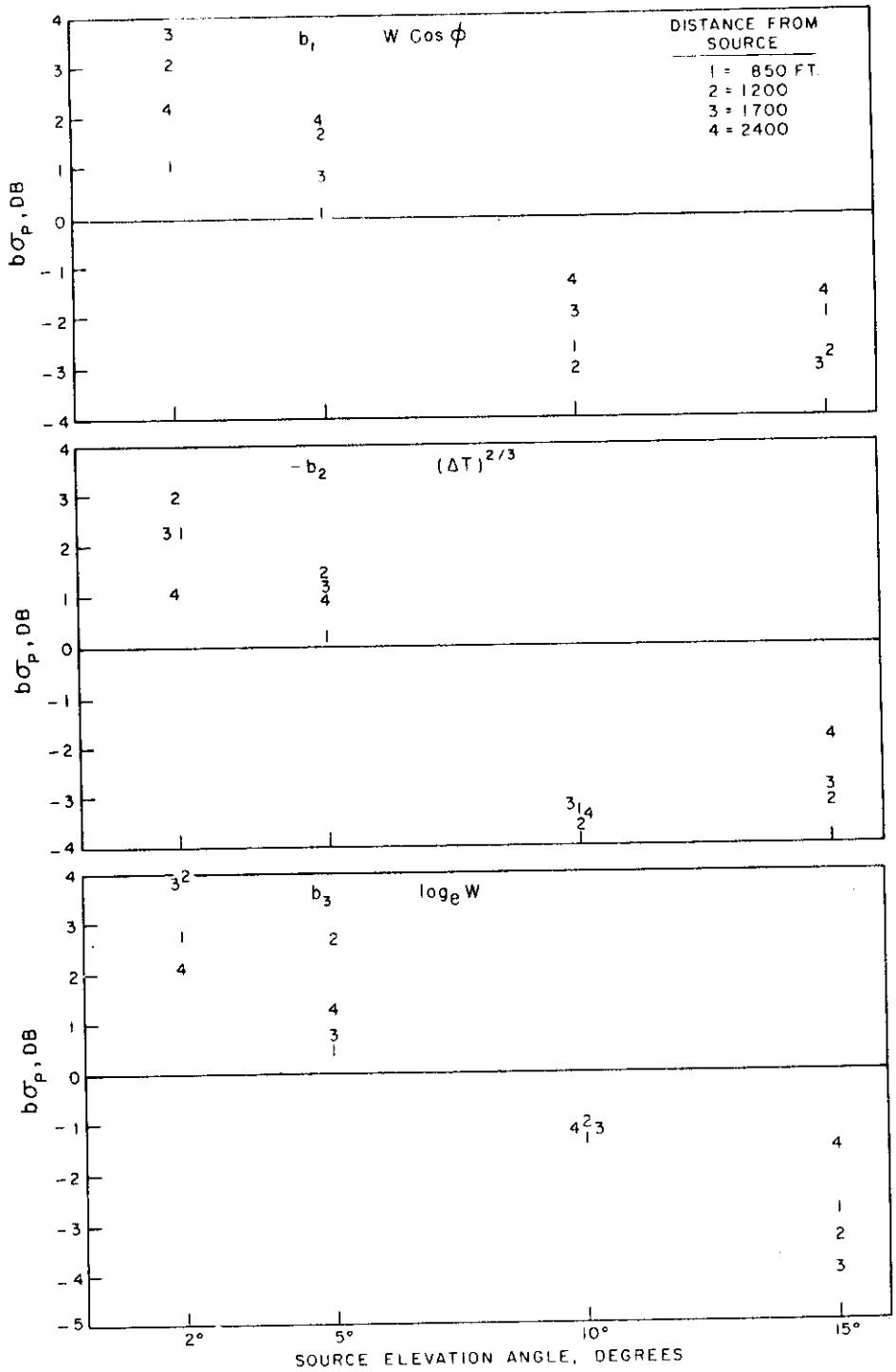

FIG. 45 - NORMALIZED REGRESSION COEFFICIENT, $b\sigma_p$, FOR DOWNWIND PROPAGATION IN THE 75-150 CPS FREQUENCY BAND, AS A FUNCTION OF SOURCE ELEVATION ANGLE

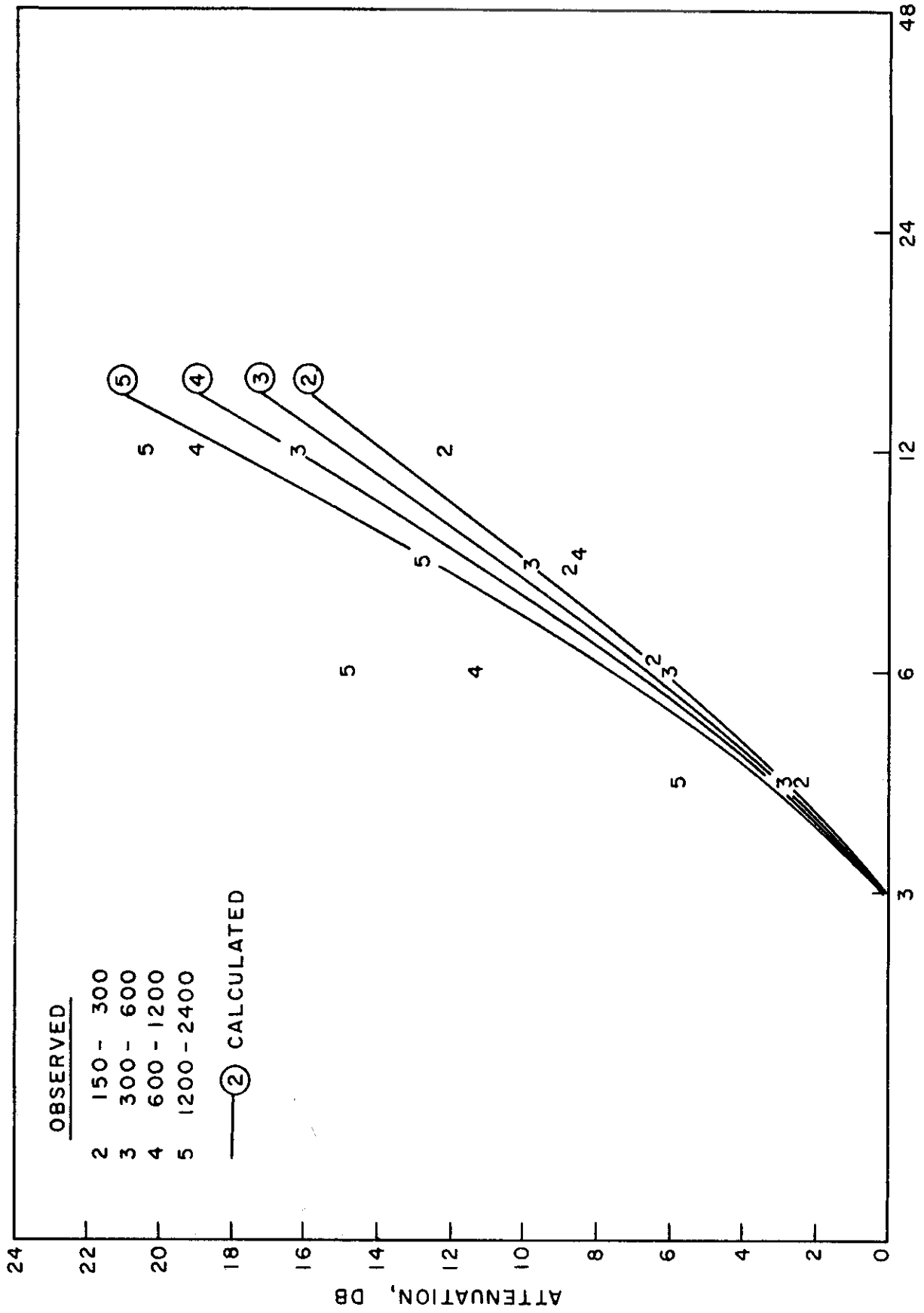

FIG. 46 - COMPARISON OF OBSERVED RESIDUAL ATTENUATIONS, A_o, AVERAGED FOR FIVE UPWIND PASSES AT 2° ELEVATION WITH THEORETICAL ATTENUATION OF SOUND DIFFRACTED INTO SHADOW ZONE, FOR ESTIMATED AVERAGE SOUND VELOCITY GRADIENT AT 5 FT. HEIGHT OF 0.4 SEC-1

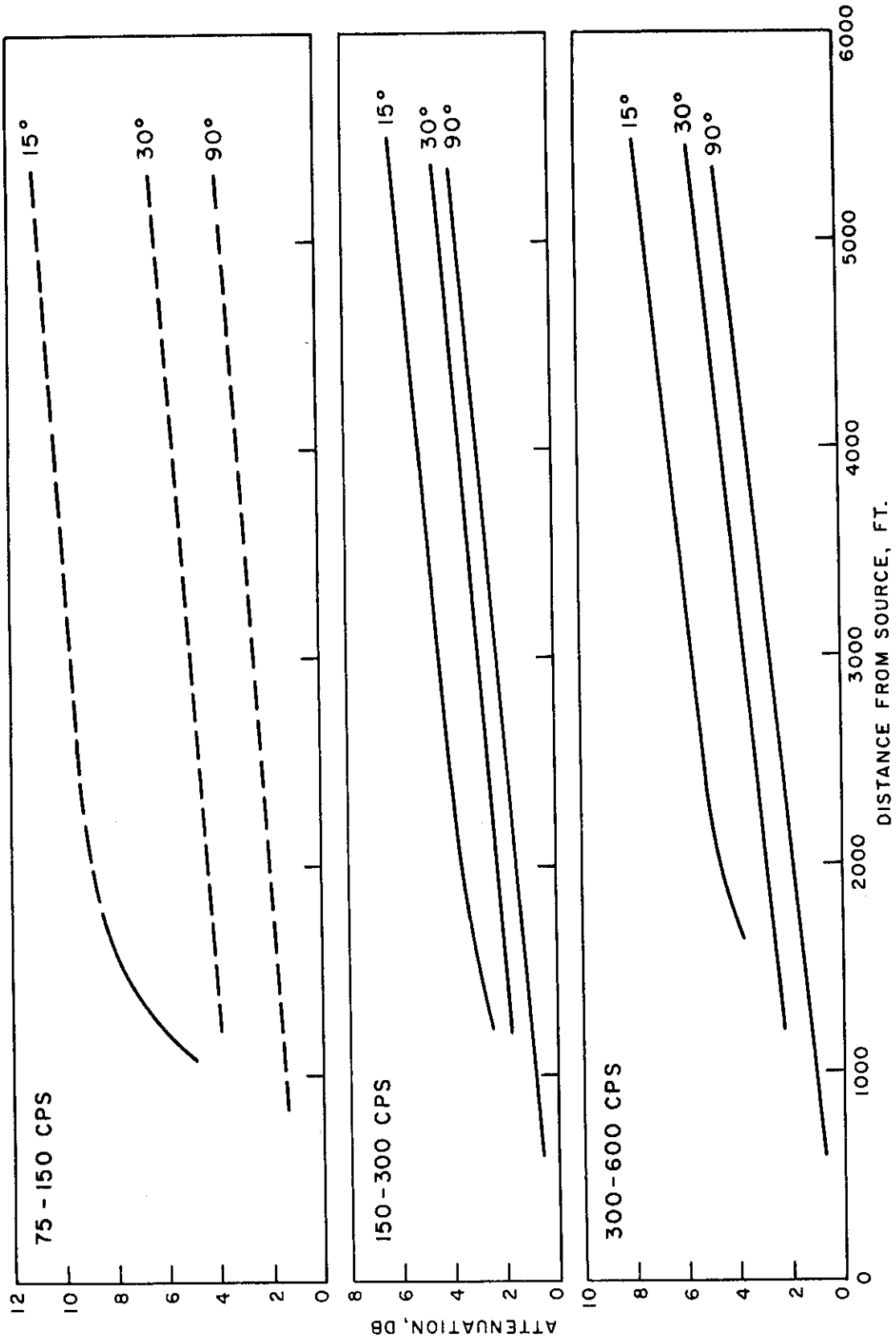

FIG. 50-A - AVERAGE RESIDUAL ATTENUATION, $\bar{A}_o$, AS A FUNCTION OF DISTANCE FROM SOURCE AND SOURCE ELEVATION FROM 15° TO 90°. 75-600 cps.

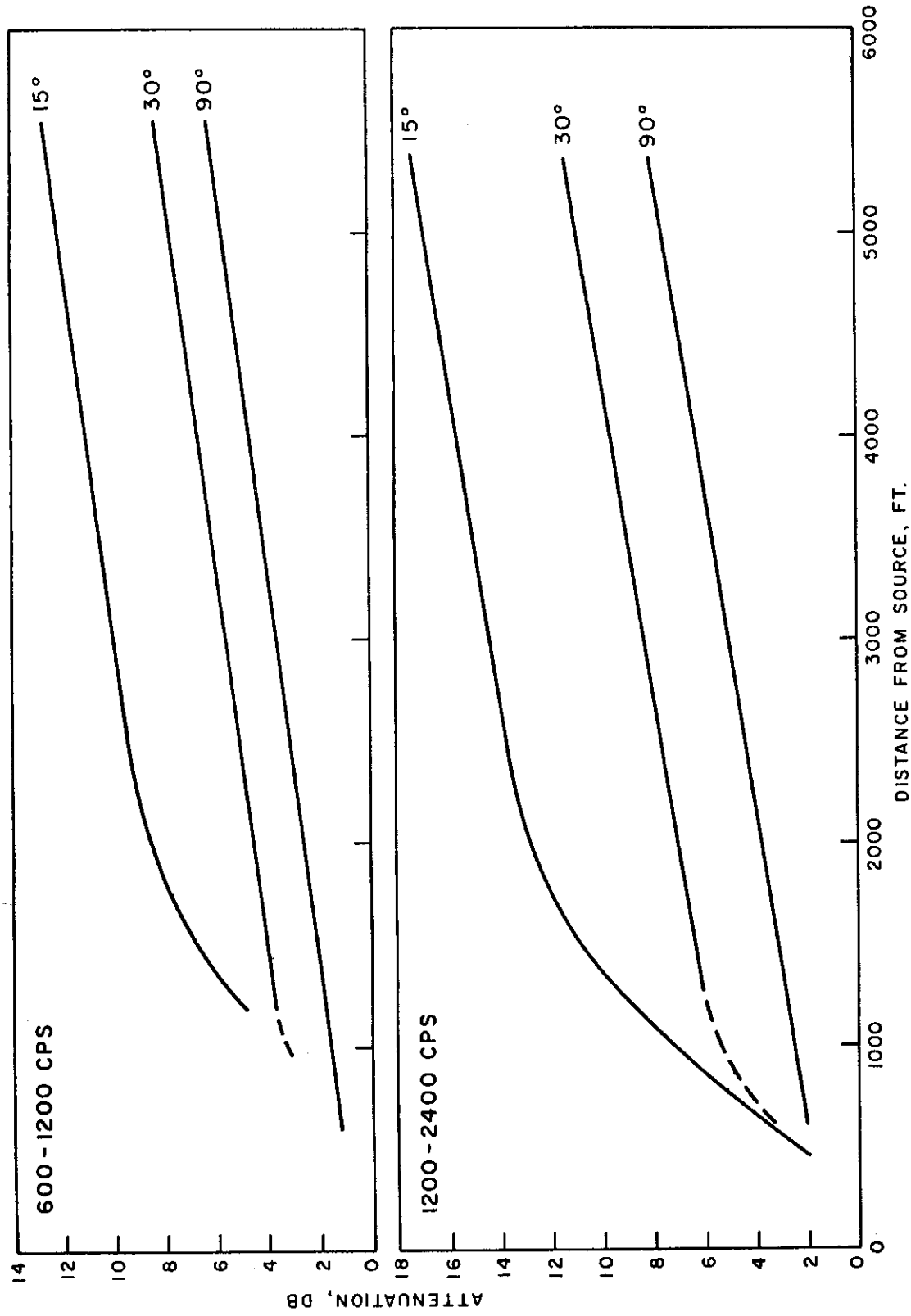

FIG. 50-B - 600-2400 CPS

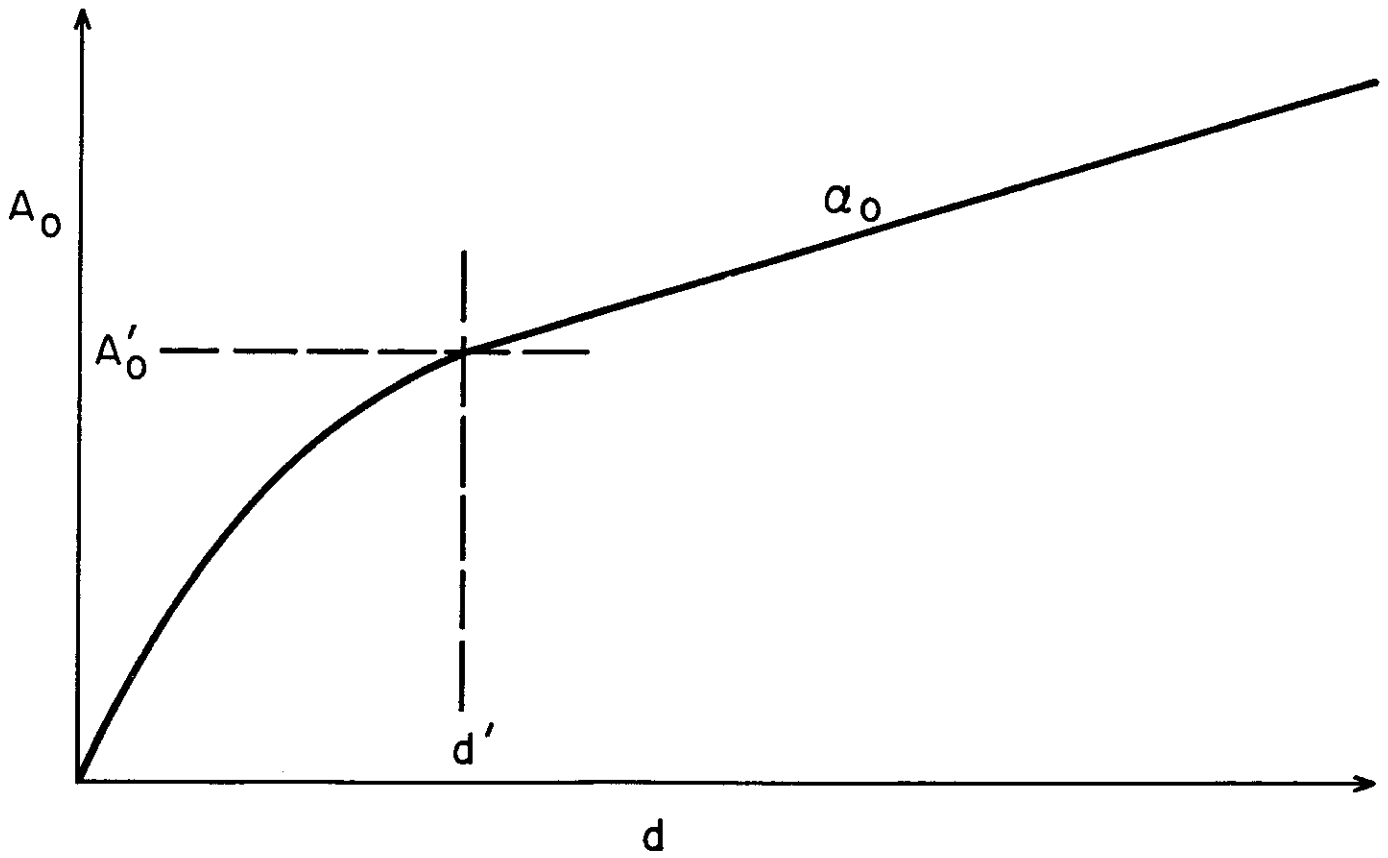

FIG. 51 - EQUATION FOR DETERMINING AVERAGE RESIDUAL ATTENUATION AS A FUNCTION OF DISTANCE FROM SOURCE d FOR SOURCE ELEVATIONS OF 15° TO 90°

APPENDIX A

TABLES

Table I

Airplane Passes

Code	Type	Altitude	Range	Elevation	Direction
1	Circle	600 ft	1200 ft	30°	
2a	Overhead	600	600	90°	Against wind
2b	Overhead	600	600	90°	Wind on plane's left
2c	Overhead	600	600	90°	With wind
2d	Overhead	600	600	90°	Wind on plane's right
3	Circle	1200	2400	30°	
4a,b,c,d	Overhead	1200	1200	90°	See pass 2
5	Circle	2400	4800	30°	
6a,b,c,d	Overhead	2400	2400	90°	See pass 2
7a,b,c,d	Overhead	4800	4800	90°	See pass 2
8	Circle	600	2400	14.5°	
9	Circle	1200	4800	14.5°	
10	Circle	2400	9600	14.5°	
11E, 11E2	Dive			15°	From East
11W, 11W2	Dive			15°	From West
12E, 12E2	Dive			10°	From East
12W, 12W2	Dive			10°	From West
13E, 13E2	Dive			5°	From East
13W, 13W2	Dive			5°	From West
14E, 14E2	Dive			2°	From East
14W, 14W2	Dive			2°	From West

Note: Overhead passes were used to obtain data on propagation from the airplane directly overhead only. Hence, the elevation angle is given as 90° and the altitude and range are the same.

Table II

Weather Parameters

Parameter	Measuring Altitude, ft	Illinois Min.	Illinois Max.	Arizona Min.	Arizona Max.	Overall Mean	Standard Deviation
T Temp., °F	5	54	87	42	83	69	8.5
	600	56	86	50	82	71	8.5
	1200	54	84	50	80	69	8.5
	2400	55	79	41	75	65	8.5
	4800	45	77	36	70	60	8.5
g Temp. gradient, °F/1000 ft, measured between 5 ft and	600	-23	10	-32	5	- 4.2	4.5
	1200	-11	8	-14	4	- 0.6	2.6
	2400	- 3	5	- 6	4	1.2	1.7
	4800	- 1	5	- 4	4	0.8	0.8
W Wind velocity, ft/sec, averaged between ground and	600	1.7	44.9	1.5	42.7	14	9
	1200	4.0	46.6	2.2	26.7	16	10
	2400	5.6	49.1	2.8	24.3	18	12
	4800	6.1	53.3	5.6	26.5	20	13
G Wind gradient, ft/sec/1000 ft, between ground and	600					17	19
	1200					14	11
	2400					15	9
	4800					20	10
h Absolute humidity, gm/m^3,	3	5	22	1	12	9.5	
(for band 5)*				2			
(for band 6)				3			
$H = (T+45)/h^2$	3	0.3	3	1	54	4.1	
(for band 5)*					20		
(for band 6)					10		
W cos ∅ Component of wind parallel to dive pass, ft/sec, averaged between ground and	600					7.7	6.9

Table II (Continued)

Parameter	Measuring Altitude, ft	Illinois Min.	Illinois Max.	Arizona Min.	Arizona Max.	Overall Mean	Standard Deviation
$(W \cos \phi)^{2/3}$						3.6	2.3
$(\Delta T)^{2/3}$ °F between ground (5') and	600					1.96	1.04
$\log_e W$ averaged between ground and	600					2.43	.70

* Values of h less than those indicated for frequency bands 5 and 6 were not used in correlations, since humidity function, H, is not valid.

Table III

Average Values of Atmospheric Attenuation, $\bar{A}_a$, in db and Residual Attenuation, $\bar{A}_o = \bar{A}_a - \bar{A}_H$, and Standard Deviations, σ_a, for Circle and Overhead Passes

Source elevation angle	Distance from source ft d_1	d_2	Distance interval ft	Frequency Bands 75-150 $\bar{A}_a$	$\bar{A}_o$	σ_a	150-300 $\bar{A}_a$	$\bar{A}_o$	σ_a	300-600 $\bar{A}_a$	$\bar{A}_o$	σ_a	600-1200 $\bar{A}_a$	$\bar{A}_o$	σ_a	1200-2400 $\bar{A}_a$	$\bar{A}_o$	σ_a	2400-4800 $\bar{A}_a$	$\bar{A}_o$	σ_a
90°	600	1200	600	1.3	1.3	1.4	1.3	1.3	1.3	1.4	1.4	1.9	1.8	1.6	1.9	3.0	2.3	2.8	5.0	2.1	6.6
	600	2400	1800	2.3	2.3	1.9	2.2	2.2	2.0	2.2	2.1	2.4	3.6	3.1	3.1	5.1	3.0	4.4	(7.0)		(7.8)
	600	4800	4200	(2.1)	(2.1)	(2.1)	2.5	2.4	2.0	3.4	3.1	2.9	5.8	4.6	3.9	9.4	4.4	8.0	(10.6)		(10.5)
30°	1200	2400	1200	2.2	2.2	2.5	2.2	2.2	2.0	1.8	1.7	1.5	1.8	1.5	2.0	3.9	2.5	2.7	(2.6)		(3.9)
	2400	4800	2400	(0.6)	(0.6)		1.1	1.1		1.7	1.5		3.2	2.5		(2.5)			(0)		
	1200	4800	3600	(2.8)	(2.8)	(3.1)	3.4	3.3	1.9	3.8	3.5	2.5	5.1	4.1	3.2	(6.4)		(4.8)	(1.1)		(6.3)
14.5°	2400	4800	2400	(0.2)	(0.2)	(2.1)	0.8	0.8	1.7	1.8	1.6	1.5	2.9	2.2	2.6	(2.8)		(3.6)			
	2400	9600	7200				0.2	0.1	2.5	3.4	2.9	2.7	(5.5)	(3.4)	(4.9)	(1.2)		(5.3)			

Values in parentheses are subject to question because of low signal-to-noise ratio.

Table IV

Comparison of Mean Weather Parameters for 1st and 2nd Years

	Illinois 1st year	Illinois and Arizona 2nd year
Temperature, °F	53	69
Temperature gradient, °F/1000 ft., between 5 ft and 600 ft	1.2	-4.2
Wind velocity, ft/sec, averaged between ground and 600 ft.	19	14
Absolute humidity, gm/m^3	6.1	9.5

Table V

Mean Value, $\bar{A}_o$, and Standard Deviation, σ, of Residual Atmospheric Attenuation, $A_o = A_a - A_H$, for Dive Passes

Source elevation angle	Direction of Propagation	Distance interval ft	Frequency Band 75-150 $\bar{A}_o$	75-150 σ	150-300 $\bar{A}_o$	150-300 σ	300-600 $\bar{A}_o$	300-600 σ	600-1200 $\bar{A}_o$	600-1200 σ	1200-2400 $\bar{A}_o$	1200-2400 σ	2400-4800 $\bar{A}_o$	2400-4800 σ
2°	Upwind	425-300	3.7	4.1	4.0	4.8	3.0	4.5	3.3	4.8	4.5	6.4	2.6	5.2
		600	3.3	6.7			5.6	6.4	6.0	8.9	6.0	9.5	2.1	8.9
		850	6.1	9.7	7.8	8.4	6.6	11.3	9.9	11.6	9.8	11.8	4.8	10.0
		1200	9.9	11.0	10.0	9.8	10.3	13.0	15.8	12.3	15.9	12.8	9.2	13.4
		1700	10.4	9.0	10.5	9.0	12.8	12.4	18.4	10.6	19.1	11.6	11.4	7.2
		2400	8.6	8.0	12.0	9.5	14.5	11.3	20.5	10.8	18.3	10.1		
		3400	7.0	6.7	11.6	8.9	14.6	11.0	20.1	11.7	16.5	10.3		
		4800	5.9	6.5	12.7	6.9	15.2	10.9	20.8	9.7				
		6800	4.2		12.4	8.8	14.3	11.6	17.1	5.8				
		9600	-.9		8.7	8.8	11.3	9.4						
	Downwind	425-300	5.7	4.3	3.8	2.9	2.3	3.3	.9	3.7	2.2	4.4	2.6	4.2
		600	4.6	5.4	2.3	4.0	.2	5.2	.1	5.0	2.4	4.6	2.0	7.1
		850	5.2	6.7	4.3	5.8	3.5	6.8	1.9	7.3	3.9	6.9	2.6	8.3
		1200	7.8	8.9	6.9	6.7	6.0	6.3	6.2	9.2	7.1	8.1	9.0	12.5
		1700	10.7	8.4	9.0	6.1	9.4	7.2	10.1	8.6	11.4	9.0	12.2	8.1
		2400	11.8	6.3	9.2	6.1	12.1	7.5	10.0	9.1	14.0	8.8		
		3400	12.2	5.3	10.4	7.1	13.7	8.3	11.3	9.8	16.5	5.0		
		4800	10.2	6.1	13.2	8.5	15.6	9.7	11.1	8.6	15.3	6.7		
		6800	7.7	3.6	15.5	8.3	17.2	9.3	12.4	9.1				
		9600	-.2	6.4	10.5	8.0	15.6	8.9	6.9	10.1				

Data below line are based on less than 80 per cent of the number of cases at 425 ft and are subject to question.

Table V (Continued)

Source elevation angle	Direction of Propagation	Distance interval ft	Frequency Band 75-150 $\bar{A}_o$	75-150 σ	150-300 $\bar{A}_o$	150-300 σ	300-600 $\bar{A}_o$	300-600 σ	600-1200 $\bar{A}_o$	600-1200 σ	1200-2400 $\bar{A}_o$	1200-2400 σ	2400-4800 $\bar{A}_o$	2400-4800 σ
5°	Upwind	425-300	2.7	4.0	1.3	2.8	.4	4.0	1.0	3.8	4.5	6.4	.1	4.4
		600	.5	5.4	-.2	3.1	-2.4	5.6	.3	5.0	6.0	9.5	.1	6.5
		850	.9	6.2	1.0	4.7	-2.6	8.0	2.1	7.3	9.8	11.8	1.1	7.4
		1200	4.8	8.3	2.5	6.3	1.0	10.5	6.4	9.2	15.9	12.8	5.2	12.0
		1700	7.3	7.0	4.5	6.7	3.6	11.4	10.4	8.7	19.1	11.6	7.2	18.0
		2400	8.3	6.9	5.1	6.9	3.5	10.8	10.4	9.0	18.3	10.1		
		3400	7.3	7.0	6.0	6.8	5.1	10.9	11.4	9.8	16.5	10.3		
		4800	3.3	7.8	6.7	6.6	5.0	9.9	11.3	8.2				
		6800	-2.8	8.0	4.3	8.7	5.6	10.6	12.3	9.0				
		9600	-7.2	9.0	-1.3	8.3	1.3	11.0	6.8	10.2				
	Downwind	425-300	5.0	4.0	1.8	2.5	1.8	3.3	1.1	3.1	2.2	4.4	2.6	4.5
		600	3.2	4.6	.9	3.7	-.6	4.0	.1	3.7	2.4	4.6	.9	7.3
		850	2.9	5.0	2.1	5.5	-1.0	4.6	1.0	5.0	3.9	6.9	2.9	6.4
		1200	6.0	7.1	4.2	6.3	1.8	6.0	4.7	6.1	7.1	8.1	8.0	9.6
		1700	9.8	7.4	6.3	6.9	4.5	6.4	6.8	5.4	11.4	9.0	8.7	13.2
		2400	10.8	7.2	7.1	6.8	6.3	6.9	8.0	5.9	14.0	8.8	6.2	12.9
		3400	10.1	7.5	7.5	6.6	6.3	6.7	10.9	6.6	16.5	5.0		
		4800	8.9	7.8	9.0	7.3	7.7	7.6	14.7	5.9	15.3	6.7		
		6800	5.9	6.6	8.2	8.1	6.1	6.6	13.9	5.6				
		9600	-2.3	5.6	4.7	8.6	5.7	7.8	6.6	7.4				

Table V (Continued)

Source elevation angle	Direction of Propagation	Distance interval ft	Frequency Band 75-150 $\bar{A}_o$	75-150 σ	150-300 $\bar{A}_o$	150-300 σ	300-600 $\bar{A}_o$	300-600 σ	600-1200 $\bar{A}_o$	600-1200 σ	1200-2400 $\bar{A}_o$	1200-2400 σ	2400-4800 $\bar{A}_o$	2400-4800 σ
10°	Upwind	425-300	1.9	3.9	-.4	3.2	5.6	2.9	1.1	3.6	1.3	3.8	1.6	6.2
		600	.5	5.4	-3.7	4.2	-1.8	3.5	-.9	4.3	1.1	4.2	1.7	7.4
		850	-.8	5.5	-3.5	4.5	.1	4.2	1.3	5.1	4.1	4.9	3.8	9.6
		1200	4.2	5.9	-2.4	6.1	3.3	5.1	4.5	5.2	8.0	5.1	7.3	14.0
		1700	5.7	6.2	-1.6	7.0	4.6	5.4	6.1	5.4	10.0	5.9	12.7	8.2
		2400	5.1	6.0	-1.0	7.3	6.2	4.9	7.9	4.9	11.6	6.1		
		3400	2.8	6.6	-1.2	7.6	7.0	6.2	8.9	5.1	14.0	5.4		
		4800	1.1	8.3	-2.2	8.3	6.5	6.6	10.5	6.0	13.1	7.8		
		6800	-2.0	10.4	-5.0	8.3	6.5	8.8	10.9	5.3				
		9600	-7.3	9.8	-1.1	10.0	-.5	7.1	3.8	7.4				
	Downwind	425-300	4.5	5.0	.9	2.9	1.3	3.1	2.1	3.5	1.7	3.3	2.8	4.6
		600	3.4	6.4	-1.8	4.4	-1.4	3.6	.5	3.6	1.3	4.5	3.0	5.8
		850	3.9	7.4	-1.8	5.4	-.6	5.3	1.6	5.2	3.8	5.0	4.9	6.6
		1200	6.9	8.7	1.0	6.0	2.3	5.0	5.4	5.7	7.0	4.8	7.3	10.4
		1700	10.8	8.3	2.4	6.3	4.2	5.7	8.4	5.5	10.2	5.3	10.0	14.6
		2400	11.1	7.5	2.9	6.3	5.5	5.4	8.7	5.0	12.4	6.6	10.0	10.4
		3400	9.5	9.1	3.3	7.0	8.0	6.7	12.1	6.9	15.1	6.0		
		4800	7.4	9.0	2.3	6.3	8.0	6.2	12.2	6.3	15.3	7.2		
		6800	5.2	8.3	3.1	7.2	8.9	7.6	11.9	6.1				
		9600	-2.6	12.9	5.6	6.6	1.2	7.1	5.9	7.6				

Table V (Continued)

Source elevation angle	Direction of Propagation	Distance interval ft	Frequency Band 75-150 $\bar{A}_o$	75-150 σ	150-300 $\bar{A}_o$	150-300 σ	300-600 $\bar{A}_o$	300-600 σ	600-1200 $\bar{A}_o$	600-1200 σ	1200-2400 $\bar{A}_o$	1200-2400 σ	2400-4800 $\bar{A}_o$	2400-4800 σ
15°	Upwind	425-300	2.9	3.8	1.0	2.5	.5	2.8	1.2	3.0	.7	3.3	2.1	4.5
		600	1.7	5.7	-.1	4.0	-2.5	3.6	-.4	3.2	1.2	4.9	2.9	6.1
		850	2.8	7.0	.7	5.8	-2.3	4.0	1.7	4.1	3.2	4.8	3.8	11.9
		1200	7.2	6.7	4.7	4.6	.2	4.5	4.6	4.3	7.4	6.2	9.5	10.2
		1700	7.6	6.7	5.0	4.1	1.9	4.5	7.6	5.3	10.5	5.9	13.6	13.1
		2400	7.0	6.5	4.5	4.5	3.8	4.5	8.3	5.2	12.2	5.9	8.1	27.6
		3400	4.5	6.5	4.4	4.8	4.0	5.1	9.7	5.8	13.8	6.3		
		4800	-4.4	6.4	2.4	5.2	6.4	6.7	12.2	6.3	15.0	5.7		
		6800	-2.3	8.2	2.2	6.0	7.8	6.4	11.4	12.1				
		9600	-8.3	8.9	-9.4	5.4	-.6	6.3	2.6	18.9				
	Downwind	425-300	1.8	3.9	1.1	3.1	2.5	2.8	1.2	3.1	2.0	2.9	3.1	4.1
		600	2.1	5.8	-.6	3.9	-.9	3.6	-.8	3.5	1.2	4.2	4.0	7.0
		850	3.2	7.9	.9	5.2	-.2	3.9	1.4	4.7	3.6	5.2	6.8	6.2
		1200	6.8	8.8	3.9	5.5	2.5	4.3	4.8	4.6	7.7	4.9	11.6	10.5
		1700	9.4	9.1	5.7	4.5	5.0	5.0	8.2	5.1	10.6	5.6	14.6	13.0
		2400	8.0	9.6	5.4	4.0	6.1	5.2	9.8	5.2	12.8	5.9	18.0	10.1
		3400	7.5	11.3	5.4	5.3	7.3	6.0	11.2	7.0	16.3	5.0		
		4800	7.3	12.9	5.2	5.5	8.9	5.9	14.0	7.1	19.0	6.5		
		6800	-3.0	12.3	3.4	6.2	10.0	7.1	12.2	12.1				
		9600	-10.7	8.3	-5.6	5.6	3.5	7.1	3.2	17.4				

Table VI

Simple Regression Coefficients, b, of Residual Atmospheric Attenuation, A_o, with Respect to Weather Parameters for Dive Passes

σ_p = standard deviation of parameter.

Frequency band	Source elevation angle	Direction of propagation	Distance interval ft	b_1 W cos ∅	b_2 $(\Delta T)^{2/3}$	b_3 $\log_e$ W	b_4 $(W \cos \emptyset)^{2/3}$
				σ_p=6.9	1.04	.70	2.25
				$1/\sigma_p$=.145	.96	1.44	.445
75-150	2°	Upwind	425-300	0.096	-1.58	1.60	0.293
			600	0	-	-	-
			850	0.432	-2.45	6.87	1.23
			1200	0.706	-4.03	8.96	2.05
			1700	0.593	-3.38	5.90	1.73
			2400	0.022	-3.98	2.05	0.036
			3400	-0.027	-1.50	0.849	-0.081
			4800	-0.126	-0.909	0.557	-0.241
			6800	-0.257	-2.99	-2.06	-0.780
			9600	-0.528	-0.119	-1.11	-1.19
		Downwind	425-300	0.085	-0.851	1.17	0.214
			600	0	-	-	-
			850	0.165	-2.24	3.96	0.383
			1200	0.442	-2.84	5.68	1.16
			1700	0.536	-2.20	5.65	1.48
			2400	0.317	-1.06	3.03	0.877
			3400	0.075	-0.508	0.652	0.266
			4800	-0.089	-0.656	0.568	-0.233
			6800	0.133	-0.162	-0.625	0.300
			9600	0.063	1.78	1.87	-0.072
	5°	Upwind	425-300	0.102	-0.895	1.67	0.333
			600	0	-	-	-
			850	0.201	-0.280	2.71	0.569
			1200	0.232	-1.50	4.89	0.656
			1700	0.326	-1.42	3.87	0.944
			2400	0.230	-1.85	2.32	0.676
			3400	0.301	-2.03	3.03	0.919
			4800	0.319	0.454	4.27	0.988
			6800	0.394	0.105	2.82	0.580
			9600	0.239	2.19	4.75	0.210
		Downwind	425-300	0.070	-0.061	0.475	0.210
			600	0	-	-	-
			850	0.012	-0.195	0.890	0.040
			1200	0.241	-1.36	3.83	0.726
			1700	0.112	-1.12	1.21	0.378
			2400	0.279	-0.966	1.71	0.699
			3400	0.100	-0.945	0.817	0.180
			4800	0.232	1.47	3.06	0.449
			6800	0.252	2.93	3.57	0.618
			9600	0.201	2.18	-1.32	0.577

Data below line are based on less than 80 per cent of the number of cases at 425 ft and are subject to question.

Table VI (Continued)

Frequency band	Source elevation angle	Direction of propagation	Distance interval ft	b_1 W cos Ø	b_2 $(\Delta T)^{2/3}$	b_3 $\log_e$ W	b_4 $(W \cos Ø)^{2/3}$
75-150	10°	Upwind	425-300	0.069	-0.224	1.54	0.199
			600	0	-	-	-
			850	-0.039	1.68	0.041	-0.114
			1200	-0.022	0.586	1.32	-0.072
			1700	0.003	0.341	0.809	0.047
			2400	0.038	-0.145	1.06	0.114
			3400	0.163	-0.666	2.10	0.455
			4800	0.203	-0.888	3.87	0.545
			6800	0.675	-0.008	6.13	1.75
			9600	0.536	-0.644	5.40	1.46
		Downwind	425-300	-0.075	0.919	-0.116	-0.222
			600	0	-	-	-
			850	-0.232	3.12	-1.85	-0.682
			1200	-0.438	3.50	-1.60	-1.29
			1700	-0.280	2.96	-1.54	-0.792
			2400	-0.183	3.26	-1.76	-0.500
			3400	-0.231	3.98	-1.54	-0.748
			4800	-0.397	2.80	-1.79	-1.11
			6800	-0.308	-0.62	-3.47	-1.01
			9600	-0.424	2.16	-1.61	-1.39
	15°	Upwind	425-300	0.0189	-0.327	0.538	0.050
			600	-	-	-	-
			850	-	-	-	-
			1200	-	-	-	-
			1700	-0.100	0.317	-0.268	-0.332
			2400	-0.049	1.49	-0.467	-0.148
			3400	0.065	0.582	2.45	0.144
			4800	0.228	0.369	2.93	0.554
			6800	0.059	1.99	8.84	-0.124
			9600	0.154	1.95	5.66	0.322
		Downwind	425-300	-0.044	-0.103	0.332	-0.087
			600	0	-	-	-
			850	-0.289	3.27	-3.98	-0.855
			1200	-0.409	3.02	-4.76	-1.23
			1700	-0.415	2.67	-4.13	-1.20
			2400	-0.229	1.73	-2.13	-0.648
			3400	-0.317	3.93	-2.01	-0.876
			4800	-0.631	6.18	-4.88	-1.81
			6800	-0.403	7.53	1.44	-1.31
			9600	-0.164	-1.80	-4.79	-0.658

Table VI (Continued)

Frequency band	Source elevation angle	Direction of propagation	Distance interval ft	b_1 W cos Ø	b_2 $(\Delta T)^{2/3}$	b_3 $\log_e W$	b_4 $(W \cos Ø)^{2/3}$
150-300	2°	Upwind	425-300	0.289	-1.05	3.39	0.862
			600				
			850	0.480	-1.80	5.99	1.50
			1200	0.810	-2.79	8.27	2.49
			1700	0.695	-2.62	5.47	1.88
			2400	0.693	-4.24	4.69	1.77
			3400	0.421	-1.58	2.42	1.04
			4800	-0.140	0.824	-1.26	-0.175
			6800	-0.588	3.37	-0.229	-1.49
			9600	-0.335	4.95	-0.162	-0.780
		Downwind	425-300	0.048	-1.17	0.938	0.154
			600	-0.067	-1.60	0.399	-0.235
			850	-0.127	-1.09	-0.081	-0.472
			1200	0.020	-1.47	1.63	0.021
			1700	0.012	-0.999	2.14	0.037
			2400	-0.103	-1.20	0.427	-0.278
			3400	-0.057	-1.20	-1.27	-0.176
			4800	-0.203	-0.210	-1.77	-0.578
			6800	-0.245	0.818	-1.74	-0.699
			9600	-0.483	3.69	-2.87	-1.20
	5°	Upwind	425-300	0.073	-0.392	0.917	0.216
			600	0.124	0.102	0.803	0.359
			850	0.243	-0.369	2.72	0.720
			1200	0.349	-1.42	3.83	1.03
			1700	0.327	-1.52	3.88	0.976
			2400	0.342	-2.25	3.82	1.04
			3400	0.330	-1.82	2.27	0.998
			4800	0.178	-0.917	2.19	0.516
			6800	0.191	1.47	-0.193	0.680
			9600	-0.047	0.608	-0.405	0.021
		Downwind	425-300	0.099	-0.040	0.530	0.309
			600	0.023	0.693	-0.113	0.086
			850	-0.077	1.21	-0.952	-0.194
			1200	0.087	0.624	1.51	0.277
			1700	0.076	0.482	0.734	0.275
			2400	0.078	0.412	1.63	0.258
			3400	0.011	0.925	0.973	0.053
			4800	-0.163	1.73	-1.03	-0.466
			6800	-0.332	2.16	-2.62	-0.783
			9600	0.094	-0.548	-1.94	0.327

Table VI (Continued)

Frequency band	Source elevation angle	Direction of propagation	Distance interval ft	b_1 W cos Ø	b_2 $(\Delta T)^{2/3}$	b_3 $\log_e W$	b_4 $(W \cos Ø)^{2/3}$
150-300	10°	Upwind	425-300	0.116	-0.397	1.46	0.366
			600	-	-	-	-
			850	0.046	-0.005	1.50	0.159
			1200	0.055	-0.826	2.54	0.221
			1700	0.020	-1.36	1.87	0.089
			2400	0.050	-2.09	1.91	0.176
			3400	-0.123	-1.28	0.420	-0.326
			4800	0.027	-1.24	2.78	0.117
			6800	0.070	-1.72	2.85	0.295
			9600	0.401	-2.56	4.67	1.13
		Downwind	425-300	0.086	0.041	1.47	0.249
			600	0	-	-	-
			850	-0.016	1.77	0.667	-0.050
			1200	-0.087	1.67	1.20	-0.273
			1700	-0.035	1.38	1.22	-0.119
			2400	-0.007	1.26	1.01	-0.023
			3400	0.026	1.57	0.838	-0.055
			4800	-0.044	0.868	0.421	-0.234
			6800	-0.012	1.43	2.20	-0.110
			9600	0.163	1.03	2.16	0.436
	15°	Upwind	425-300	0.017	-0.108	-0.225	0.039
			600	0	-	-	-
			850	-0.068	1.99	-2.48	-0.219
			1200	-0.059	1.28	-1.33	-0.198
			1700	-0.160	1.40	-1.83	-0.471
			2400	-0.035	0.419	-0.654	-0.101
			3400	-0.125	0.250	-0.875	-0.403
			4800	-0.201	0.704	-1.77	-0.598
			6800	0.110	-0.115	2.23	0.302
			9600	-0.003	0.946	-3.85	0.076
		Downwind	425-300	0.110	-0.209	1.49	0.352
			600	0	-	-	-
			850	-0.056	0.990	-0.320	-0.145
			1200	-0.191	1.29	-0.693	-0.585
			1700	-0.031	1.48	0.210	-0.102
			2400	-0.051	0.861	-0.253	-0.141
			3400	0.017	1.23	0.391	0.045
			4800	0.002	1.26	-0.700	-0.023
			6800	-0.286	2.00	-3.67	-0.764
			9600	-0.097	0.136	0.358	-0.210

Table VI(Continued)

Frequency band	Source elevation angle	Direction of propagation	Distance interval ft	b_1 W cos Ø	b_2 $(\Delta T)^{2/3}$	b_3 $\log_e W$	b_4 $(W \cos Ø)^{2/3}$
300-600	2°	Upwind	425-300	0.286	-1.57	2.92	0.827
			600	0.350	-0.812	3.53	1.06
			850	0.727	-4.98	8.74	2.19
			1200	1.19	-5.71	10.87	3.35
			1700	1.23	-4.80	9.75	3.31
			2400	0.699	-3.63	7.20	2.11
			3400	0.318	-3.03	4.57	1.05
			4800	0.297	-1.51	1.88	0.942
			6800	-0.201	3.67	-0.710	-0.329
			9600	-0.337	1.59	-1.58	-0.705
		Downwind	425-300	-0.032	0.181	-0.620	-0.035
			600	-0.004	-1.84	0.541	-0.003
			850	-0.27	0.649	-2.46	-0.823
			1200	-0.024	-0.265	0.499	-0.025
			1700	0.024	0.873	-0.193	0.174
			2400	-0.032	0.883	-1.23	0.014
			3400	-0.136	1.13	-2.92	-0.344
			4800	-0.218	2.35	-4.02	-0.652
			6800	-0.314	3.27	-3.81	-1.01
			9600	-0.275	3.36	-4.59	-0.855
	5°	Upwind	425-300	0.094	-0.736	1.47	0.244
			600	0.213	-0.724	2.43	0.589
			850	0.303	-1.92	4.30	0.834
			1200	0.477	-3.38	6.37	1.34
			1700	0.611	-3.84	7.64	1.77
			2400	0.576	-3.77	6.13	1.61
			3400	0.487	-4.42	6.33	1.45
			4800	0.329	-4.59	6.14	0.857
			6800	0.305	-4.74	4.50	0.940
			9600	0.302	-5.37	4.23	0.927
		Downwind	425-300	0.067	0.319	0.434	0.223
			600	0.063	0.651	0.438	0.180
			850	-0.021	0.559	0.496	-0.056
			1200	0.145	-0.417	2.28	0.422
			1700	0.167	0.573	1.15	0.514
			2400	0.202	0.378	3.22	0.634
			3400	0.151	0.378	2.46	0.472
			4800	0.282	-0.392	3.48	0.768
			6800	0.190	-0.183	2.00	0.630
			9600	0.254	-0.501	2.90	0.813

Table VI (Continued)

Frequency band	Source elevation angle	Direction of propagation	Distance interval ft	b_1 W cos ∅	b_2 $(\Delta T)^{2/3}$	b_3 $\log_e W$	b_4 $(W \cos \emptyset)^{2/3}$
300-600	10°	Upwind	425-300	0.057	0.050	1.14	0.175
			600	0.107	0.027	1.57	0.304
			850	0.031	0.454	0.734	0.121
			1200	-0.041	0.413	0.423	-0.097
			1700	-0.075	0.420	-0.192	-0.178
			2400	-0.149	-0.166	0.136	-0.441
			3400	-0.177	-0.414	0.844	-0.510
			4800	-0.343	0.122	-0.219	-1.05
			6800	-0.288	-0.849	-0.455	-0.929
			9600	-0.038	-1.96	2.13	-0.389
		Downwind	425-300	0.151	-0.058	1.85	0.447
			600	0.145	0.171	2.27	0.441
			850	0.027	1.64	1.35	0.097
			1200	-0.024	1.01	1.12	-0.083
			1700	0.034	0.834	1.84	0.096
			2400	0.087	0.478	1.64	0.343
			3400	0.107	0.308	2.47	0.255
			4800	0.166	0.308	2.94	0.456
			6800	0.332	-0.661	5.12	1.05
			9600	0.095	-1.37	2.38	0.317
	15°	Upwind	425-300	0.021	-0.330	0.640	0.071
			600	0.081	-0.158	0.619	0.265
			850	-0.014	1.02	-0.714	-0.057
			1200	0.047	0.050	1.73	0.126
			1700	-0.052	0.701	0.572	-0.154
			2400	0.036	0.454	1.16	0.135
			3400	-0.058	-0.391	-0.163	-0.107
			4800	0.198	0.016	0.667	0.674
			6800	0.036	0.487	0.085	0.199
			9600	-0.020	0.519	-1.21	0.013
		Downwind	425-300	0.027	0.404	0.009	0.068
			600	0.128	0.488	0.843	0.371
			850	0.020	1.14	-0.131	0.063
			1200	0.045	0.924	0.850	0.129
			1700	0.127	1.03	1.26	0.324
			2400	0.036	1.16	0.264	0.109
			3400	0.159	2.28	-0.240	0.493
			4800	0.024	0.481	-1.13	0.096
			6800	-0.163	1.48	-0.933	-0.401
			9600	-0.066	0.134	1.12	-0.214

Table VI (Continued)

Frequency band	Source elevation angle	Direction of propagation	Distance interval ft	b_1 W cos ∅	b_2 $(\Delta T)^{2/3}$	b_3 $\log_e W$	b_3 $(W \cos \emptyset)^{2/3}$
600-1200	2°	Upwind	425-300	0.187	-1.28	2.35	0.542
			600	0.736	-3.79	7.08	2.06
			850	0.997	-4.98	9.37	2.72
			1200	1.14	-4.19	9.66	3.21
			1700	0.964	-3.33	6.14	2.75
			2400	0.662	-1.85	5.98	1.89
			3400	0.866	-2.39	3.75	2.35
			4800	0.807	-4.50	3.66	1.91
			6800	0.053	-3.90	-0.576	0.072
			9600	-0.344	-7.45	-0.309	-0.922
		Downwind	425-300	0.066	-0.248	1.54	0.177
			600	-0.071	0.683	0.102	-0.199
			850	0.053	-0.00	1.77	0.110
			1200	0.148	-0.568	3.69	0.358
			1700	0.311	-0.793	4.05	0.809
			2400	0.252	-0.478	3.79	0.633
			3400	0.511	-1.55	4.78	1.38
			4800	0.250	-2.48	3.06	0.542
			6800	-0.200	-2.85	1.03	-0.540
			9600	-0.165	-3.44	1.41	-0.630
	5°	Upwind	425-300	0.072	-0.264	1.56	0.198
			600	0.058	0.632	0.152	-0.156
			850	0.079	-0.118	1.88	0.191
			1200	0.157	-0.562	3.70	0.396
			1700	0.340	-0.844	4.12	0.905
			2400	0.324	-0.715	4.07	0.836
			3400	0.520	-1.47	4.75	1.42
			4800	0.249	-2.36	3.06	0.566
			6800	-0.359	-2.42	0.597	-0.873
			9600	-0.313	-2.88	0.957	-0.990
		Downwind	425-300	0.041	0.230	0.549	0.135
			600	-0.044	0.669	-0.832	-0.109
			850	0.024	0.753	0.105	0.041
			1200	0.286	0.255	3.11	0.709
			1700	0.282	0.693	2.11	0.759
			2400	0.297	0.403	2.87	0.840
			3400	0.189	-0.284	1.97	0.563
			4800	0.020	-0.702	1.73	0.020
			6800	-0.141	-0.771	2.44	-0.139
			9600	-0.182	-3.45	0.055	-0.563

Table VI (Continued)

Frequency band	Source elevation angle	Direction of propagation	Distance interval ft	b_1 W cos Ø	b_2 $(\Delta T)^{2/3}$	b_3 $\log_e W$	b_4 $(W \cos Ø)^{2/3}$
600-1200	10°	Upwind	425-300	0.171	0.677	1.69	0.470
			600	0.159	0.135	1.63	0.395
			850	0.122	0.324	1.14	0.305
			1200	0.079	-0.496	0.769	0.233
			1700	0.064	-0.052	-0.168	0.240
			2400	-0.153	-0.927	-0.447	-0.389
			3400	-0.002	-1.15	0.151	0.0169
			4800	-0.294	-0.582	-1.48	-0.799
			6800	-0.434	1.20	-2.01	-1.19
			9600	-0.107	-0.904	1.57	-0.153
		Downwind	425-300	0.099	-1.07	2.41	-0.794
			600	0.050	-0.996	2.12	-0.171
			850	-0.068	0.417	1.32	0.066
			1200	-0.073	-0.363	2.05	0.084
			1700	0.092	-0.054	2.25	-0.204
			2400	0.065	-0.786	2.18	-0.239
			3400	0.047	-1.25	3.21	-0.135
			4800	-0.239	-0.137	0.115	-0.278
			6800	-0.145	-0.614	1.82	-0.286
			9600	-0.245	-0.299	1.64	0.336
	15°	Upwind	425-300	-0.055	-0.683	0.999	-0.171
			600	0.193	0.293	0.381	0.066
			850	0.048	0.983	0.069	0.084
			1200	-0.064	0.628	0.803	0.204
			1700	-0.074	1.00	0.348	-0.239
			2400	-0.043	0.602	0.569	-0.135
			3400	-0.112	-0.162	0.037	-0.278
			4800	-0.088	0.807	1.25	-0.287
			6800	0.147	-3.20	4.26	0.336
			9600	-0.505	-4.03	2.70	-0.653
		Downwind	425-300	0.082	-0.553	1.24	0.238
			600				
			850	0.027	0.527	0.613	0.082
			1200	-0.110	0.588	0.244	-0.304
			1700	0.046	1.17	0.721	0.111
			2400	-0.077	0.051	-0.005	-0.172
			3400	0.022	0.267	-0.199	0.567
			4800	0.122	-0.517	1.08	0.270
			6800	-0.492	-2.51	0.516	-1.44
			9600	-0.256	-3.11	3.17	-0.929

Table VI (Continued)

Frequency band	Source elevation angle	Direction of propagation	Distance interval ft	b_1 W cos Ø	b_2 $(\Delta T)^{2/3}$	b_3 $\log_e$ W	b_4 $(W \cos Ø)^{2/3}$
1200-2400	2°	Upwind	425-300	.41	-.97	3.46	1.22
			600	.85	-2.42	6.94	2.28
			850	1.09	-3.10	9.44	3.07
			1200	.87	-3.90	9.59	2.60
			1700	.608	-2.75	4.69	1.79
			2400	.245	-2.13	1.25	.643
			3400	-.003	-.093	.708	.013
			4800	.143	3.15	1.92	.707
			6800	.144	1.56	.05	.865
			9600	-.35	-3.66	-2.7	-.77
		Downwind	425-300	0.063	-0.018	1.10	0.250
			600	0.014	-0.094	0.575	-0.061
			850	0.076	-0.664	1.94	0.171
			1200	0.269	-2.33	5.02	0.747
			1700	0.134	-1.93	3.37	0.477
			2400	-0.433	-0.648	-2.62	-1.34
			3400	-0.122	-1.32	-1.90	-0.335
			4800	0.073	-3.50	-5.51	0.361
			6800	1.89	1.26	3.17	3.94
			9600	0.945	-4.29	-0.874	1.93
	5°	Upwind	425-300	-0.012	-0.516	-0.149	-0.019
			600	0.140	-0.159	0.187	0.412
			850	0.130	-1.05	0.491	0.352
			1200	0.432	-0.626	2.59	1.23
			1700	0.475	0.314	2.00	1.35
			2400	0.219	0.251	0.941	0.561
			3400	0.124	-2.08	-0.851	0.407
			4800	0.399	-2.48	-2.27	1.31
			6800	-0.023	-1.49	-1.05	0.577
			9600	-0.032	-3.88	-3.15	0.150
		Downwind	425-300	0.192	-0.807	2.20	0.558
			600	0.085	-0.400	1.11	0.201
			850	0.159	-0.455	1.90	0.458
			1200	0.386	-1.21	3.13	1.02
			1700	0.371	-0.964	2.75	1.07
			2400	0.061	-0.115	1.90	0.224
			3400	0.107	-0.738	0.616	0.280
			4800	0.538	-1.17	2.80	1.71
			6800	1.47	-0.346	-0.229	3.21
			9600	0.332	-6.09	-4.15	0.525

Table VI(Continued)

Frequency band	Source elevation angle	Direction of propagation	Distance interval ft	b_1 W cos ∅	b_2 $(\Delta T)^{2/3}$	b_3 $\log_e$ W	b_4 $(W \cos \emptyset)^{2/3}$
1200-2400	10°	Upwind	425-300	0.020	-0.602	1.15	0.102
			600	0.051	0.425	1.14	0.167
			850	-0.031	0.656	0.236	-0.073
			1200	-0.009	0.275	-0.281	0.023
			1700	0.058	0.663	0.703	0.288
			2400	-0.278	0.382	-1.29	-0.753
			3400	-0.297	-0.301	-2.25	-0.761
			4800	-0.247	0.290	0.162	-0.443
			6800	1.29	1.30	2.75	3.14
			9600	1.08	6.48	-3.59	2.00
		Downwind	425-300	0.051	-1.08	1.80	0.163
			600	0.094	-1.09	2.23	0.284
			850	-0.021	-0.062	0.821	-0.025
			1200	-0.085	-0.455	0.146	-0.201
			1700	0.038	-0.374	1.22	0.143
			2400	-0.034	-2.49	0.711	0.012
			3400	-0.228	-0.218	-1.77	-0.623
			4800	-0.149	0.531	-2.13	-0.321
			6800	-0.030	0.776	1.25	0.472
			9600	0.136	-4.94	-2.86	0.465
	15°	Upwind	425-300	-0.074	-0.240	-0.426	-0.203
			600	-0.029	0.691	-0.858	-0.001
			850	-0.075	1.70	-1.05	-0.211
			1200	-0.300	1.29	-1.54	-0.853
			1700	-0.028	1.61	0.503	-0.115
			2400	-0.131	0.780	0.396	-0.383
			3400	-0.300	0.242	-1.82	-0.833
			4800	-0.360	1.63	-5.04	-0.893
			6800	1.75	4.08	3.57	4.31
			9600	0.305	-0.739	-1.68	0.906
		Downwind	425-300	0.106	-0.451	1.41	0.338
			600	0.213	-0.316	2.27	0.637
			850	0.110	0.938	-0.064	0.345
			1200	0.104	1.20	0.789	0.285
			1700	0.072	1.18	0.432	0.144
			2400	-0.047	0.178	0.378	-0.179
			3400	0.085	0.95	0.002	0.133
			4800	-0.071	-1.04	0.090	-0.064
			6800	1.48	3.47	4.39	3.77
			9600	1.37	-0.633	0.599	3.00

Table VII

Deviation from Average Level of Circular Pass as Function of Wind-Sound Angle.

Tabulated figures are averages for indicated number of flights.

Frequency band, cps	Site	Wind Vel., mph	Time	Pass No.	No. of Flights	Wind - Sound Octant 0	1	2	3	4	5	6	7
1200-2400	Ill.	0-5	Spring-Fall '55	3	12	-.3	-2.4	-.9	.9	2.2	1.4	.8	.1
			Winter '55-56	3	14	-2.2	-2.3	-.3	1.5	1.8	1.0	.8	-.3
				8	15	-1.2	-1.4	-.6	.7	.7	1.4	.7	-.5
			Summer '56	3	10	-.1	.7	.9	.5	-.5	-.6	-.3	-.4
				8	8	0	0	0	-.1	.1	.5	.2	-.1
					Ave.	-.8	-1.1	-.2	.7	.9	.7	.4	-.2
		10-15	Spring-Fall '55	3	12	-2.6	-2.1	-.8	1.3	2.6	2.7	.8	-1.3
			Winter '55-56	3	11	-4.4	-2.4	1.2	2.2	2.6	1.9	1.1	-2.3
				8	11	-3.3	-2.8	.3	1.4	3.3	2.9	.6	-1.5
			Summer '56	3	22	-1.1	-2.1	-1.0	.1	.7	1.9	.9	.6
				8	18	-1.9	-2.1	-.5	.9	2.5	1.7	.6	-.9
					Ave.	-2.7	-2.3	-.2	1.2	2.3	2.2	.8	-1.1
		20-25	Spring-Fall '55	3	8	-1.9	-2.6	-1.2	1.7	2.7	3.2	1.4	.2
			Winter '55-56	3	8	-6.9	-6.0	-.5	3.3	4.0	4.7	2.3	-1.0
				8	8	-6.7	-3.9	2.0	3.3	4.3	3.6	.6	-2.9
			Summer '56	3	4	-2.2	-3.4	-1.7	.1	1.6	3.3	2.8	-.2
				8	3	-3.0	-2.3	0	1.4	1.7	2.0	1.4	-1.3
					Ave.	-4.1	-3.6	-.3	2.0	2.9	3.4	1.7	-1.0
1200-2400	Ariz.	5-15	Winter '56-57	3	10	-.9	-.7	-.6	.1	.6	.9	.4	.1
				8	10	-.6	-.6	-.3	.3	.2	.4	.1	-.4
					Ave.	-.8	-.7	-.5	.2	.4	.7	.3	-.2
150-300	Ill.	0-5	Summer '56	3	10	0	.1	-.1	.3	-.1	-.2	-.4	-.4
				8	9	-.1	.1	.2	-.5	-.5	-.5	-.1	.2
		10-15	Summer '56	3	26	-.1	-.1	-.1	-.3	-.1	.4	.2	.4
				8	26	0	0	-.1	-.1	0	0	.1	.1
		20-25	Summer '56	3	6	0	-.5	-.5	-.8	-.3	.7	.7	.8
				8	7	-.6	-1.3	-1.7	-1.0	-.4	1.0	1.9	1.4

Table X

Values of Maximum Molecular Absorption, a_m, and Absolute Humidity, h_m, for Maximum Absorption

Octave frequency band, cps	h_m gm/m^3	a_m, db/1000 ft., for temperatures, °F				
		0	20	40	60	80
75- 150	.32	.2	.3	.5	.6	.7
150- 300	.46	.5	.7	.9	1.1	1.3
300- 600	.65	1.0	1.4	1.8	2.2	2.7
600-1200	.92	1.9	2.8	3.6	4.5	5.3
1200-2400	1.31	3.8	5.5	7.2	8.9	10.6
2400-4800	1.84	7.6	11.1	14.4	17.9	21.2

APPENDIX B

INTERPRETATION OF DIVE PASSES

To obtain sound propagation at low angles of elevation, dive passes were flown, as explained in the body of the report. During these passes the airplane was approaching the microphone at constant air speed on a straight line until the plane was within about 100 feet of the microphone, at which point the pilot pulled out of the dive and climbed back to altitude.

The airplane noise received by the microphone was recorded in the usual manner on magnetic tape and played back in the laboratory through an octave band filter and recorded on a waxed paper chart on a high speed level recorder.

The levels at different distances were obtained from this level-time chart by subdividing the record between the instant at which the plane was at a fixed reference distance and the instant of closest approach.

The instant of closest approach is very clearly defined on the records by the very high level reached as the plane passes. The instant of passage over the fixed reference was radioed by the pilot to the observer on the ground and recorded on the auxiliary channel of the magnetic tape. At the same time a 20 db attenuator in the microphone was switched into the circuit showing a sudden level change in the final chart for convenience in reading the charts without reference to the other tape channel. The latter was useful, however, for those higher octave bands for which the instrument noise was greater than airplane noise at these distances.

The principal use of the additional 20 db attenuator in the microphone line consisted of reducing the gain of the recording equipment as the plane approached the microphone. That is, it essentially increased the dynamic range of the recorder, preventing overloading.

Subdivision of the level-time chart was effected by means of the device shown in Fig. B-1. This consisted of a set of parallel wires mounted in a parallelogram frame with hinged corners as shown. By changing the vertical angle of the parallelogram the total distance between the left frame edge and the last wire could be adjusted to correspond to the start and finish of the chart, irrespective of the actual ground speed of the airplane.

Allowance was made for the finite time it takes the sound to travel to the microphone by placing the start mark at a distance corresponding to $L/(1-v/c)$ where L is the actual distance to the starting point, v the airplane velocity, and c the velocity of sound.

This correlation, of course, does depend on the airplane ground speed, but the error in taking the mean value was not considered sufficiently large to introduce the inconvenience and possible reading error of a more complex set-up. Another small error which was similarly ignored involved the fact

that the slant distance increases about 3.5 per cent as the dive angle changes from 2° to 15°.

The overall distance error depends on the wind speed and was greatest for a 15° dive with tail wind which resulted in readings being taken with the plane at distances about 10 per cent greater than nominal.

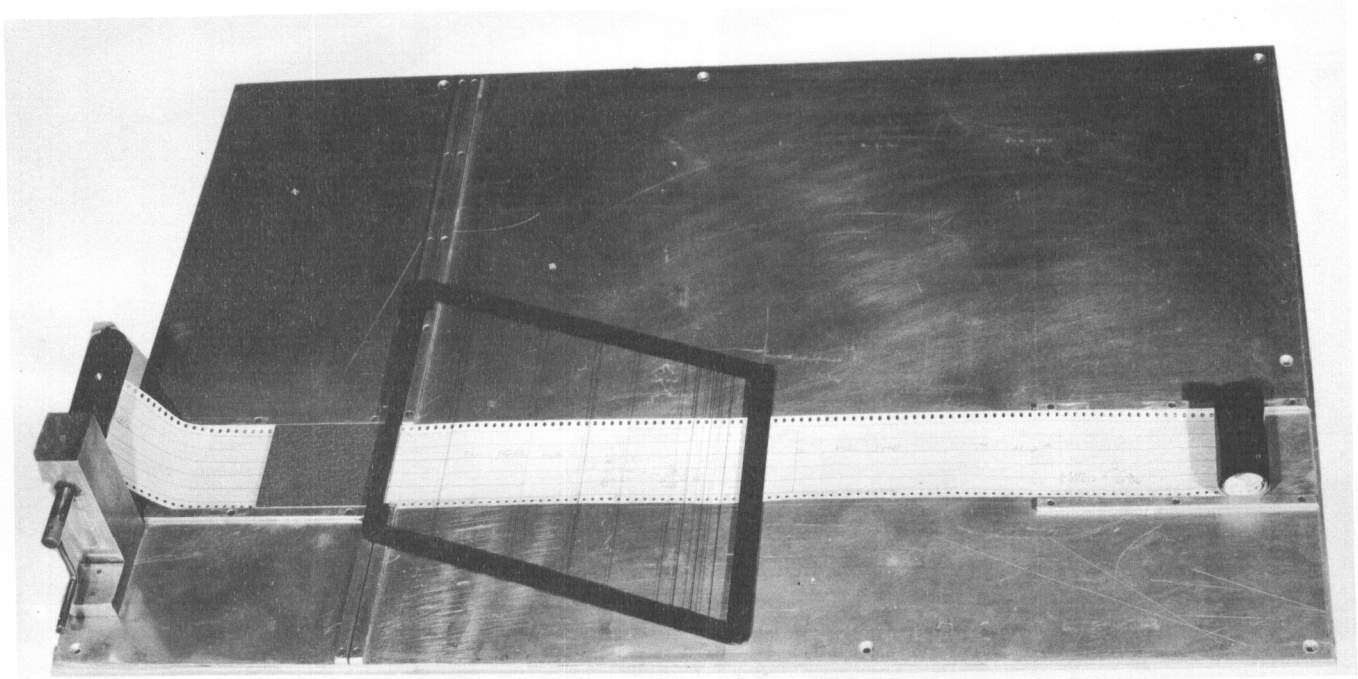

FIG. B-1 - BOARD FOR DETERMINING LEVELS IN DIVE PASSES